Earth-Science Reviews 215 (2021) 103576

Contents lists available at ScienceDirect

Earth-Science Reviews

journal homepage: www.elsevier.com/locate/earscirev

The North American Cordilleran Anatectic Belt

James B. Chapman [a,*], Simone E. Runyon [a], Jessie E. Shields [a], Brandi L. Lawler [a], Cody J. Pridmore [a], Shane H. Scoggin [a], Nathan T. Swaim [a], Adam E. Trzinski [a], Hannah N. Wiley [a], Andrew P. Barth [b], Gordon B. Haxel [c]

[a] University of Wyoming, Department of Geology and Geophysics, Laramie, WY 82071, United States of America
[b] Indiana University–Purdue University Indianapolis, Department of Earth Sciences, Indianapolis, IN 46202, United States of America
[c] Northern Arizona University, School of Earth and Sustainability, Division of Geosciences, Flagstaff, AZ 86011, United States of America

ARTICLE INFO

Keywords:
Two-mica granite
Peraluminous
Crustal melting
Anatexis
Metamorphic core complex
Decompression
Fluid-flux
Leucogranite
Orogenic plateau
Magmatism

ABSTRACT

The North American Cordilleran Anatectic Belt (CAB) is a ~3,000 km long region in the hinterland of the Cordillera that comprises numerous exposures of Late Cretaceous to Eocene intrusive rocks and anatectic rocks associated with crustal melting. As such, it is comparable in size and volume to major anatectic provinces including the Himalayan leucogranite belt. The CAB rocks are chiefly peraluminous, muscovite-bearing leucogranite produced primarily by anatexis of Proterozoic to Archean metasedimentary rocks. The CAB rocks lack extrusive equivalents and were typically emplaced as thick sheets, laccoliths, and dike/sill complexes. The extent, location, and age of the CAB suggests that it is integral to understanding the tectonic evolution of North America, however, the belt is rarely considered as a whole. This paper reviews localities associated with crustal melting in the CAB and compiles geochemical, geochronologic, and isotopic data to evaluate the melt conditions and processes that generated these rocks. The geochemistry and partial melting temperatures (ca. 675–775 °C) support water-absent muscovite dehydration melting and/or water-deficient melting as the primary melt reactions and are generally inconsistent with water-excess melting and high-temperature (biotite to amphibole) dehydration melting. The CAB rocks are oldest in the central U.S. Cordillera and become younger towards both the north and south. At any single location, partial melting appears to have been a protracted process (≥10 Myr) and evidence for re-melting and remobilization of magmas is common. End-member hypotheses for the origin of the CAB include decompression, crustal thickening, fluid-flux melting, and increased heat flux from the mantle. Different parts of the CAB support different hypotheses and no single model may be able to explain the entirety of the anatectic event. Regardless, the CAB is a distinct component of the Cordilleran orogenic system.

1. Introduction

The North American Cordillera is an archetypal Cordilleran (ocean-continent subduction) orogenic system and has been the foundation for many tectonic and geodynamic concepts (Burchfiel and Davis, 1975; DeCelles, 2004; Dickinson, 2004; Yonkee and Weil, 2015; Fitz-Díaz et al., 2018). One of the fundamental components of the North American Cordillera is a belt of Mesozoic to Cenozoic, peraluminous, muscovite-bearing granite (*sensu lato*) exposures in the orogenic hinterland, stretching from southern British Columbia, Canada to northern Sonora, Mexico (Miller and Bradfish, 1980; Miller and Barton, 1990) (Fig. 1). These rocks are located landward, or cratonward, of the Mesozoic Cordilleran coastal batholiths (e.g., the Sierra Nevada, Coast Mountains, and Peninsular Ranges batholiths) and are colloquially called the belt of two-mica (biotite + muscovite) granites. The belt of peraluminous, muscovite-bearing granite is generally considered to have formed by crustal melting (anatexis) (Miller and Bradfish, 1980; Lee et al., 1981; Farmer and DePaolo, 1983; Haxel et al., 1984; Miller and Barton, 1990; Patiño-Douce et al., 1990; Wright and Wooden, 1991). However, detailed experimental and field studies suggest that a variety of processes could have created these peraluminous compositions and mineral assemblages, including crustal anatexis, fractional crystallization, crustal assimilation, hydrothermal alteration, high-pressure differentiation, and localized melting of country rock during the emplacement of mantle-derived magmas (see review in Patiño-Douce, 1999 and Clarke, 2019). Likewise, depending on the source rock, crustal melting may not

* Corresponding author.
E-mail address: jay.chapman@uwyo.edu (J.B. Chapman).

https://doi.org/10.1016/j.earscirev.2021.103576
Received 16 January 2021; Accepted 22 February 2021
Available online 24 February 2021

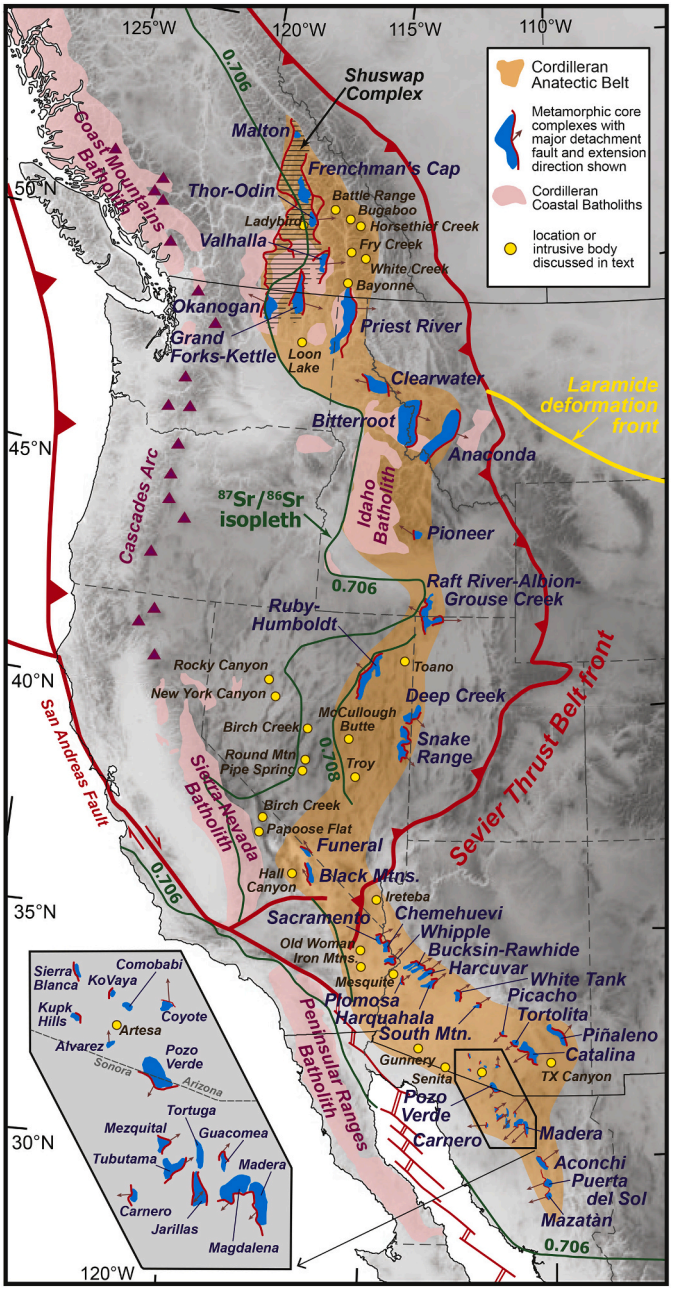

Fig. 1. Overview map of the North American Cordilleran Anatectic Belt (CAB). Feature locations were compiled from previously published works including core complexes (Rehrig and Reynolds, 1980; Armstrong, 1982; Wust, 1986; Roldán-Quintana, 1991; Nourse et al., 1994, 1995; Foster and John, 1999; Miller et al., 1999; Foster et al., 2001, 2007, 2010; Vanderhaeghe et al., 2003; Laberge and Pattison, 2007; Kruckenberg et al., 2008; Howard et al., 2011; Konstantinou et al., 2013; Hoisch et al., 2014; Singleton, 2015; Stevens et al., 2016; Lee et al., 2017; Gottardi et al., 2020), Sevier thrust belt and Laramide deformation front (Yonkee and Weil, 2015; Fitz-Díaz et al., 2018),), and $^{87}Sr/^{86}Sr_i$ isopleths (Armstrong, 1988; Kistler and Anderson, 1990; Miller et al., 2000; Valencia-Moreno et al., 2001). CAB locations, data, and data sources presented in Table 1 and Supplementary File 2. Map projection: UTM, NAD 83 Zone 12N.

always produce strongly peraluminous compositions (see review in Gao et al., 2016).

The primary goal of this review is to update the classic compilation of Miller and Bradfish (1980) and to distinguish igneous bodies and suites related to crustal melting from peraluminous, muscovite-bearing rocks generated by other processes. Crustal melting is defined here as *partial melting of pre-existing crustal rocks that does not directly involve the formation, crystallization, and differentiation of mantle-derived mafic magmas* (cf., Clemens et al., 2020). We refer to these rocks as the North American Cordilleran Anatectic Belt (CAB). Anatectic belts are generally associated with continental collisional orogens including the Himalayan (e.g., Kohn, 2014; Weinberg, 2016), Grenville (Rivers et al., 2002), and Alpine orogens (Burri et al., 2005). The CAB is one of the best examples of an anatectic province related to Cordilleran-style orogenesis and may provide an analog for deep crustal processes in other Cordilleran orogenic systems. With an along-strike length of ~3,000 km, the scale of the CAB rivals or exceeds the size of major continental collision-related anatectic belts, making it one of the largest anatectic provinces globally, regardless of tectonic setting (Fig. 2). Thinking about this belt in terms of process (crustal anatexis) rather than composition (aluminosity) or mineralogy (presence of muscovite) yields insight into the tectonic and thermal evolution of the North American Cordillera (Miller and Gans, 1989; Hodges and Walker, 1992; Foster et al., 2001; Vanderhaeghe and Teyssier, 2001; Whitney et al., 2004a; Wells and Hoisch, 2008; Bendick and Baldwin, 2009; Gervais and Brown, 2011; Konstantinou and Miller, 2015).

First, we describe how CAB rocks produced by crustal melting are distinguished from granitic bodies produced by other processes with an emphasis on locations previously included in the compilation by Miller and Bradfish (1980). Next, we document locations of crustal melting in the CAB and compile geologic, geochronologic, geochemical, and isotopic data for each occurrence. This information is summarized and the shared characteristics and commonalities among the CAB rocks are presented. Then, melt conditions and processes are evaluated, including water-absent dehydration melting, water-deficient melting, and water-excess (fluid-flux) melting. Finally, we evaluate the various tectonic mechanisms that have been proposed to have caused crustal melting.

2. Geologic setting

The North American Cordillera was constructed as a result of prolonged eastward subduction of the oceanic Farallon and Kula plates

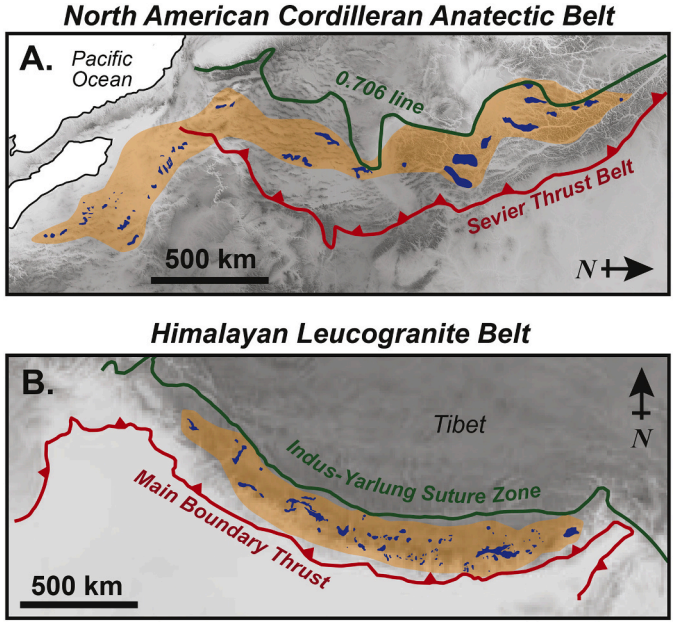

Fig. 2. A comparison between the A) North American Cordilleran Anatectic Belt (CAB) and the B) Himalayan leucogranite belt, both shaded orange and shown at the same scale. Blue polygons are metamorphic core complexes in the CAB and leucogranite bodies in the Himalaya (Whitney et al., 2013; Kohn, 2014).

beneath the North American plate during Triassic to Eocene time and the accretion of various terranes during this interval of time (Dickinson, 2006). This paper focuses on the Cordillera between 53° N and 29° N, which is the range of latitudes where the CAB is exposed. The orogenic system comprises several key fundamental tectonic components including a retroarc thrust belt, orogenic hinterland, and a continental arc (Fig. 1).

2.1. The retroarc and orogenic interior

The thin-skinned Sevier retroarc thrust belt extends from northernmost Canada to the Mojave region of southeast California (Fig. 1) and was active during the Early Cretaceous to Paleogene (Yonkee and Weil, 2015). The thrust belt records up to 350 km of horizontal shortening (DeCelles and Coogan, 2006) and precursor thrust belts like the Luning-Fencemaker, Central Nevada, and Eastern Sierra thrust belts accommodated another ~100 km of shortening during early Mesozoic time (Wyld, 2002). To the east (cratonward) of the Sevier thrust belt is the Laramide foreland belt that was most active from 80 to 40 Ma and temporally overlaps with the end of Sevier deformation (Copeland et al., 2017). The Laramide foreland belt is characterized by thick-skinned, basement-involved deformation with limited horizontal shortening (<50 km) (Yonkee and Weil, 2015).

Pre-Sevier, Sevier, and Laramide-related shortening thickened the crust in the orogenic hinterland and created a high-elevation plateau, called the Nevadaplano in the central U.S. Cordillera (DeCelles, 2004) and the Arizonaplano in the southern U.S. and northern Mexican Cordillera (Chapman et al., 2020). Maximum crustal thickness estimates range from 50 to 65 km in the U.S. and Mexican Cordillera (Coney and Harms, 1984; Chapman et al., 2015, 2020) and may have been as high as 80 km in southeastern British Columbia (Hinchey and Carr, 2006). Exposures of recumbently folded and stacked nappes in metamorphic core complexes like the Ruby-East Humboldt Mountains suggest that upper crustal shortening was balanced by middle to lower crustal shortening and thickening (McGrew et al., 2000).

The regions of thickest crust in the orogenic hinterland during the Cretaceous to early Paleogene are thought to roughly coincide with the current position of the Cordilleran metamorphic core complexes (Coney and Harms, 1984), which were most active from 60 Ma to 10 Ma (Bendick and Baldwin, 2009; Konstantinou and Miller, 2015; Gottardi et al., 2020). There is also a close spatial correlation between the CAB and the Cordilleran metamorphic core complexes (Fig. 1). We adopt the terminology of Whitney et al. (2013) who divided the Cordilleran core complexes into northern, central, and southern belts. The northern belt encompasses core complexes from the Shuswap complex (British Columbia, Canada) to the Pioneer Mountains (Idaho, USA). The central belt extends from the Raft River-Albion-Grouse Creek complex (Utah-Idaho, USA) to the Black Mountains (California, USA). The southern belt stretches from the Sacramento Mountains (California, USA) to Sierra Mazatán (Sonora, Mexico). We use the same geographic divisions when referring to the northern, central, and southern CAB hereafter.

2.2. Cordilleran magmatism

The North American Cordillera has a rich magmatic history related to subduction and extension that overlaps with the CAB in both time and space. The North American Cordilleran continental arc is chiefly preserved as the belt of giant Mesozoic Cordilleran coastal batholiths including the Peninsular Ranges, Sierra Nevada, Idaho, and Coast Mountains batholiths located west of the CAB (Fig. 1). However, magmatism extended into the orogenic interior, particularly during the Jurassic, and some Jurassic igneous rocks were originally included in the belt of muscovite-bearing granite of Miller and Bradfish (1980). In southern British Columbia, the Jurassic Kootenay arc overlaps spatially with the CAB and includes units such as the Kuskanax and Nelson suites that range in composition from diorite to peraluminous two-mica ± garnet granite (Armstrong, 1988; Ghosh, 1995). In the Great Basin region, Jurassic igneous rocks located in a hinterland/back-arc position spatially overlap with the CAB and range in composition from gabbro to peraluminous, two-mica granite (e.g., Dawley Canyon granite; Kistler et al., 1981; Barton et al., 2011). Subsequent to Miller and Bradfish's (1980) study of muscovite-bearing granite, petrologic and isotopic studies indicated that Jurassic to Early Cretaceous magmatism that spatially overlaps with the CAB was chiefly produced from subduction-related (mantle-involved) melting and overwhelmingly tends to be metaluminous or weakly peraluminous (Farmer and DePaolo, 1983; Miller and Barton, 1990; Wright and Wooden, 1991; Brandon and Smith, 1994). Strongly peraluminous, Jurassic-age rocks, like the Dawley Canyon granite, may be related to localized crustal melting associated with the intrusion of mafic magmas at depth (Jones, 1999). In the eastern Great Basin, Jurassic magmatism has also been linked to mantle upwelling during back-arc extension (Elison, 1995; Miller et al., 1995; Miller and Barton, 1990) as well as a slab break-off event (Dickinson, 2006). We do not include any Jurassic or older rocks in the CAB.

2.2.1. Laramide magmatism

Subduction-related, calc-alkaline, metaluminous magmatism ended in the Mesozoic coastal batholiths during the Late Cretaceous (Chen and Moore, 1982; Silver and Chappell, 1988; Gehrels et al., 2009; Gaschnig et al., 2010; Cecil et al., 2012). In the U.S. and Mexican Cordillera, subduction-related magmatism then migrated eastward, sometimes referred to as the "magmatic sweep," as the subduction angle shallowed during the Laramide Orogeny (Coney and Reynolds, 1977; Constenius et al., 2003; Yonkee and Weil, 2015; Fitz-Díaz et al., 2018). This eastward sweep was most pronounced to the north and south of the central U.S. Cordillera - the Great Basin region today. The central U.S. Cordillera contains only scattered evidence for magmatic activity during the Laramide Orogeny and has been referred to as a magmatic gap that is associated with low-angle subduction (Dickinson and Snyder, 1978). We refer to igneous rocks produced during this eastward sweep of magmatism as "Laramide magmatism" or the "Laramide arc," as it is referred to in the southern U.S. and northern Mexican Cordillera (Lang and Titley, 1998; González-León et al., 2011; Leveille and Stegen, 2012; Seedorff et al., 2019). Laramide magmatism is compositionally distinct from rocks in the CAB and is generally characterized as calc-alkaline, quartz-poor to intermediate, metaluminous, containing biotite + hornblende ± clinopyroxene, and is more isotopically juvenile than rocks associated with the CAB (Barton, 1990, 1996). The eastward migration of subduction-related, Laramide magmatism reached or passed through the future position of the CAB during the Late Cretaceous to early Paleogene. Magmatism associated with the Laramide magmatic sweep is generally older than anatectic intrusive rocks in the CAB, but in some cases the two igneous suites overlap both spatially and temporally (e.g., Wright and Haxel, 1982; Miller and Barton, 1990).

2.2.2. Mid-Cenozoic ignimbrite flare-up

Soon after Laramide magmatism reached its most eastward extent during the Laramide orogeny, magmatism rapidly swept back westward toward the trench, producing the mid-Cenozoic (*née* mid-Tertiary) ignimbrite flare-up and several large-volume volcanic eruptive centers (Ferrari et al., 2002; Best et al., 2009). The mid-Cenozoic ignimbrite flare-up is related to the foundering or rapid roll-back of the previously shallowly-dipping Farallon plate (Humphreys et al., 2003). The majority of mid-Cenozoic flare-up magmatism has been interpreted to have originated by melting of hydrated mantle lithosphere to produce mafic magmas that then experienced various degrees of fractional crystallization and assimilation within the crust to produce a range of compositions (basaltic to rhyolitic) (Farmer et al., 2008; Henry and John, 2013). In some locations, intrusion of mantle-derived mafic magmas into the crust locally caused crustal melting and produced magmas with similar geochemical and isotopic compositions to the CAB rocks (e.g., Watts et al., 2016). In the northern and central U.S. Cordillera, the mid-

Cenozoic flare-up migrated southward while in the southern U.S. and Mexican Cordillera, the flare-up migrated west-northwestward (Armstrong and Ward, 1991; Humphreys, 1995). The oldest flare-up related rocks in the Canadian and northern U.S. Cordillera are the Eocene Kamloops-Challis-Absaroka volcanics (Moye et al., 1988; Breitsprecher et al., 2003) and the oldest related rocks in the southern U.S. and Mexican Cordillera are the Eocene volcanic rocks in the Big Bend National Park region in Texas, USA (Barker, 1987; Parker et al., 2012). Igneous rocks related to the mid-Cenozoic ignimbrite flare-up (including intrusive rocks) are generally younger than rocks in the CAB (Konstantinou and Miller, 2015). There is a close temporal association between the migration or passage of the ignimbrite flare-up and the onset of extension in the Cordilleran metamorphic core complexes (Gans, 1989; Best and Christiansen, 1991). Closely following the mid-Cenozoic ignimbrite flare-up, widespread magmatism associated with lithospheric extension commenced and continues to the present in the Basin and Range province (Best and Brimhall, 1974; Hawkesworth et al., 1995).

3. Examples of peraluminous, muscovite-bearing rocks not produced by crustal melting

In our review of North American Cordilleran magmatism, we identified many examples of Mesozoic to Cenozoic peraluminous, muscovite-bearing granites that were produced by processes other than crustal melting, including fractional crystallization, crustal assimilation, hydrothermal alteration, and localized crustal melting associated with mantle-derived mafic intrusions. Below, we provide a few examples with an emphasis on locations previously included in the compilation by Miller and Bradfish (1980).

3.1. Fractional Crystallization and Crustal Assimilation

Fractional crystallization of pyroxene or subaluminous amphibole (aluminum saturation index [ASI] = ~0.5) can lead to peraluminous compositions during magmatic differentiation (Cawthorn and Brown, 1976; Zen, 1986). Throughout this contribution, we use ASI = molecular $Al_2O_3/[CaO - (3.33*P_2O_5) + Na_2O + K_2O]$ (Frost et al., 2001). Assimilation of aluminous sedimentary country rock during differentiation may also result in peraluminous compositions (Barbarin, 1996). In both cases, the simplest way to recognize these processes is to examine whether or not the felsic peraluminous rocks in question are part of a co-magmatic suite that ranges in composition and exhibits chemical or isotopic evidence for fractional crystallization or assimilation (e.g., decreasing εNd_i with increasing SiO_2) (DePaolo, 1981).

An example of peraluminous granite created by fractional crystallization is the Late Cretaceous (ca. 90 Ma) Chemehuevi Mountains plutonic suite in California, USA, which is part of the Chemehuevi metamorphic core complex (John, 1988; John and Mukasa, 1990). The Chemehuevi Mountains plutonic suite has evolved Pb and Sr isotopic values, similar to nearby Proterozoic-age crust, and is compositionally and temporally zoned with older, metaluminous to weakly peraluminous biotite granodiorite on the margins and younger, peraluminous two-mica ± garnet granite in the center, forming a "bullseye" map pattern (John and Wooden, 1990) (Fig. 3). The occurrence of cogenetic magmas of variable composition as well as the nested geometry suggest that the strongly peraluminous granite differentiated from a more mafic, metaluminous magma and the evolved isotopic compositions suggest that the magma assimilated significant amounts of Proterozoic crust (John, 1988; John and Wooden, 1990). In contrast, igneous suites in the CAB generally have a comparatively limited compositional range, usually lacking intermediate to low SiO_2 and metaluminous members (Fig. 3). The Chemehuevi Mountains plutonic suite and similarly aged suites nearby have been interpreted to be part of the Cordilleran (Laramide) arc and to have formed by (mantle-derived) mafic magma influx, hybridization, and partial remelting of the lower crust (Miller and Wooden, 1994; Economos et al., 2010).

3.2. Hydrothermal Alteration

Hydrothermal alteration can also influence the apparent peraluminosity of an intrusive rock unit (Luth et al., 1964; Miller et al., 1981; Zen, 1988; Clarke et al., 2005). There are many different forms of hydrothermal alteration, broadly categorized by the elements gained in comparison to the original protolith composition (e.g., Seedorff et al., 2005, 2008). Greisen alteration and coarse muscovite alteration are characterized by the dominant hydrothermal mineral assemblage muscovite-quartz ± albite ± K-feldspar with or without additional accessory minerals. Coarse muscovite alteration is commonly formed during fluid exsolution from a metaluminous intrusion and results in a relative increase in Al and Rb and relative decrease in Ca and Sr as muscovite ± end-member albite replaces plagioclase (Runyon et al., 2019). As a result, peraluminosity for coarse muscovite altered rocks is commonly higher than the original igneous composition (Fig. 4). Another form of hydrothermal alteration that may affect peraluminosity is hydrolytic (acidic) alteration, which strips cations from the host rock. In hydrolytic alteration, feldspar is commonly altered to fine-grained muscovite (sericite) or clay and original mafic minerals may be

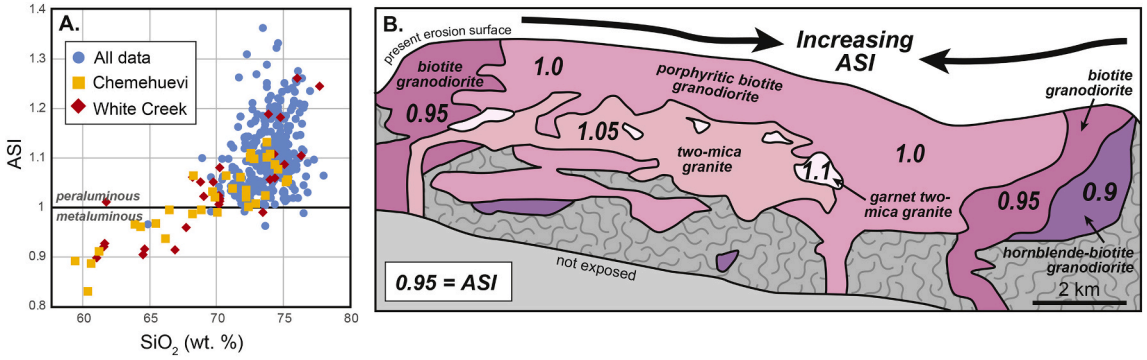

Fig. 3. A) Cordilleran Anatectic Belt (CAB) rocks (blue circles) are silica-rich (SiO_2 > 70 wt. %) and peraluminous with aluminum saturation indices (ASI) of ca. 1.0-1.3. Silica-rich, peraluminous compositions can also be generated from originally metaluminous intrusive rocks with protracted fractional crystallization or assimilation as represented by the Chemehuevi Mountains plutonic suite, California (orange squares; John and Wooden, 1990) and the White Creek batholith, Kootenay arc, British Columbia (red diamonds; Brandon and Lambert, 1993). B.) A down-plunge cross-section view of the Chemehuevi Mountains plutonic suite shows zoned or nested intrusive rocks with increasing ASI toward the center (modified from John, 1988; John and Wooden, 1990), which is not observed in CAB intrusive suites. Data and data sources are presented in Supplementary File 2. (For interpretation of the references to color in this figure legend, the reader is referred to the web version of this article.)

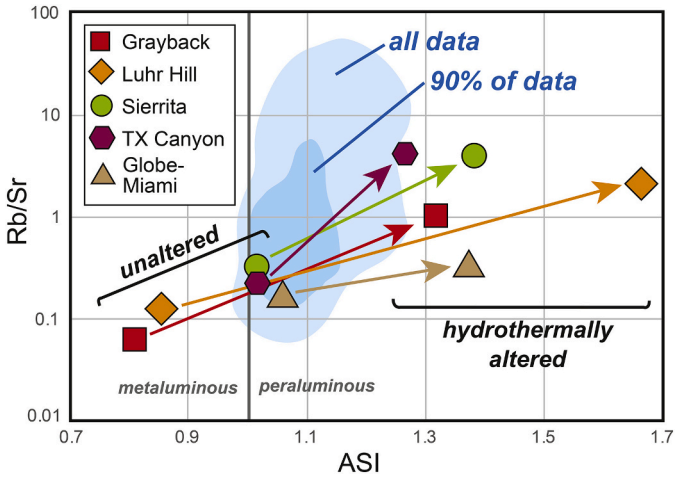

Fig. 4. Pairs of unaltered and hydrothermally altered intrusive rocks from the southern U.S. Cordillera that display elevated Rb/Sr and peraluminosity as a result of hydrothermal alteration, ASI = aluminum saturation index. Cordilleran Anatectic Belt rocks (blue polygons) generally have ASI < 1.3. Data and data sources are presented in Supplementary File 2.

altered to chlorite with or without accessory minerals. In these cases, cations like Na, Ca, and K are more easily mobilized into the fluid than Al, resulting in an apparent increase in peraluminosity (Fig. 4). These two examples are among the more well-known types of hydrothermal alteration that could increase peraluminosity, however, there are many factors including fluid composition, intensity of alteration, host rock composition, and pressure/temperature conditions that will all influence the apparent changes in peraluminosity during hydrothermal alteration of a given rock.

In coarse muscovite alteration, muscovite is commonly found as dispersed, euhedral booklets, replaces igneous minerals (e.g., biotite, feldspars, amphibole), and occurs in veins, and fractures, and small "vugs" or open space that can develop in areas of pervasive wall-rock replacement (Runyon et al., 2019). Hydrothermal versus magmatic muscovite can be distinguished both chemically (e.g., Ti content) and texturally (Miller et al., 1981). Hydrothermally altered rocks may also be hyperaluminous, with an aluminum saturation index (ASI) > 1.3 (Clarke, 2019) and have very high Rb/Sr ratios – with values significantly higher than unaltered anatectic rocks (Fig. 4).

Many of the muscovite-bearing granite locations originally documented in Miller and Bradfish (1980) have been hydrothermally altered (e.g., Barton, 1987). An example of hydrothermal alteration creating an apparently strongly peraluminous, muscovite granite is the Texas Canyon stock in the Little Dragoon Mountains, Arizona (Cooper and Silver, 1964). Unaltered samples of the Texas Canyon stock are commonly biotite ± muscovite quartz monzonite in composition and metaluminous to weakly peraluminous. Coarse muscovite alteration is strongly developed within the Texas Canyon quartz monzonite, ranging from incomplete replacement of biotite by hydrothermal muscovite to pervasive wall-rock replacement by muscovite-albite-K-feldspar ± fluorite mineral assemblages (Runyon et al., 2019). The alteration is well-developed over large areal extents (Cooper and Silver, 1964) and samples of the coarse muscovite altered Texas Canyon quartz monzonite have a significantly higher ASI than unaltered samples (Fig. 4).

3.3. Localized Melting from Mantle-Derived Intrusions

Another way to create peraluminous granite is to locally melt the crust by underplating or intrusion of mantle-derived (basaltic) magmas (Barbarin, 1996). The majority of Phanerozoic granite suites in the North American Cordillera are hybrids with both mantle and crustal inputs, however, added heat or exsolved fluids from basaltic rocks can generate crustal melts with little to no geochemical or isotopic mantle signature (Patiño-Douce, 1999; Annen et al., 2006). As a result, peraluminous granite generated in this fashion is particularly difficult to distinguish from instances of crustal melting that does not involve the intrusion of mantle-derived mafic magmas. Recognition of a mantle-derived, basaltic precursor is mainly achieved through thermal arguments (e.g., a regional heating event) or by exposure of the basaltic intrusions themselves (including as mafic enclaves) and/or igneous rocks derived from these intrusions (e.g., Ireteba pluton, Eldorado Mountains, Nevada; Kapp et al., 2002).

An example of this process to create peraluminous granite comes from the Raft River-Albion-Grouse Creek metamorphic core complex. When examined in isolation, the 32–25 Ma Cassia plutonic complex in the Albion Range and northern Grouse Creek Mountains is a good candidate for a crust-derived magma. The Cassia plutonic complex is 1) silica rich (> 70 wt. % SiO_2), 2) peraluminous (ASI=1.0–1.2), 3) isotopically very evolved ($\varepsilon Nd_i < -25$; $^{87}Sr/^{86}Sr_i > 0.71$), 4) was emplaced into amphibolite-grade metamorphic rocks during or close to peak pressure-temperature conditions (4 kbar, 650°C), and 5) is synkinematic with early core complex extension (Egger et al., 2003; Strickland et al., 2011; Konstantinou et al., 2013). However, emplacement of the Cassia plutonic complex was immediately preceded by the intrusion of the 42–31 Ma Emigrant Pass plutonic complex, which ranges from mafic to felsic compositions (55–75 wt. % SiO_2), is more isotopically primitive, and ranges from metaluminous to peraluminous compositions (Egger et al., 2003; Strickland et al., 2011; Konstantinou et al., 2013). In addition, both the Emigrant Pass and Cassia plutonic complexes have mantle-like, autocrystic (not inherited) zircon $\delta^{18}O$ compositions (Strickland et al., 2011). Added heat from the mantle-derived Emigrant Pass magmatic event has been interpreted to have locally melted the crust to produce the Cassia plutonic suite (Strickland et al., 2011; Konstantinou et al., 2013). Rocks of the Cassia plutonic complex were included in the belt of muscovite-bearing granite of Miller and Bradfish (1980) but are excluded from our compilation of rocks in the CAB.

In the compilation and summary of CAB rocks presented below, locations that involved mantle-derived magmas were excluded. We omitted locations that contain cogenetic igneous rocks interpreted as primitive magmas or products of assimilation and/or fractional crystallization from primitive magmas. This distinction follows previous classification schemes that suggest only peraluminous leucogranite represents crustal melts with no mantle-input and that all other granitic rocks are crust-mantle hybrids, including the Cordilleran coastal batholiths (Collins, 1996; Patiño-Douce, 1999; Annen et al., 2006; Kemp et al., 2007). Alternative models for producing metaluminous granite of intermediate composition (representative of the Cordilleran coastal batholiths) by crustal anatexis include restite unmixing (Chappell et al., 1987) and peritectic assemblage entrainment (Clemens and Stevens, 2012).

4. The North American Cordilleran Anatectic Belt

The CAB includes most of the anatectic rocks in the Omineca Crystalline Belt in southern British Columbia, Canada (Monger et al., 1982; Parrish et al., 1988; Nelson et al., 2013), the "Late Cretaceous-Cenozoic plutonic suite" of Wright and Wooden (1991) and "S-type subzone" of Solomon and Taylor Jr (1989) in the eastern Great Basin region of the United States, the "strongly peraluminous suite" of "Cordilleran Interior plutonism" of Miller and Barton (1990) in the U.S. Cordillera, the "compositionally restricted granites" of Haxel et al. (1984) in southern Arizona, U.S.A., and the "Aconchi granitic suite" in Mexico (Grijalva-Noriega and Roldan-Quintana, 1998). In the following section, we list and briefly describe all main exposures of anatectic rocks that collectively form the CAB. A summary of this information is presented in Table 1. We acknowledge that there are likely additional locations we are unaware of that were unintentionally omitted from the compilation.

Table 1
Summary of details for locations in the North American Cordilleran Anatectic Belt.

State/ Province	Core complex/ region	Core Complex Extension Timing		Metamorphism Timing and Peak Conditions			Cordilleran Anatectic Belt Magmatism								References
		Rapid Extension (Ma)	Extension Onset (Ma)	Peak Timing (Ma)	Max Press. (kbar)	Max. Temp. (°C)	Unit Names	Age (Ma)	SiO_2 (wt. %)	ASI	$\varepsilon Nd_{(t)}$	$^{87}Sr/^{86}Sr_{(i)}$	$^{18}\delta O$ (‰)	Zircon Sat. Temp. (°C)	
BC	Adam's River area						Adams River leucogranite	63–60	73–75	1.1	−19 to −17	0.716–0.742	10–11 (WR)	710 ± 10	1
BC	Frenchmans Cap	51 ± 2	55 ± 3	59–50	10–12	800	migmatite								2–4
BC	Thor Odin complex	52 ± 4	56 ± 2	60–55	8–10	750–800	Ladybird Suite, South Fosthall pluton	62–52	71–76	1.0–1.2	−24 to −5	0.706–0.766	10–13 (qtz)	700 ± 50	5–11
BC	Kootenay Arc						White Creek, Fry Creek, Horsethief Creek, Battle Range, Bugaboo, Bayonne batholiths	117–95	60–78	0.9–1.0	−20 to −5	0.707–0.740	7–11 (WR)	740 ± 50	12–15
BC	Valhalla complex	50 ± 2	60 ± 2	60–57	8–9	800–820	Ladybird and Airy Suite	60–50	71–75	1.0–1.2	−24 to −5	0.706–0.766	11–12 (qtz)	700 ± 50	8, 16–18
BC/WA	Kettle/Grand Forks complex	51 ± 2	52 ± 2	74–56	5–8	725–800	Christina Lake leucogranite	59–50							19–21
WA	Okanogan complex	49 ± 2	51 ± 2	61–49	9–10	700–850	Colville Igneous Complex, Keller Butte Suite, Coulee Dam Suite	61–49	68–78	1.1–1.2		0.706–0.709		760 ± 30	22–24
ID/WA	Priest River complex	50 ± 2	55 ± 2	75–64	7–10	780–800	Silver Point, Wrencoe, Rathdrum plutons	54–44			−21 to −19				25–28
WA	Lake Roosevelt area						Loon Lake bahtolith		70–76	1.0–1.1		0.712–0.729			29
ID	Clearwater complex	45 ± 3	48 ± 3	64–56	8–11	650–750	Roudtop, Beaver Creek, Bungalow plutons	50–45							30–32
ID/MT	Bitterroot complex	50 ± 2	53 ± 2	80–75	7–8	650–750	Bear Creek, Atlanta, Bitterroot Suites	83–53	71–75	1.0–1.1	−19 to −8	0.707–0.715	7 (zrc) 10–11 (qtz)	760 ± 20	33–37
MT	Anaconda complex	45 ± 5	53 ± 2	80–75	4–6	600–700	Hearst Lake pluton	53–46							38, 39
ID	Pioneer Mtns.	36 ± 3	50 ± 4		4		Pioneer Intrusive Suite	53–48							40, 41
NV	Toano Range						Toano Springs pluton	77–72	73–76	1.1–1.2	–23	0.725	9–10 (qtz)	700 ± 10	42–45
NV	Ruby-E. Humboldt complex	22 ± 2	50 ± 3	85–80	8–10	700–800	Ruby Mtns. pegmatitic leucogranite complex	92–68	70–76	1.0–1.2	−17 to −16	0.715–0.720	10–14 (qtz)	690 ± 50	46–51
NV	Fish Creek Range						McCullough Butte, Rocky Canyon plutons	84							52
NV	Snake Range	20 ± 2	45 ± 3	90–70	6–8	500–650	Lexington Creek, Pole Canyon, Can Young Canyon plutons	86–70	71–76	1.0–1.2	−17 to −13	0.711–0.719	10–11 (WR) 11–12 (qtz)	750 ± 25	53–57
NV	Kern Mtns.						Tungstonia pluton	75–66	72–75	1.0–1.1	−19 to −18	0.719–0.788	10–11 (qtz)	715 ± 15	56, 59
NV	Grant Range					550	Troy granite	84							59–61
CA	Funeral Mtns.	9 ± 1	11 ± 1	70–90	7–9	600–700	leucogranite dikes	64–62							62–64
CA	Black Mtns.	5 ± 2	10 ± 1				leucogranite dikes	64–55							65, 66
CA	Panamint Mtns.						Hall Canyon pluton	72	72–76	1.1–1.2	−19 to −18	0.716–0.723		745 ± 40	67
CA	Old Woman–Piute Mtns.						Sweetwater Wash, Lazy Daisy, Painted Rock plutons	75–70	70–76	1.0–1.2	−17 to −10	0.709–0.718	7–9 (WR)	740 ± 10	43, 68

(*continued on next page*)

Table 1 (*continued*)

State/ Province	Core complex/ region	Core Complex Extension Timing		Metamorphism Timing and Peak Conditions			Cordilleran Anatectic Belt Magmatism								References
		Rapid Extension (Ma)	Extension Onset (Ma)	Peak Timing (Ma)	Max Press. (kbar)	Max. Temp. (°C)	Unit Names	Age (Ma)	SiO_2 (wt. %)	ASI	$\varepsilon Nd_{(t)}$	$^{87}Sr/^{86}Sr_{(i)}$	$^{18}\delta O$ (‰)	Zircon Sat. Temp. (°C)	
AZ	Buckskin-Rawhide-Harcuvar complex	17 ± 3	24 ± 2				Tank Pass granite	70	71–74						69–72
AZ	Harquahala complex	19 ± 2	21 ± 2				Browns Canyon, Stone Corral granites	77	72–74	1.0–1.1				750 ± 10	73–76
AZ	White Tank Mtns.	20 ± 5					White Tank granite	72	73–75	1.0–1.2				715 ± 60	76, 77
AZ	Picacho Mtns.	20 ± 2	22 ± 2				Picacho Peak granite, Newman Peak leucogranite	59							78, 79
AZ	Pinaleno complex	25 ± 5					Relleno Suite	54–57	66–75	1.0	−12 to −9	0.707–0.710	7–9 (qtz)	750 ± 50	80, 81
AZ	Tortolita Mtns.	22 ± 3					Fresnal Canyon granite	46	71–74	1.1				725 ± 10	82, 83
AZ	Catalina-Rincon complex	25 ± 2	30 ± 4				Wilderness Suite	57–46	71–76	1.1–1.3	−10 to −8	0.711–0.712		720 ± 10	84–89
AZ	Sierra Blanca Mtns.						granite of Sierra Blanca		75–77	1.1–1.2				700 ± 30	90
AZ	Comobabi Mtns.						granite of Comobabi		75–76	1.1–1.2				650 ± 10	90
AZ	Coyote Mtns. complex	29 ± 2	30 ± 3				Pan Tak granite	58	73–77	1.1			9 (qtz)	730 ± 40	91–93
AZ	Artesa Mtns.						Artesa granite		74–76						90
AZ	N. Sonoyta Mtns.						Senita Basin granite	67	74–80	1.0–1.2				720 ± 35	83, 90
AZ	Kupt Hills						Kupt Hills granite		74–75	1.0–1.1				730 ± 20	90
AZ	Pozo Verde complex		25 ± 3				Presumido Peak granite	58	71–77	1.1–1.2	–12	0.721		720 ± 45	90, 94–95
SO	Guacomea complex						leucogranite dikes	78							96
SO	Mezquital complex						granite of Sierra San Juan	59–51	70–77	1.1				730 ± 10	90, 97
SO	Aconchi complex	23 ± 3	26 ± 3				Huepac granite, El Babizo leucogranite	71–50		1.1–1.3	−14 to −9	0.707–0.714			98–100
SO	Puerta del Sol complex						El Pajarito leucogranite	68–59	74–76	1.0				690 ± 10	101
SO	Matzatan complex	19 ± 2	25 ± 3				Aconchi-El Jaralito batholith	58	72–75	1.1–1.2					96, 99, 102

Data Sources: 1 = Sevigny and Parrish (1993); 2 = Armstrong and Ward (1991); 3 = Crowley et al., 2001; 4 = Crowley et al., 2008); 5 = Norlander et al. (2002); 6 = Carr, 1992; 7 = Holk and Taylor Jr (1997); 8 = Holk and Taylor Jr (2000); 9 = Vanderhaeghe et al. (1999); 10 = Vanderhaeghe et al. (2003); 11 = Hinchey et al. (2006); 12 = Leclair et al. (1993); 13 = Brandon and Lambert (1993); 14 = Brandon and Lambert (1994); 15 = Brandon and Smith (1994); 16 = Spear and Parrish (1996); 17 = Spear (2004); 18 = Gordon et al. (2008); 19 = Laberge and Pattinson (2007); 20 = Cubley et al. (2013); 21 = Cubley et al. (2013); 22 = Carlson et al. (1991); 23 = Hansen and Goodge (1988); 24 = Kruckenberg et al. (2008); 25 = Doughty and Price (1999); 26 = Stevens et al. (2015); 27 = Stevens et al. (2016); 28 = Whitehouse et al. (1992); 29 = Asmerom et al. (1988); 30 = Guevara (2012); 31 = Foster et al. (2007); 32 = Doughty and Chamberlain (2007); 33 = Foster and Raza (2002); 34 = Gaschnig et al. (2010); 35 = Gaschnig et al. (2011); 36 = Foster et al. (2001); 37 = King and Valley (2001); 38 = Wallace et al. (1992); 39 = Foster et al. (2010); 40 = Silverberg (1990); 41 = Vogl et al. (2012); 42 = Lee and Marvin (1981); 43 = Miller et al. (1990); 44 = Wright and Wooden (1991); 45 = Wooden et al. (1999); 46 = McGrew and Snee (1994); 47 = Lee et al. (2003); 48 = Howard et al. (2011); 49 = Henry et al. (2011); 50 = Hallett and Spear (2014); 51 = Hallett and Spear (2015); 52 = Barton (1987); 53 = Evans et al. (2015); 54 = Lee et al. (2017); 55 = Lee and Christiansen (1983); 56 = King et al. (2004); 57 = Gottlieb (2017); 58 = Miller et al. (1999); 59 = Fryxell (1988); 60 = Lund et al. (2014); 61 = Long and Soignard (2016); 62 = Applegate et al. (1992); 63 = Holm and Dokka (1991); 64 = Mattinson et al. (2007); 65 = Sizemore et al. (2019); 66 = Lima et al. (2018); 67 = Mahood et al. (1996); 68 = Miller and Wooden (1994); 69 = Bryant and Wooden (2008); 70 = Wong et al. (2011); 71 = Dewitt and Reynolds (1990); 72 = Singleton et al. (2014); 73 = Isachsen et al. (1998); 74 = Prior et al. (2016); 75 = Richard et al. (1990); 76 = Shaw and Guilbert (1990); 77 = Shafiqullah et al. (1980); 78 = Gottardi et al. (2020); 79 = Spencer et al. (2003); 80 = S. Scoggin (unpublished); 81 = Long et al. (1995); 82 = Creasey et al. (1977); 83 = J. Chapman (unpublished); 84 = Fornash et al. (2013); 85 = Fayon et al. (2000); 86 = Terrien (2012); 87 = Peterman et al. (2014); 88 = Davis et al. (2019); 89 = Ducea et al. (2020); 90 = G. Haxel (unpublished); 91 = Wright and Haxel (1982); 92 = Gottardi et al. (2020); 93 = C. Pridmore (unpublished); 94 = Arnold (1986); 95 = Goodwin and Haxel (1990); 96 = Anderson et al. (1980); 97 = Mallery et al. (2018); 98 = Wong et al. (2010); 99 = Roldán-Quintana (1991); 100 = González-León et al. (2011); 101 = González-Becuar et al. (2017); 102 = Wong and Gans (2008).

Following the descriptions, some of the shared characteristics of the CAB rocks are discussed.

4.1. The Northern Belt

4.1.1. The Shuswap complex

The Shuswap is the largest Cordilleran metamorphic core complex and contains several migmatite-cored gneiss domes that are often treated as core complexes individually, including the Matton, Frenchman's Cap, Thor-Odin, Valhalla, Okanagan, and Grand Forks-Kettle complexes (Vanderhaeghe et al., 1999) (Fig. 1). Peraluminous granites interpreted as anatectic melts are found throughout the Shuswap complex as leucosome in migmatite and as numerous intrusive bodies (plutons, dikes, sills, laccoliths, and veins). Among the more well-known intrusive bodies are the large, sheet-like Ladybird, Airy, and Adams River leucogranites, which have been interpreted to be derived from partial melting in migmatite (Sevigny and Parrish, 1993; Hinchey and Carr, 2006). The ages of Shuswap migmatite and leucogranite range from 61 to 49 Ma and exhibit a wide range of ages ($\geq$ 10 Myr) in most individual locations (Vanderhaeghe et al., 1999; Hinchey et al., 2006; Gordon et al., 2008; Kruckenberg et al., 2008; Cubley et al., 2013). Metamorphic rocks and migmatite in the Shuswap complex record prograde metamorphism from ca. 85 to 55 Ma, with peak pressure and temperature conditions of 8–12 kbar and 700–850 °C ca. 60 to 55 Ma (see review in Bendick and Baldwin, 2009), coincident with or slightly older than the age of crustal melting.

4.1.2. Mid-Cretaceous Kootenay arc

Partly overlapping and east of the Shuswap metamorphic core complex is the Kootenay arc, which contains a suite of mid-Cretaceous (117–95 Ma; Leclair et al., 1993) intrusions that have been associated with crustal melting (Brandon and Lambert, 1993, 1994; Brandon and Smith, 1994) and were included in the belt of muscovite-bearing granite of Miller and Bradfish (1980). These rocks include the White Creek, Fry Creek, Horsethief Creek, Battle Range, Bugaboo, and Bayonne batholiths (Fig. 1). The batholiths are typically zoned or nested and contain a wide range of compositions (60–78 wt. % SiO_2) from metaluminous quartz monzodiorite to biotite-hornblende granodiorite to strongly peraluminous two-mica granite (Brandon and Lambert, 1993, 1994; Brandon and Smith, 1994). Whole rock $\delta^{18}O$ (7.1–11.2 ‰) increases and radiogenic isotope ratios become more evolved (−5 to −20 εNd_i; 0.707–0.74 $^{87}Sr/^{86}Sr$) with increasing differentiation of the magmatic suite with the most evolved values represented by the two-mica granite (Brandon and Lambert, 1993, 1994; Brandon and Smith, 1994). These compositional trends are consistent with crustal contamination of a basaltic precursor during differentiation. However, Brandon and Lambert (1994) note that there are no nearby exposures of basalt, that low Cr and Ni contents and weak negative Eu anomalies are inconsistent with fractional crystallization of plagioclase from a basaltic source, and that the more mafic mid-Cretaceous igneous rock compositions are similar to experimental melt compositions of amphibolite (Rapp et al., 1991; Beard and Lofgren, 1991). The mid-Cretaceous Kootenay arc rocks were interpreted to form by dehydration melting as a zone of anatexis migrated upward through the crust; initially melting Proterozoic amphibolite to tonalitic gneiss to produce the quartz monzodiorite and biotite-amphibole granodiorite and then melting Proterozoic metapelites to produce the two-mica granite (Brandon and Lambert, 1993, 1994; Brandon and Smith, 1994). The mid-Cretaceous suite was emplaced at 2–4 kbar and postdates Early Cretaceous (144–134 Ma) regional Barrovian metamorphism that records peak pressures and temperatures of 6–7 kbar and 650–700 °C (Moynihan and Pattison, 2013; Webster et al., 2017). The mid-Cretaceous Kootenay arc is significantly older (20–80 Myr) than the rest of the CAB (Table 1) and crustal melting has been associated with accretion events on the plate margin specific to this longitude (ca. 50 °N) that may not be relevant to other parts of the CAB (Monger et al., 1982; Brandon and Lambert, 1993, 1994).

4.1.3. Priest River-Clearwater complexes

Prograde metamorphism occurred from ca. 75 to 64 Ma in the Priest River metamorphic core complex, with peak pressure and temperature conditions of 10 kbar and 790 °C, followed by nearly isothermal decompression ca. 60–57 Ma (Stevens et al., 2015) (Fig. 1). Migmatite exposures are estimated to contain 25–45% leucosome and are classified as metatexite (Stevens et al., 2016). Crustal anatexis, via dehydration melting, occurred during both prograde metamorphism and decompression with a majority of melt crystallization occurring ca. 54–44 Ma (Stevens et al., 2015). Intrusive rocks in the Priest River complex are generally Late Cretaceous or Eocene in age. The Late Cretaceous intrusive rocks (e.g., Spokane granite) partly precede prograde metamorphism, span a range of compositions including two-mica granite, and have radiogenic isotopic compositions that may require the involvement of a mantle-derived juvenile component (Whitehouse et al., 1992), which suggests that they are not crustal melts and are not included in the CAB. The Eocene intrusive rocks (e.g., Silver Point, Wrencoe, Rathdrum plutons) overlap in age (50–45 Ma) with leucosome in migmatite and include biotite-hornblende-bearing and biotite-bearing granite (Miller et al., 1975; Stevens et al., 2016) that have been interpreted to be crustal melts of Proterozoic basement (metapelite to orthogneiss) based on their highly evolved isotopic composition (zircon $\varepsilon Hf_i = -22$ to -27; $\varepsilon Nd_i = -19$ to -21; Whitehouse et al., 1992; Stevens et al., 2016) and are included in the CAB. Eocene magmatism also occurs outside (in the hanging wall) of the complex including the peraluminous two-mica granite in the Loon Lake batholith that has been attributed to crustal melting (Asmerom et al., 1988).

The Clearwater metamorphic core complex experienced peak metamorphism at 8–11 kbar and 650–750 °C during ca. 64–56 Ma, followed by the onset of decompression at ca. 59 Ma (Doughty and Chamberlain, 2007). Migmatite is absent, but intrusion of muscovite-bearing granite (e.g., Roundtop, Beaver Creek, Bungalow plutons) during the early Eocene (ca. 50–45 Ma) may record crustal melting at depth (Marvin et al., 1984; Foster et al., 2007). Undated pegmatitic two-mica leucogranite dikes and sills also intrude and cross-cut Proterozoic metasedimentary units (Guevara, 2012).

4.1.4. The Idaho Batholith and Bitterroot complex

Unlike the other large Mesozoic coastal arc batholiths, the Idaho batholith was emplaced entirely into Proterozoic basement and is dominated by peraluminous granite including the 83–67 Ma peraluminous Atlanta suite in the Atlanta lobe and the 66–53 Ma (mostly 55–53 Ma; e.g., Bear Creek and Paradise plutons) peraluminous Bitterroot suite in the Bitterroot lobe (Hyndman, 1983; Johnson et al., 1988; Foster et al., 2007; Gaschnig et al., 2010) (Fig. 1). Whether the peraluminous suites represent crustal melts or extensive crustal assimilation has been a topic of debate for the last half-century (see review in Gaschnig et al., 2011). Emplacement of both peraluminous suites was immediately preceded by cogenetic metaluminous arc magmatism and the batholith generally exhibits increasingly evolved radiogenic isotopes through time (Gaschnig et al., 2011). These patterns, along with the presence of mafic igneous rocks that overlap in age with the Bitterroot suite (Hyndman and Foster, 1988) and mantle-like zircon $\delta^{18}O$ (King and Valley, 2001), support models linking the formation of the Idaho batholith to injection of mantle-derived magmas that eventually led to melting of continental crust. However, the highly evolved isotopic compositions and limited compositional range of the peraluminous suites suggest that if mantle-derived magmas were involved in petrogenesis of the suites, they likely provided heat and not mass input (Gaschnig et al., 2011). Gaschnig et al. (2011) interpreted the Atlanta peraluminous suite to have formed by dehydration melting of greywacke or biotite-bearing granitic rocks and the Bitterroot suite to have formed by dehydration melting of orthogneiss, both at relatively high pressure.

The Bitterroot peraluminous suite is located within the Bitterroot metamorphic core complex and has been interpreted in terms of core complex formation as well as part of the Cordilleran coastal batholith system. The region experienced crustal thickening and prograde metamorphism during the Sevier-Laramide orogeny (80–50 Ma) and the intrusion of the Bitterroot peraluminous suite ("main phase" plutons) as a series of thick (3–4 km) sills and laccoliths has been interpreted to be related to anatexis of Proterozoic basement gneisses (Foster et al., 2001, 2010). Migmatite is locally exposed in the Bitterroot metamorphic core complex and records anatectic melting (leucosome and pegmatite intrusions) at ~53 Ma and peak metamorphic pressures and temperatures of 7–8 kbar and 650–750 °C, resulting in muscovite breakdown (Foster et al., 2001).

4.1.5. Anaconda-Pioneer complexes

The Anaconda metamorphic core complex shares many similarities with the Priest River, Clearwater, and Bitterroot complexes and they are linked by the dextral Lewis and Clark fault zone (Foster et al., 2007) (Fig. 1). The footwall of the Anaconda complex exposes recumbently folded nappes that record deformation and metamorphism related to crustal thickening during the Late Cretaceous (80–75 Ma) with peak pressures and temperatures of 4–6 kbar and 600–700 °C (Grice, 2006; Haney, 2008). Eocene plutons and abundant pegmatite and aplite dikes and sills intrude Proterozoic host rocks, which are locally migmatitic (Foster et al., 2007). The Eocene (53–50 Ma) intrusive rocks include the Hearst Lake pluton, a peraluminous, two-mica leucogranite (Wallace et al., 1992; Foster et al., 2007).

The footwall of the Pioneer metamorphic core complex locally contains migmatite and is pervasively intruded by leucogranite dikes and sills with crystallization ages of 52–46 Ma, which overlap in age with the Pioneer Intrusive Suite (50–48 Ma) (Silverberg, 1990; Vogl et al., 2012).

4.2. The Central Belt

4.2.1. Ruby-East Humboldt core complex

Fold nappes exposed in the core of the Ruby-East Humboldt metamorphic core complex and thrust faults in nearby mountain ranges record crustal thickening and prograde metamorphism, starting during the mid-Cretaceous (ca. 100–95 Ma) and peaking during the Late Cretaceous (ca. 85–80 Ma) (Camilleri and Chamberlain, 1997; McGrew et al., 2000; Hallett and Spear, 2015) (Fig. 1). Metamorphic rocks indicate that the complex experienced decompression from ca. 85–55 Ma, although the amount of decompression (1–6 kbar) varies and there is little to no upper crustal or basinal record of this event (Hodges et al., 1992; McGrew et al., 2000; Henry et al., 2011; Hallett and Spear, 2014; Hallett and Spear, 2015). Some authors have related decompression to vertical ductile thinning (Hallett and Spear, 2014; Long and Kohn, 2020). Migmatite is exposed at deep structural levels in the complex (Howard, 1980) and partial melting in these migmatites has been linked to pervasive intrusion of leucogranite at higher structural levels during the Late Cretaceous (Lee et al., 2003; Premo et al., 2008). Late Cretaceous pegmatitic leucogranite is the dominant intrusive component of the Ruby-East Humboldt complex and forms an injection complex of innumerable dikes and sills (Howard et al., 2011). The pegmatitic leucogranite has been interpreted to have formed by muscovite dehydration melting of Proterozoic metapelite and to be related to crustal anatexis during both prograde metamorphism and decompression (Wright and Snoke, 1993; McGrew et al., 2000; Lee et al., 2003; Howard et al., 2011; Hallett and Spear, 2014; Hallett and Spear, 2015). A younger population (46–29 Ma) of leucogranite bodies is also present in the Ruby-East Humboldt complex and overlaps in age with a compositionally expanded suite of igneous rocks (e.g., Harrison Pass pluton) ranging from gabbro to two-mica granite that involve a mantle-derived component (Barnes et al., 2001; Lee et al., 2003; Howard et al., 2011). These younger rocks are volumetrically less significant and geochemically and isotopically distinct from the Late Cretaceous pegmatitic granite (Barnes et al., 2001; Lee et al., 2003). Howard et al. (2011) suggested that mafic underplating during the younger phase of magmatism (Eocene-Oligocene) provided heat ± fluids that resulted in additional crustal melting and re-melting and remobilization of the Late Cretaceous pegmatitic granite. Regionally, Eocene-Oligocene magmatism is related to the mid-Cenozoic ignimbrite flare-up and rollback of the Farallon slab (Humphreys, 1995; Konstantinou and Miller, 2015) and is not included in the CAB.

East of the Ruby-East Humboldt complex, Late Cretaceous two-mica ± garnet leucogranite, pegmatite, and aplite dikes interpreted to have formed by crustal melting are present in the Wood Hills, Pequop Mountains, and Toano Range (Lee and Marvin, 1981; Miller et al., 1990; Camilleri and Chamberlain, 1997; Milliard et al., 2015). The 77–72 Ma Toano Springs pluton in the Toano Range marks the northeastern extent of Late Cretaceous crustal anatexis in the Great Basin as interpreted by Wright and Wooden (1991).

4.2.2. Snake Range-Kern Mountains-Deep Creek range

The Snake Range, Kern Mountains, and Deep Creek Range are part of a single metamorphic core complex/extensional fault system (Miller et al., 1999), herein referred to as the Snake Range complex (Fig. 1). No migmatite is exposed in the Snake Range complex, but the region experienced peak metamorphism during the Late Cretaceous (90–70 Ma) associated with the Sevier orogeny (Miller and Gans, 1989). Metamorphic rocks in the footwall record maximum pressures and temperatures of 6–8 kbar and 500–650 °C (Cooper et al., 2010). Late Cretaceous (ca. 86–70 Ma), strongly peraluminous, two-mica granite (e.g., Lexington Creek, Pole Canyon-Can Young Canyon, Tungstonia plutons) in the Snake Range complex have been interpreted to be crustal melts formed by dehydration melting of Proterozoic metapelite (Lee et al., 1981; Lee et al., 1986; Farmer and DePaolo, 1983; Lee and Christiansen, 1983; Wright and Wooden, 1991; Gottlieb, 2017). Eocene peraluminous, muscovite-bearing granite (e.g., Young Canyon-Kious Basin plutons; ~37 Ma) is also present in the Snake Range complex (Lee and Christiansen, 1983) and may have formed in a similar way to the Eocene peraluminous rocks in the Ruby-Humboldt Mountains (i.e., associated with the mid-Cenozoic ignimbrite flare-up). The Eocene intrusive rocks have more juvenile $^{87}Sr/^{S6}Sr$ ratios, are more oxidized, and have lower $\delta^{18}O$ ratios compared to the strongly peraluminous Cretaceous intrusions (Lee and Christiansen, 1983; King et al., 2004).

Swarms of pegmatitic leucogranite sills and dikes are common in the Snake Range complex as well as in neighboring ranges (e.g., Schell Creek Range) and may also be associated with crustal anatexis (Lee et al., 1981; Miller and Gans, 1989). Miller et al. (1999) reported an age of 82 Ma on a leucogranite dike in the Smith Creek region, Kern Mountains. Two-mica granite, potentially equivalent with the strongly peraluminous Cretaceous intrusions in the Snake Range, is also exposed in some surrounding ranges, including the ca. 84 Ma Troy Granite in the Grant Range (Fryxell, 1988; Lund et al., 2014) and the ca. 84 Ma McCullough Butte and Rocky Canyon plutons in the Fish Creek Range (Barton, 1987).

4.2.3. Central Great Basin two-mica granite

All the rocks in the central CAB described in the preceding sections (Sections 4.2.1 and 4.2.2) occur east of the $^{87}Sr/^{86}Sr = 0.708$ isopleth and east of the Roberts Mountain thrust, which marks a suture zone separating accreted (para)allochthonous terranes to the west from North American cratonic basement to the east (Kistler and Peterman, 1973; Stewart, 1980). Small exposures of Late Cretaceous, peraluminous, two-mica granite occur throughout the Great Basin region west of the $^{87}Sr/^{86}Sr = 0.708$ isopleth (Fig. 1). These granites are interpreted to have a significant sedimentary input and were included in previous compilations of strongly peraluminous rocks (Miller and Bradfish, 1980; Barton, 1987, 1990; Miller and Barton, 1990; Barton and Trim, 1991). In Nevada, these granites include the Pipe Springs (80 Ma) and Round Mountain plutons (95 Ma) in the Toquima Range (Shawe et al., 1986),

the Birch Creek pluton (89 Ma) in the Toiyabe Range (Stewart et al., 1977), and the New York Canyon and Rocky Canyon plutons (73–71 Ma) in the Humboldt and Stillwater Ranges (Johnson, 1977; McFarlane, 1981; Barton and Trim, 1991). In eastern California, these include the Birch Creek and Papoose Flat plutons (83–82 Ma) in the White and Inyo Mountains (Sylvester et al., 1978; Barton, 2000). Two-mica granite intrusions in the central Great Basin are generally considered to be satellites of the Sierra Nevada batholith and occur along with more common Late Cretaceous metaluminous intrusive rocks (Sylvester et al., 1978; McFarlane, 1981; Barton, 1987, 2000; Brown et al., 2018). Besides slightly more juvenile radiogenic isotopic compositions (compared to the eastern Great Basin), these rocks have lower zircon $\delta^{18}O$ ratios (King et al., 2004) and, where studied in detail, are associated with rare mafic dikes and enclaves (e.g., Barton, 2000). Late Cretaceous, two-mica granite in the central Great Basin has been interpreted to be an evolved, high-pressure equivalent to more metaluminous, calc-alkaline continental arc rocks (Patiño-Douce, 1999) or related to increased mantle heat flow (e.g., basaltic underplating or intrusion, mantle upwelling; Barton, 1990). Wright and Wooden (1991) suggested that none of the Late Cretaceous two-mica granite located west of $^{87}Sr/^{86}Sr = 0.708$ isopleth are crustal melts and they are not included in the CAB here.

4.3. The Southern Belt

4.3.1. Death Valley area, California

The Funeral Mountains metamorphic core complex contains migmatite that record Late Cretaceous prograde metamorphism and maximum pressures and temperatures of 7–9 kbar and 600–700 °C during ca. 90–70 Ma (Hodges and Walker, 1990; Hoisch and Simpson, 1993; Mattinson et al., 2007) (Fig. 1). The migmatite is cut by Paleocene (64–62 Ma) two-mica leucogranite dikes and sills that were emplaced syn-kinematically and have been interpreted to have formed by water-excess to water-deficient melting of muscovite-bearing metasedimentary rocks (Mattinson et al., 2007).

Leucogranite dikes and pegmatite (59–55 Ma) are also present in the Black Mountains metamorphic core complex in the Badwater, Mormon Point, and Copper Canyon turtlebacks (antiformal footwall corrugations) (Miller and Friedman, 1999; Lima et al., 2018) and in the Panamint Mountains (Mahood et al., 1996). The ~72 Ma Hall Canyon pluton, a two-mica granodiorite, in the Panamint Mountains was interpreted by Mahood et al. (1996) to be a product of water-absent biotite dehydration melting.

Late Cretaceous muscovite-garnet granite is found south and west of Death Valley in the western Mojave Desert region and is interpreted to have formed in part by partial melting and assimilation of Pelona-Orocopia-Rand Schist, which was underplated in this area during Laramide low-angle subduction (Miller et al., 1996, 2000; Grove et al., 2003). Despite significant involvement of the Pelona-Orocopia-Rand Schist in the source region, these muscovite-garnet granites are still interpreted to be subduction-related and to have originated in the upper mantle (Miller et al., 1996; Saleeby, 2003). They are considered distinct from the Cordilleran interior belt of muscovite-granite (Miller and Barton, 1990; Miller et al., 1996), and are not included in the CAB.

4.3.2. Colorado river extensional corridor

The Colorado River extensional corridor extends from southern Nevada to the Phoenix, Arizona area and consists of a series of top-to-the-northeast metamorphic core complexes and extensional fault systems (Howard and John, 1987). Numerous magmatic rocks occur throughout this corridor that have been or could be interpreted as crustally-derived magmas. The Ireteba pluton (~66 Ma) in the Eldorado Mountains, Nevada is a two-mica ± garnet granite that was included in the belt of muscovite-bearing granite of Miller and Bradfish (1980). However, the Ireteba granite shows extensive interaction with mafic magmas and has been interpreted to be related to injection of juvenile basaltic magmas causing melting of the crust (Kapp et al., 2002).

Late Cretaceous peraluminous granite in the Sacramento and Chemehuevi core complexes, California has been interpreted to be related to fractional crystallization and crustal assimilation of mantle-derived magmas as discussed in Section 3.1 (John and Wooden, 1990). Likewise, Late Cretaceous (~89 Ma) peraluminous granite in the Whipple Mountains metamorphic core complex has been interpreted to have formed in a subduction setting and involved a mantle input (Anderson and Cullers, 1990).

Late Cretaceous (75–70 Ma), strongly peraluminous two-mica granite in the Old Woman-Piute batholith, California (e.g., Sweetwater Wash, Lazy Daisy, Painted Rock plutons) has been interpreted to represent crustal melts with limited mantle input (Foster et al., 1989; Miller et al., 1990b; Miller and Wooden, 1994). The strongly-peraluminous plutons were emplaced along with metaluminous rocks of the same age, show a spectrum of major element and isotopic compositions, and in some cases are nested within the metaluminous rocks, similar to the peraluminous granite in the Chemehuevi Mountains (John and Wooden, 1990; Miller et al., 1990). However, the peraluminous stocks in the Old Woman-Piute batholiths have been interpreted to reflect anatexis of a hybridized lower crustal source consisting of older basement rocks and mantle-derived Jurassic arc igneous rocks (Miller et al., 1990; Miller and Wooden, 1994). The nearby Iron Mountains, California also contain Late Cretaceous (ca. 75–70 Ma) strongly peraluminous two-mica ± garnet granite equivalent to the Old Woman-Piute batholith (Wells et al., 2002; Wells and Hoisch, 2008). The Iron Mountains intrusive suite and nearby Coxcomb intrusive suite comprise the Cadiz Valley batholith, which has been interpreted to be subduction-related (Howard, 2002; Economos et al., 2010).

Widespread exposures of two-mica ± garnet leucogranite occur in the Buckskin-Rawhide, Harcuvar, Harquahala, and White Tank metamorphic core complexes, Arizona, including the Tank Pass granite (ca. 80–78 Ma; Dewitt and Reynolds, 1990; Bryant and Wooden, 2008), the Brown's Canyon granite (ca. 72 Ma; Richard et al., 1990; Isachsen et al., 1998), and the White Tank granite (ca. 72 Ma; Reynolds et al., 2002; Prior et al., 2016) which intruded primarily as large sills, but also form dense networks of smaller dikes and sills. Locally, areas of particularly voluminous intrusions have been referred to as migmatitic injection complexes (Bryant and Wooden, 2008), although evidence for *in situ* melting during the Late Cretaceous is not documented in Arizona. Bryant and Wooden (2008) report a ~110 Ma mylonitized, "migmatitic" gneiss in the Harcuvar Mountains, and Knapp and Heizler (1990) report a ~67 Ma partially mylonitized, "migmatitic" gneiss in the Mesquite Mountains, Arizona.

4.3.3. Southern Arizona

Strongly peraluminous, two-mica ± garnet leucogranite is exposed throughout southern Arizona, primarily within the footwalls of

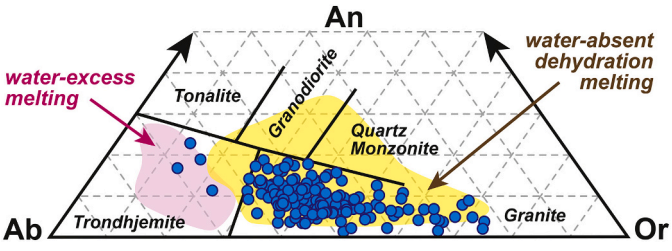

Fig. 5. Cordilleran Anatectic Belt rocks (blue circles) generally plot as granite on a normative Ab–An–Or ternary diagram and overlap with metasedimentary melt compositions for water-absent dehydration melting experiments (Patiño-Douce and Beard, 1995; Patiño-Douce and Harris, 1998; Patiño Douce, 2005) rather than water-excess melting experiments (Conrad et al., 1988; Patiño-Douce and Harris, 1998). Data and data sources are presented in Supplementary File 2. (For interpretation of the references to color in this figure legend, the reader is referred to the web version of this article.)

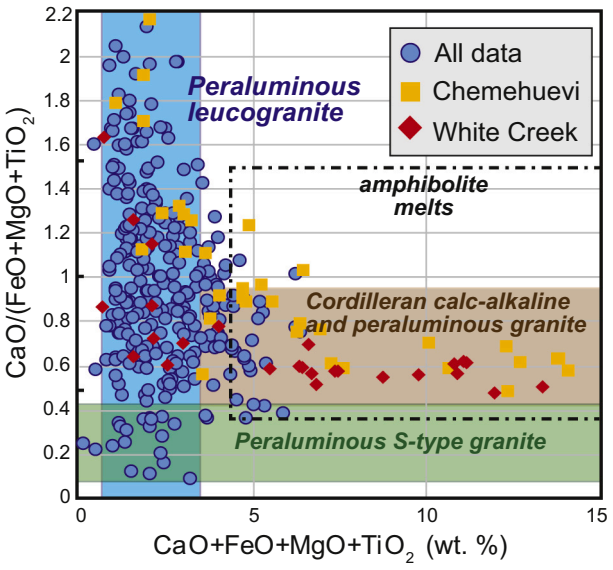

Fig. 6. The majority of Cordilleran Anatectic Belt (CAB) rocks (blue circles) have compositions consistent with peraluminous leucogranite melts produced by experimental melting of mica-rich metasedimentary rocks (shaded blue) rather than amphibolite (black outline). CAB rock compositions are also largely distinct from S-type granite and Cordilleran granite. The Chemehuevi Mountains plutonic suite (orange squares; John and Wooden, 1990) and White Creek batholith (red diamonds; Brandon and Lambert, 1993) are shown for comparison. Compositional fields are from Patiño-Douce (1999). Data and data sources are presented in Supplementary File 2.

metamorphic core complexes. The Paleocene to Eocene (ca. 60–45 Ma) Wilderness Suite in the Catalina-Rincon metamorphic core complex was emplaced as series of thick (≤ 2 km) sills and has been interpreted to have formed by crustal melting of Proterozoic Oracle granite (Keith et al., 1980; Farmer and DePaolo, 1984; Force, 1997; Fornash et al., 2013; Davis et al., 2019) or from other unexposed lithologies (Ketcham, 1996). Equivalent rocks (e.g., Fresnal Canyon granite) are exposed in the Picacho and Tortolita Mountains core complexes as well (Banks, 1980; Spencer et al., 2003; Ferguson et al., 2003). The Wilderness suite was estimated to have been emplaced at 3–4 kbar and ca. 625–725 °C (Anderson et al., 1988).

The Pan Tak granite in the Coyote Mountains core complex and the Presumido Peak granite in the Pozo Verde Mountains core complex are both ~58 Ma, two-mica ± garnet leucogranites that have been interpreted to have formed by crustal anatexis of Proterozoic basement, potentially the Pinal schist (Wright and Haxel, 1982; Goodwin and Haxel, 1990). Haxel et al. (1984) report similar peraluminous granite in the Kupk Hills, Sierra Blanca, and Comobabi core complexes. Apart from the southern Arizona metamorphic core complexes, peraluminous two-mica leucogranite occurrences include the Texas Canyon stock (~55 Ma), Senita Basin granite, and Artesa Mountains granite (Cooper and Silver, 1964; May and Haxel, 1980; Shafiqullah et al., 1980; Haxel et al., 1984; Chapman et al., 2018). Arnold (1986) interpreted the Gunnery Range batholith and Texas Canyon stock (Fig. 1) to represent crustal melting of a deep granulitic source terrane, although the strongly peraluminous compositions of the Texas Canyon stock may be related to hydrothermal alteration as discussed in Section 3.2 (Runyon et al., 2019).

4.3.4. Northern Sonora

The Aconchi suite in northern Sonora comprises Late Cretaceous to Paleogene two-mica ± garnet leucogranite that has been interpreted as crustal melts and has been mapped throughout the region, primarily within the footwalls of metamorphic core complexes, including in the Mesquital (59–51 Ma), Tubutama, Carnero (ca. 55 Ma), Tortuga, Guacomea (78 Ma), Magdalena, Madera, Aconchi (58–55 Ma), Puerta del Sol (68–59 Ma), and Mazatán (58 Ma) complexes (Anderson et al., 1980; Hayama et al., 1984; Nourse et al., 1994; Nourse et al., 1995; Grijalva-Noriega and Roldan-Quintana, 1998; González-León et al., 2011; González-Becuar et al., 2017; Mallery et al., 2018). Relatively little information is available on many of these localities, although the intrusions are often described as laterally extensive sills, laccoliths, small plutons, and networks of small dikes and sills. The largest exposure is the Aconchi-El Jaralito batholith located between the Mazatán and Aconchi complexes, which contains the Huépac (58–55 Ma) and El Babizo leucogranites (71 Ma) among others (Roldán-Quintana, 1991; González-León et al., 2011). Late Cretaceous to Paleocene (68–59 Ma) orthogneiss migmatite is reported from the Puerta del Sol complex and has been interpreted as the source for the El Pajarito (68 Ma) garnet-bearing leucogranite (González-Becuar et al., 2017). The youngest leucogranite in the Puerta del Sol complex is the ~42 Ma El Oquimonis granite, a two-mica + garnet leucogranite (González-Becuar et al., 2017).

5. Common Characteristics of the Cordilleran Anatectic Belt

The most straightforward way to recognize igneous rocks produced by crustal anatexis is to observe them in situ – leucosome in migmatite. Leucosome often represents the initial stages of crustal anatexis and has been interpreted to feed larger-scale intrusive bodies or represent crystal fractionation from these bodies (Solar and Brown, 2001; Johannes et al., 2003). Migmatite (of similar age to the CAB) is common in the northern CAB, but rare to absent in the central and southern CAB. In some locations, leucosomes have been shown to be the source for more voluminous CAB magmas (e.g., Ladybird Suite in the Shuswap complex; Hinchey and Carr, 2006). However, in most instances a direct relationship between migmatitic leucosomes and CAB magmas has not been demonstrated. Most exposures of migmatite associated with the CAB record mid-crustal (5–10 kbar), amphibolite facies conditions (Table 1). In rare cases, evidence is present suggesting that significant leucosome accumulation ± melt extraction took place at these conditions (e.g., Priest River complex; Stevens et al., 2015, 2016). In the majority of locations, however, CAB igneous rocks were derived from deep structural levels not exposed at the surface.

The emplacement geometry of CAB igneous rocks varies greatly, but commonly forms dike and sill networks, injection complexes, or large sheets and laccoliths (e.g., Ruby-East Humboldt complex and Catalina-Rincon complex; Howard et al., 2011; Fornash et al., 2013). This is similar to the geometry of igneous bodies in other major anatectic provinces (e.g., Manaslu laccolith in the Himalaya leucogranite belt, Le Fort et al., 1987). Where CAB rocks are exposed as stocks or plutons, they are commonly pervasively intruded by late-phase pegmatite and aplite dikes that are generally interpreted to have been derived from closed-system crystallization of water-bearing felsic magmas (e.g., Coyote Mountains complex; Wright and Haxel, 1982). To our knowledge, there are no extrusive rocks equivalent to the intrusive rocks of the CAB. The inferred high water contents of the CAB melts likely caused them to reach their solidus and freeze at moderate pressure (depth) during ascent (Miller, 1985; Clemens and Droop, 1998), which may explain the lack of extrusive equivalents.

5.1. Geochemistry, isotopic composition, and protoliths

The CAB igneous rocks are silica-rich (≥ 70 wt. % SiO_2; Fig. 3; Table 1), consistent with experimentally produced melts from a wide range of crustal protoliths (e.g., greywacke, schist, gneiss; Patiño-Douce, 1999). The paucity of anatectic rocks of intermediate composition (< 70 wt. % SiO_2) suggest that crustal melting of more mafic source rocks (e.g., basaltic amphibolite) is less common (Beard and Lofgren, 1991; Patiño-Douce and Beard, 1995; Rapp and Watson, 1995; Gao et al., 2016). CAB rocks are usually identified in the field as leucogranite and are

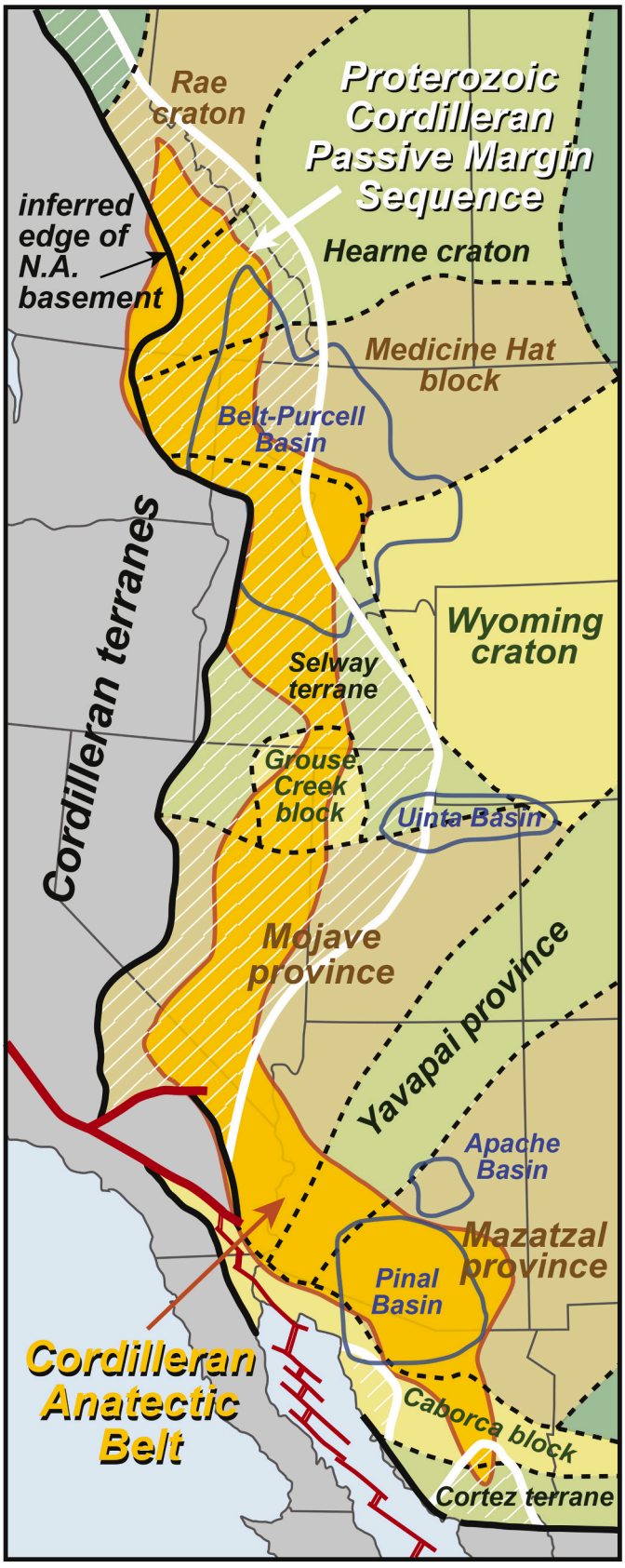

(caption on next column)

Fig. 7. The North American Cordilleran Anatectic Belt (CAB) crosses many Proterozoic to Archean basement provinces/terranes. The northern and central CAB overlaps with areas where Proterozoic rocks are present in the Cordilleran passive margin sequence (Miogeocline), which has been proposed as one possible protolith. Metasedimentary rocks from the Mesoproterozoic Belt-Purcell Basin and Paleoproterozoic Pinal Basin have also been proposed as possible protoliths. The inferred edge of North American basement is based on the position of the $^{87}Sr/^{86}Sr_i = 0.706$ isopleth (Fig. 1). Map projection: UTM, NAD 83 Zone 12N.

geochemically and mineralogically classified as granite or rarely, as trondhjemite (Fig. 5). Potassium feldspar is common, but always significantly less abundant than plagioclase. Compositions range from alkalic to calcic on modified alkali–lime index (MALI; $Na_2O + K_2O - CaO$) diagrams, consistent with global compilations of leucogranites (Frost et al., 2001). CAB rocks are weakly to moderately peraluminous (ASI = 1.0–1.3; Fig. 3; Table 1) and are corundum normative with modal minerals more aluminous than biotite, chiefly muscovite and garnet, characteristic of crustal melting of metasedimentary protoliths (Castro et al., 1999; Chappell et al., 2012). Biotite is generally more abundant than muscovite and cordierite is very rare, which is one of the reasons why the CAB rocks are not strictly classified as S-type granites (White et al., 1986; Chappell and White, 2001). Another difference between the CAB and classic S-type granites is that magnetite, rather than ilmenite, is the dominant opaque oxide in CAB rocks (White et al., 1986), which suggests that the CAB magmas may be more oxidized. Crustal melts originating from (meta)sedimentary protoliths containing small amounts of organic material tend to be reduced ($fO_2 <$ FMQ) (Nabelek, 2019). However, there has been no comprehensive investigation of the oxidation state of CAB rocks. Peraluminous S-type granites as well as peraluminous, calc-alkaline Cordilleran (subduction-related) granite are enriched in FeO, MgO, and TiO_2 compared to CAB rocks (Patiño-Douce, 1999; Fig. 6). Despite their geochemical and mineralogical differences, CAB rocks have been informally referred to as S-type granites because the large majority have been interpreted to have formed from melting of metasedimentary protoliths (Miller and Bradfish, 1980; Patiño-Douce et al., 1990; Wright and Wooden, 1991). Additional geochemical data for CAB rocks is presented below in Section 6, focusing on melt processes.

The CAB rocks exhibit highly evolved radiogenic isotopic compositions (e.g., low $\varepsilon Nd_{(t)}$, $\varepsilon Hf_{(t)}$, high $^{87}Sr/^{86}Sr_i$; Table 1) that reflect the composition and age of local basement rocks. In North America, the $^{87}Sr/^{86}Sr_i = 0.706$ isopleth ("0.706 line") is often interpreted to represent the western edge of autochthonous, North American crystalline basement (Kistler and Peterman, 1973) and the CAB is almost everywhere located east (cratonward) of this isopleth (Fig. 1). For the Great Basin region, Wright and Wooden (1991) suggested that Mesozoic to Cenozoic crustal melting was limited to areas east of the $^{87}Sr/^{86}Sr_i = 0.708$ isopleth and east of the $\varepsilon Nd_i = -7$ isopleth (Farmer and DePaolo, 1983), although the relationship between these isopleths and the CAB is less clear to the north and south (Fig. 1). The CAB crosses multiple Archean to Proterozoic basement/lithospheric provinces including, from north to south, the Rae craton, Hearne craton, Medicine Hat block, Selway terrane, Grouse Creek block, Mojave province, Yavapai province, Mazatzal province, and Caborca block (Whitmeyer and Karlstrom, 2007; Fig. 7).

CAB rocks generally have high $\delta^{18}O$ ratios (2–5 ‰ above mantle array values) as reflected in whole rock and single mineral (e.g., quartz, zircon) analyses (Table 1). The high $\delta^{18}O$ ratios have been interpreted to reflect crustal melting of metasedimentary rocks, rather than (meta) igneous rocks (Solomon and Taylor Jr, 1989; King et al., 2004; Gottlieb, 2017). In the northern and central CAB, upper Proterozoic metasedimentary rocks are present as part of the Cordilleran passive margin sequence (Cordilleran Miogeocline) and are often cited as a possible protolith (e.g., Neoproterozoic McCoy Creek Group, Ruby-East Humboldt complex; Lee et al., 2003). Metasedimentary members of the

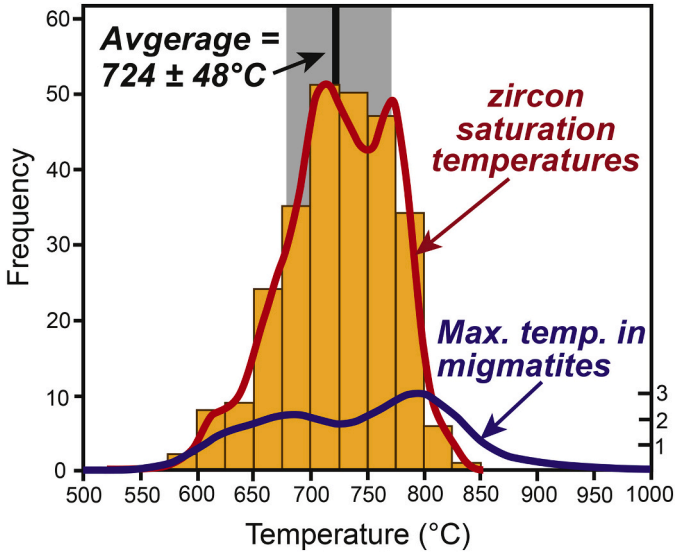

Fig. 8. A histogram and kernel density estimate (red curve) of zircon saturation temperatures (Watson and Harrison, 1983) for rocks in the Cordilleran Anatectic Belt (CAB). The uncertainty of the average is based on the standard deviation (1σ). Data and data sources are presented in Supplementary File 2. A kernel density estimate (blue curve) shows the maximum (peak) temperatures in migmatite within the CAB as reported by previous studies (Table 1). (For interpretation of the references to color in this figure legend, the reader is referred to the web version of this article.)

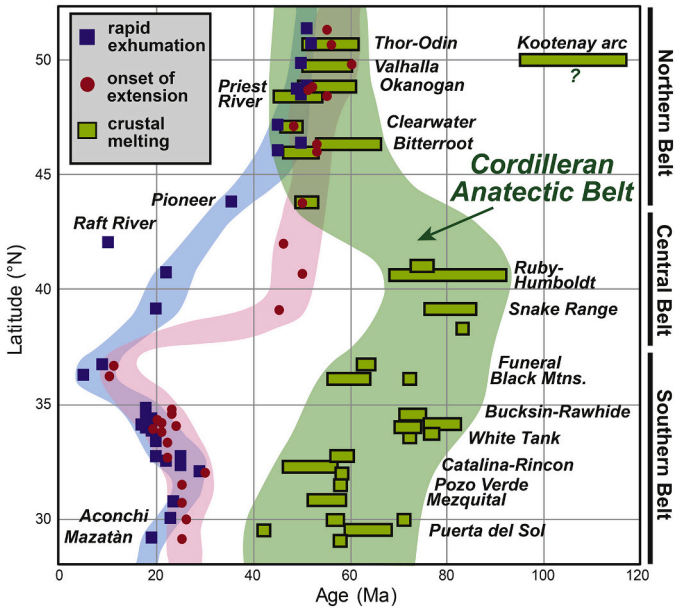

Fig. 9. A plot of age vs. latitude for crystallization ages of rocks in the Cordilleran Anatectic Belt (CAB; green rectangles), rapid exhumation/cooling ages for the Cordilleran metamorphic core complexes (blue squares), and timing for the onset of extension in the core complexes (red circles) (Table 1). Most major core complexes are labelled for reference. Data and data sources are presented in Supplementary Files 1 and 2. (For interpretation of the references to color in this figure legend, the reader is referred to the web version of this article.)

Mesoproterozoic Belt-Purcell Supergroup and the overlying Neoproterozoic Windermere Supergroup have also been suggested as potential protoliths in the northern CAB (e.g., Shuswap complex; Norlander et al., 2002). The southern CAB does not contain metasedimentary rocks associated with the Mesoproterozoic basins or Neoproterozoic metasedimentary rocks associated the Cordilleran passive margin sequence (Stewart et al., 1984) (Fig. 7). Paleoproterozoic metasedimentary rocks in the Pinal Basin in southern Arizona and northern Sonora (Meijer, 2014; Bickford et al., 2019) have been proposed as a potential source for the southern CAB (e.g., Pinal Schist; Haxel et al., 1984). Proterozoic (meta)igneous rocks and Jurassic arc rocks in the southern CAB have also been mentioned as possible protoliths (Miller and Wooden, 1994; Fornash et al., 2013; Mallery et al., 2018).

5.2. Melt temperature estimates

Zircon saturation temperatures were calculated using the calibration of Watson and Harrison (1983) for CAB rocks that meet the compositional criteria for this thermometer (Table 1). The dataset indicates an average temperature of 724 ± 48 °C (1σ) (Fig. 8). The calibration of Watson and Harrison (1983) results in higher calculated zircon saturation temperatures than other recently revised calibrations (Boehnke et al., 2013; Gervasoni et al., 2016; Borisov and Aranovich, 2019) and can be considered a maximum estimate. For intrusive rocks, zircon saturation temperature has been used as a proxy for the temperature of partial melting or magma temperature (e.g., Collins et al., 2016). Zircon saturation temperature is a dynamic variable that predicts when zircon saturation begins in a cooling magma and increases during crystallization (Clemens et al., 2020). Siégel et al. (2018) suggest that magma temperature and zircon saturation temperature are only approximately equal when SiO_2 contents increase to a certain value, which was determined to be 64–74 wt. % based on a limited dataset. For higher SiO_2 values, calculated zircon saturation temperatures may overestimate the magma temperature. Because CAB rocks have $SiO_2 > 70$ wt. %, we interpret the calculated zircon saturation temperatures to be close to or a slight overestimate of the partial melting temperature. In addition, almost all zircon U-Pb analyses of CAB rocks report inherited (antecrystic or xenocrystic) zircon components (Applegate et al., 1992; Wright and Snoke, 1993; Vanderhaeghe et al., 1999; Vogl et al., 2012; Gaschnig et al., 2013; Stevens et al., 2016; Davis et al., 2019). Intrusions with abundant inherited zircon indicate saturation at the source and suggest that calculated zircon saturation temperatures are a maximum since part of the bulk Zr concentration is from inherited crystals rather than the melt (Miller et al., 2003; Barth and Wooden, 2006). Our compilation of CAB rocks also contains some analyses of late-stage, highly fractionated melts (chiefly aplite and pegmatite dikes). Zircon saturation temperatures of these rocks can be interpreted as minimum estimates of magma temperature at the time of melt segregation (Miller et al., 2003).

Peak metamorphic temperature estimates from migmatite in the central and northern CAB are plotted in Figure 8 and show a broad maxima from 650–825 °C that overlaps with the average CAB zircon saturation temperature. For individual localities, zircon saturation temperatures are consistently 50–100 °C lower than estimates of peak metamorphic temperatures obtained using equilibria thermobarometry or pseudosection analysis (Table 1). Kohn (2014) made a similar observation in his review of the Himalayan leucogranite belt.

5.3. Age relationships

A compilation of crystallization or emplacement ages of rocks in the CAB are presented in Figure 9 and Table 1. Ages range from 92 to 42 Ma, with the majority of ages between 80 and 50 Ma. Ages are youngest in the northern and southern CAB and oldest in the central CAB. The age pattern suggests that anatectic magmatism started in the central U.S. Cordillera and simultaneously migrated (or "swept") northward and southward with crustal melting shutting down in its wake. Many locations in the CAB only have a few dated samples, but where sufficient geochronologic data are available, the duration of anatexis is typically protracted, lasting 10 Myr or more. Examples of well-studied locations

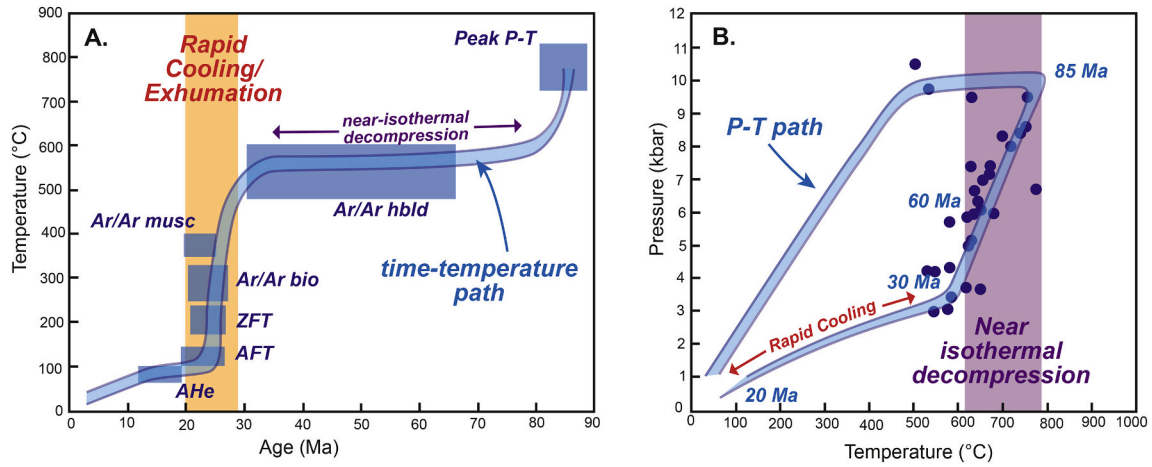

Fig. 10. A) Time-temperature and B) pressure-temperature (P-T) diagrams for the Ruby-East Humboldt metamorphic core complex (modified from Henry et al., 2011) used to illustrate periods of rapid cooling and near-isothermal decompression in the Cordilleran core complexes in general. Rapid cooling is chiefly identified using thermochronology (AHe = apatite U-Th/He, AFT = apatite fission track, ZFT = zircon fission track) whereas periods of near-isothermal decompression are not well-resolved or recorded at all by thermochronometers and may have occurred up to several 10s of Myr prior to rapid exhumation.

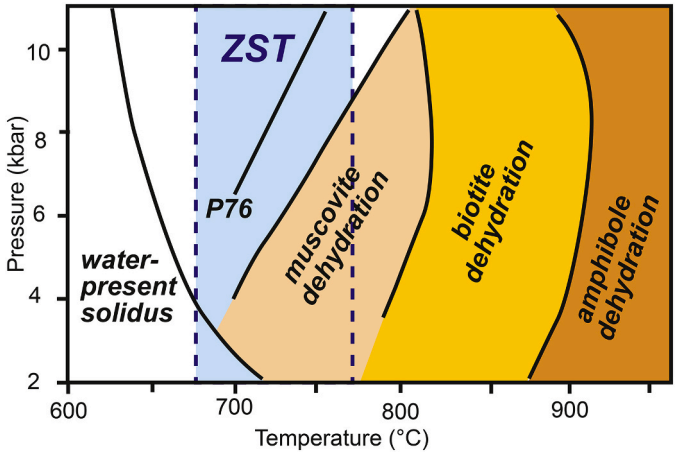

Fig. 11. Melt reactions for metasedimentary protoliths showing solidus curves for water-present melting (Stevens and Clemens, 1993), muscovite dehydration melting (Patiño-Douce and Harris, 1998; P76 = Peto, 1976), biotite dehydration melting (Vielzeuf and Montel, 1994), and amphibole dehydration melting (Wyllie and Wolf, 1993). The range of calculated zircon saturation temperatures (ZST) from the Cordilleran Anatectic Belt is shown in blue and presented in Fig. 8.

with a wide range of ages include the Shuswap complex (60–50 Ma; Vanderhaeghe et al., 1999; Hinchey et al., 2006; Gordon et al., 2008; Kruckenberg et al., 2008), the Ruby-East Humboldt complex (70–40 Ma; Howard et al., 2011), and the Catalina-Rincon complex (65–45 Ma; Fornash et al., 2013; Davis et al., 2019). Similar observations have been made in the Himalayan leucogranite belt with anatectic magmatism lasting ~10 Myr in any single location (Lederer et al., 2013; Weinberg, 2016). The reasons for protracted anatexis in the CAB are unclear but may be related to fluid and/or magma pulses, magma mixing and age hybridization, slow fractionation and cooling, evolving metamorphic and thermal conditions, or combinations of these. Despite the uncertainty, prolonged remobilization and reworking of melts appears to have been a common feature of CAB intrusive rocks. Protracted periods of crustal melting imply that either the source region was not completely melted (fusible components remain to be melted later) or that conditions changed throughout the melt process (e.g., increasing temperature) so that melting could proceed. Apart from the Kootenay arc (Brandon and Lambert, 1993, 1994; Brandon and Smith, 1994) (e.g., White Creek batholith; Figs. 3 and 6), there is no geochemical evidence that more refractory minerals or restitic components were melted during later stages of crustal melting in the CAB.

Figure 9 also shows the timing for the onset of extension and the period of most rapid cooling for the Cordilleran metamorphic core complexes (see Supplementary File 1 for the data compilation). The period of most rapid cooling is generally constrained by thermochronological data and represented by the steepest segment of time-temperature cooling histories (Fig. 10). The onset of extension is constrained by thermochronological data as well as by other geologic data (e.g., timing of normal faulting, extensional basins, P-T-t modelling, etc.). The period of rapid cooling/exhumation occured shortly after ($\leq$ 5 Myr) the onset of extension for most core complexes, except for the central belt of core complexes where it may have been delayed by up to ca. 30 Myr (Fig. 9). Extension and exhumation in these areas is thought to have occurred in two or more stages (Miller et al., 1999; Henry et al., 2011; Konstantinou et al., 2012). The younger stage is generally associated with extensional tectonics, whereas the older stage of extension has been related to gravitational collapse of tectonically thickened crust and/or heating, magmatism, and uplift accompanying delamination/roll-back of the Farallon slab (McGrew and Snee, 1994; Humphreys, 1995; Constenius, 1996; Dickinson et al., 2009; Konstantinou et al., 2013; Cassel et al., 2018). The timing of core complex extension and the age of CAB magmatism overlap in the northern CAB, however, extension/exhumation is up to 50 Myr younger than crustal melting in the central and southern CAB.

6. Melting conditions and processes

The following section explores melting conditions, processes, and sources using compiled geochemical compositions of the CAB rocks (Supplementary File 2). One of the fundamental questions we seek to address is the role of water in the production of the CAB. We refer to water regardless of its state (vapor or liquid) and use water as a more general term for mixed-fluid solutions (e.g., containing CO_2). We distinguish three types of partial melting based on the amount of available water; water-absent melting, water-excess melting, and water-deficient melting (cf., Clemens et al., 2020).

We use the term water-absent melting synonymously with dehydration melting to describe conditions in which the water present is entirely structurally bound in hydrous minerals, chiefly mica and amphibole. Water released from these minerals during dehydration melting is dissolved into the melt, which is water-undersaturated.

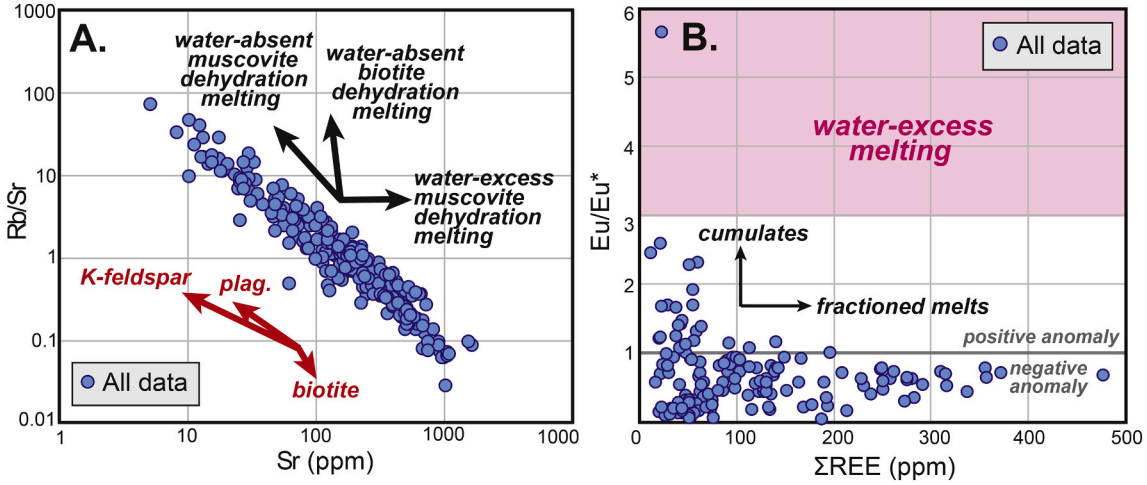

Fig. 12. A) Cordilleran Anatectic Belt (CAB) rocks (blue circles) plot along Rb/Sr vs. Sr trends consistent with water-absent muscovite dehydration melting and fractional crystallization of plagioclase. Black arrows show trends produced by melting experiments and red arrows show trends expected from crystallization of the phase listed (modified from Inger and Harris, 1993). B) Strongly positive (> 3) Eu anomalies were suggested by Prince et al. (2001) to distinguish water-excess melting. Feldspar-rich cumulate rocks may also have positive Eu anomalies, but can be recognized by their low total REE (Rudnick, 1992). Data and data sources are presented in Supplementary File 2. (For interpretation of the references to color in this figure legend, the reader is referred to the web version of this article.)

Water-absent melting is buffered by the amount and type of hydrous minerals. Muscovite dehydration melting occurs at the lowest temperatures (ca. 700 °C at 5 kbar), followed by biotite dehydration melting (ca. 800 °C at 5 kbar) and then amphibole dehydration melting (ca. 900 °C at 5 kbar) (Patiño-Douce and Harris, 1998) (Fig. 11). Amphibole dehydration melting is relatively uncommon in orogenic anatectic terranes because of the high temperatures (>850 °C) required (Thompson and Connolly, 1995). For metapelitic rocks, muscovite dehydration melting reactions (Reaction 1; Peto, 1976) produce K-feldspar and sillimanite (or kyanite) as peritectic products and biotite dehydration melting reactions (Reaction 2; Le Breton and Thompson, 1988) produce peritectic K-feldspar and cordierite (or garnet at high-pressure).

$$Ms + Pl + Qtz = Kfs + Als + Melt \quad (1)$$

$$Bt + Als + Pl + Qtz = Kfs + Crd/Grt + Melt \quad (2)$$

Water-excess melting describes melting in water-saturated conditions where water remains present in the protolith above the (wet) solidus and the melt is water-saturated. Most experimental studies with added water are water-excess experiments and for most studies water-excess, water-flux, and fluid-flux melting are synonymous (e.g., Patiño-Douce, 1996). Water-excess melting requires an external source of water to sustain melting and is buffered by the amount of available water. Water-excess melting of metasedimentary protoliths, including muscovite- and/or biotite-bearing schist (Reactions 3–5; Yardley and Barber, 1991; Patiño-Douce and Harris, 1998; Vielzeuf and Schmidt, 2001) and metagreywacke (Reaction 6; Genier et al., 2008) occurs at relatively low temperatures (ca. 650 °C at 5 kbar) and may or may not produce an aluminosilicate (including garnet) peritectic phase.

$$Ms + Pl + Qtz + H_2O = Melt \quad (3)$$

$$Bt + Als + Kfs + Qtz + H_2O = Crd/Grt + Melt \quad (4)$$

$$Ms + Bt + Kfs + Pl + Qtz + H_2O = Melt \quad (5)$$

$$Qtz + Kfs + Pl + H_2O = Melt \quad (6)$$

Water-deficient melting describes an intermediate condition (between water-absent and water-excess melting) where a free water phase is present (e.g., pore-space fluid), but limited. In this case, the protolith is water-undersaturated and excess water is consumed at or just above the wet solidus. Melting continues along a dehydration path after the excess water is exhausted. Water-deficient melting is generally rock-buffered and produces water-undersaturated melts ($aH_2O<1$) above the wet solidus (Nabelek, 2019). Water-absent and water-excess melting are end-members and can be distinguished geochemically (see review in Weinberg and Hasalová, 2015), however, water-deficient melting is considered geochemically indistinguishable from dehydration melting and is generally only inferred based on melt volumes and temperature (Schwindinger and Weinberg, 2017; Schwindinger et al., 2019).

6.1. *Water-absent melting vs. water-excess melting*

In this section, we use CAB geochemistry to evaluate the roles of water-absent and water-excess melting in generating these rocks. Although there are various hypotheses concerning the tectonic mechanisms involved (see discussion in Section 7 below), the large majority of anatectic rocks in the CAB have been previously interpreted to have formed by dehydration melting (Coney and Harms, 1984; Haxel et al., 1984; Armstrong, 1988; Miller and Gans, 1989; Barton, 1990; Patiño-Douce et al., 1990; Wright and Wooden, 1991; Brandon and Lambert, 1993; Mahood et al., 1996; Vanderhaeghe et al., 1999; Foster et al., 2001; Norlander et al., 2002; Teyssier and Whitney, 2002; Lee et al., 2003; Hinchey et al., 2006; Mattinson et al., 2007; Gaschnig et al., 2011; Stevens et al., 2015). An exception is the Big Maria Mountains, California that contain field and petrographic evidence for widespread fluid infiltration during Late Cretaceous metamorphism (Hoisch, 1987). The metamorphic rocks in the Big Maria Mountains are not migmatitic but are intruded by numerous pegmatitic leucogranite dikes that have been interpreted to result from water-excess/fluid-flux melting (Hamilton, 1987; Hoisch, 1987). The fluid source in the Big Maria Mountains could be metamorphic reactions within the crust, crystallizing magmas at depth (Hoisch, 1987), or the dehydrating Farallon slab (Wells and Hoisch, 2008).

Micas have high Rb and low Sr concentrations, whereas plagioclase has the opposite – low Rb and high Sr concentrations. Water-absent melting, involving the breakdown of muscovite and biotite, enriches the melt in Rb. Restitic feldspar increases during muscovite dehydration melting, depleting the melt in Sr, but does not increase during (relatively higher temperature) biotite dehydration melting, causing little change in Sr concentrations in the melt (Harris and Inger, 1992). As a result, mica dehydration melting is often associated with geochemical trends showing increasing Rb/Sr and decreasing Sr (muscovite dehydration) or near constant Sr (biotite dehydration) concentrations (Inger and Harris,

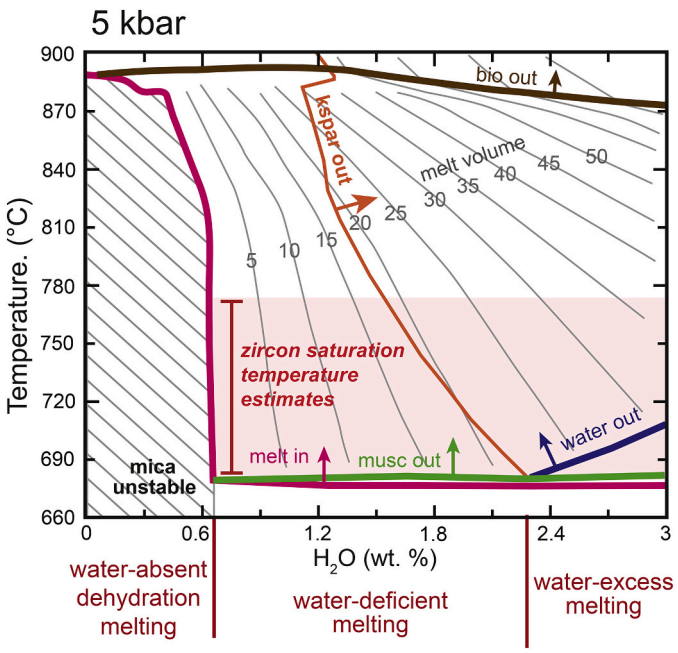

Fig. 13. An isobaric (5 kbar) temperature-X_{H2O} assemblage diagram for a quartz- and muscovite-rich metasedimentary rock from the Pinal Schist that illustrates differences between water-absent, water-deficient, and water-excess melting. Constructed using Perple_X (Connolly, 2005). See text for modeling details. Average zircon saturation temperatures calculated for the Cordilleran Anatectic Belt are shaded red (Fig. 8).

1993). Conversely, water-excess melting breaks down plagioclase before mica, resulting in increased Sr in the melt and low Rb/Sr that remains relatively constant during melt evolution (Conrad et al., 1988; Harris and Inger, 1992; Inger and Harris, 1993). There is no absolute value of Rb/Sr that can be used to discriminate water-absent melting from water-excess melting, but Harris et al. (1993) suggested that water-excess melting was unlikely for granite with Rb/Sr >3.5 for most metasedimentary protoliths. Figure 12A shows that the rocks of the CAB have a wide range of Rb/Sr values (4 orders of magnitude) and follow Rb/Sr geochemical trends consistent with muscovite dehydration melting. However, this trend is also consistent with fractional crystallization of feldspar (particularly plagioclase) and could be produced by strongly differentiated rocks with high Rb/Sr and cumulates with low Rb/Sr.

Melting of feldspar during water-excess melting has also been linked to positive Eu anomalies. Prince et al. (2001) used strongly positive (> 3) Eu anomalies in Eocene Himalayan leucogranites to identify water-excess melting. Negative Eu anomalies are generally produced by fractional crystallization of feldspar and positive Eu anomalies may record a complementary feldspar-rich cumulate (Sawyer, 1987; Rudnick, 1992). Cumulates may also be recognized by low total REE, which increases for more strongly fractionated melts. Fig. 12B plots Eu anomaly vs. total REE for CAB rocks and shows that rocks with weak positive Eu anomalies (1–3) also have low total REE and are probably cumulates. Removal of trivalent REE during crystallization of accessory phases can also produce low total REE and positive Eu anomalies (Bea and Montero, 1999). Few CAB rocks have strong positive Eu anomalies associated with water-excess melting or other processes (Fig. 12B).

Potassium concentration relative to Na and Ca (or normative orthoclase relative to albite and anorthite) in melts produced from crustal anatexis is another method used to qualitatively assess the role of water-excess melting. The melting of plagioclase prior to mica, particularly biotite, during water-excess melting results in melts with tonalite to trondhjemite compositions (Conrad et al., 1988; Scaillet et al., 1995; Patiño-Douce, 1996). Conversely, the preferential melting of mica prior to plagioclase during water-absent melting results in more potassic compositions and rocks with significant modal K-feldspar. With few exceptions, CAB intrusive rocks have normative Ab/Or (albite/orthoclase) ratios < 2 and do not have the tonalite or trondhjemite compositions produced experimentally by water-excess melting of metasedimentary protoliths (Patiño-Douce and Beard, 1996; Patiño-Douce, 1996; Patiño-Douce and Harris, 1998) (Fig. 5). Studies have also proposed that ferromagnesian contents increase during water-excess melting (e.g., FeO_{total} > 2 wt. %; Weinberg and Hasalová, 2015), but are sequestered by refractory residual mineral phases during water-absent melting of metasedimentary protoliths (Naney, 1983; Holtz and Johannes, 1991; Patiño-Douce, 1996). The majority of CAB rocks have low total FeO (< 2 wt. %), consistent with water-absent melting.

The geochemistry and magma temperature estimates (Fig. 8) for the CAB are most consistent with muscovite dehydration (water-absent) melting at middle to lower crustal pressures (≥ 5 kbar) (Fig. 11) and the composition of the CAB rocks compare favorably to experimental studies of muscovite dehydration melting (e.g., Patiño-Douce, 1999). Textural heterogeneity and numerous pegmatite and aplite dikes/sills associated with the CAB indicate exsolution of water throughout the crystallization processes from relatively hydrous melts. These observations further support muscovite dehydration melting over biotite dehydration melting. Biotite dehydration melting at higher temperature requires less water to stabilize the melt and produces relatively dry melts that are more texturally homogenous (Clemens and Vielzeuf, 1987; Villaros et al., 2018; Nabelek, 2019). Muscovite dehydration melting of metasedimentary protoliths at 750 °C and 5 kbar results in ca. 6 wt. % H_2O in the melt compared to ca. 2 wt. % H_2O at 850 °C for biotite breakdown at the same pressure (Patiño-Douce and Beard, 1995; Patiño-Douce and Harris, 1998; Castro, 2013).

6.2. *Water-deficient melting*

There are two main problems with invoking water-absent, muscovite dehydration melting as the dominant processes to produce the CAB rocks. Both problems can potentially be resolved if water-deficient melting is involved. The first problem is that muscovite dehydration melting may not produce enough melt volume to initiate melt migration and accumulation (Clemens and Vielzeuf, 1987; Barton, 1990; Patiño-Douce et al., 1990; Wells and Hoisch, 2008). Melt extraction is thought to be limited by a melt-connectivity threshold (~7 % melt), at which point melt/solid segregation can occur if the solid residue is able to deform and/or compact (Rosenberg and Handy, 2005; Vanderhaeghe, 2009). Under inefficient melt extraction conditions, a migmatite may accumulate large amounts of leucosome/melt (diatexite) until the solid-liquid threshold (20–40% melt) is reached and the migmatite starts to behave as a crystal mush (van der Molen and Paterson, 1979). A very muscovite-rich (20–30 %) schistose protolith could generate ca. 10 % melt during muscovite dehydration melting (Wyllie, 1977), but most metasedimentary compositions are estimated to produce <5 % melt by volume (Patiño-Douce et al., 1990; Johannes and Holtz, 1996; Droop and Brodie, 2012). Biotite dehydration melting of common metasedimentary protoliths can produce up to 40 % melt (Miller, 1985; Clemens and Vielzeuf, 1987; Patiño-Douce et al., 1990; Stevens et al., 1997), but the geochemical data and melting temperature estimates discussed above do not appear to support biotite dehydration melting.

Many locations in the CAB expose significant (approaching batholith-scale) volumes of muscovite-bearing peraluminous granite related to crustal melting that suggest relatively large melt fractions. For example, ~600 km^3 of CAB rocks are exposed in the Lamoille Canyon area in the Ruby-East Humboldt core complex and several times that amount is estimated to be present in the subsurface (Howard et al., 2011). Unless melt is being drained laterally from areas beyond the Ruby-East Humboldt Mountains, 5–10 % melting cannot produce the observed rock volumes. Water-deficient melting that incorporates small amounts of externally-derived water (~1 wt. % added) can result in large increases in melt fractions, 2–3 times larger than by dehydration

melting alone – resulting in a 10–20 % increase in melt volume (Sola et al., 2017; Nabelek, 2019; Schwindinger et al., 2019).

To illustrate this issue, we constructed an isobaric (5 kbar) temperature-X_{H2O} assemblage diagram for a muscovite-rich metasedimentary protolith (Fig. 13). The whole rock starting composition was modeled after a muscovite-bearing quartz wacke from the Pinal Schist in Arizona (sample "B" in Copeland and Condie, 1986). This composition is comparable to other muscovite-bearing metasedimentary rocks from the Neoproterozoic Cordilleran passive margin sequence (e.g., McCoy Creek Group in Nevada; Misch and Hazzard, 1962) and comparable to generic metasedimentary rocks compositions used in modeling partial melting of other anatectic provinces (cf., Nabelek, 2019), but is more quartz-rich than the most melt-fertile rocks (e.g., muscovite schist). Closed-system phase assemblages and melt volumes were calculated with Perple_X version 6.8.7. (Connolly, 1990, 2005; Connolly and Petrini, 2002) in the NCKMASHTO model system (Na_2O,CaO, K_2O, Al_2O_3, SiO_2, H_2O, TiO_2, O_2, FeO_t, and MgO), using a quartz-fayalite-magnetite assemblage for fO_2 buffering and thermodynamic data from Holland and Powell (2011). One way to read the assemblage diagram in Fig. 13 is to consider the average zircon saturation temperature estimate for the CAB and examine changes in melt content (shown as volume precent) as the amount of water in the protolith is increased (moving to the right along the x-axis). Muscovite dehydration melting occurs at ~0.7 wt. % H_2O, which is the amount of structurally bound water in mica in the protolith, not a free fluid phase. Water-absent muscovite dehydration melting produces < 5 % melt. Water-excess melting occurs above ~2.3 wt. % H_2O, at which point free water remains in the protolith above the solidus (pink line labeled "melt in") and > 20 % melt is produced. Water-deficient melting (ca. 0.7–2.3 wt. % H_2O) consumes all free water at the solidus and produces water-undersaturated melts but results in significant increases of melt volume. For example, 1 wt. % of free water in the protolith (1.7 wt. % H_2O in Fig. 13) increases melt volume from 1.2 % (water-absent, muscovite dehydration melting) to 16.9 % at 725 °C. Debate continues about whether any amount of free water is reasonable to expect in the middle to lower crust (Thompson, 1983; Weinberg and Hasalová, 2015).

The second problem with muscovite dehydration melting is that, despite relatively low FeO and MgO values in CAB rocks, biotite is very common, which requires partial melting of a phase more mafic than muscovite. Additional Fe and Mg can be added to the melt with added water (water-deficient or water-excess) melting (Holtz and Johannes, 1991; Patiño-Douce, 1996). Water-deficient melting is one possible mechanism to increase ferromagnesian components in CAB melts, although our modeling (Fig. 13) as well as other studies of water-deficient melting (Schwindinger et al., 2019) have indicated relatively small to insignificant increases in FeO and MgO (≤ 0.5 wt. %) from water-absent melting. Other processes such as restite/peritectic mineral entrainment have also been proposed to increase Fe and Mg in crustal melts (Stevens et al., 2007). The importance of water-deficient melting has only recently been emphasized globally (e.g., Nabelek, 2019) and it has not been previously considered for intrusive suites in the CAB, but it deserves future investigation.

7. Tectonic causes of crustal melting

There is no consensus on the underlying causes of Late Cretaceous to Paleogene crustal anatexis in the CAB, but hypotheses can be generally grouped into four categories: 1) decompression melting, 2) melting resulting from radiogenic heating and thermal relaxation following crustal thickening, 3) melting resulting from the introduction of slab-derived fluids, and 4) melting associated with increased heat flux from the mantle. These hypotheses are not all mutually exclusive and there is no requirement for a single process to explain the entire CAB. However, the CAB occupies a relatively narrow time interval and appears to be a coherent spatial feature, which supports treating it as a distinct component of the North American Cordilleran orogenic system, on par with other components such as the continental arc and retroarc thrust belt. Previous researchers have favored different hypotheses in the northern, central, and southern CAB, but it is instructive to consider how hypotheses favored in one region may be extended or extrapolated into other areas.

7.1. Decompression melting related to exhumation

There is a close spatial association between the CAB and the Cordilleran metamorphic core complexes (Fig. 1), suggesting a possible petrogenetic relationship as well (Armstrong, 1982). One possible scenario is that core complex extension and exhumation caused decompression melting. Decompression melting is a form of dehydration melting and is commonly invoked when melting and exhumation of the crust are contemporaneous (Harris and Massey, 1994). Decompression melting has received the most attention in the northern CAB, particular within the Shuswap complex, where anatectic crystallization ages, cooling ages, extension timing, and the timing of near-isothermal decompression in reconstructed P-T paths all overlap (Vanderhaeghe et al., 1999; Norlander et al., 2002; Teyssier and Whitney, 2002; Whitney et al., 2004b; Gordon et al., 2008; Stevens et al., 2016) (Fig. 9). The Shuswap complex is cored by several migmatitic gneiss domes that display structural fabrics and geometries supporting vertical motion within the domes and flattening above the domes – consistent with diapiric-like rise of the deep crust (e.g., Duncan, 1984; Whitney et al., 2004b). Relatively hot, ductile middle-to-lower crust is a prerequisite for diapirism although a variety of processes could trigger initial ascent, including a density inversion resulting from underthrusting of (meta) sedimentary rocks into the deep crust, low-degrees of partial melting causing density reduction, focused erosion at the surface, localized crustal thickening or buckling, and rapid tectonic denudation (Teyssier and Whitney, 2002). Estimates for diapir-related exhumation rates from migmatitc gneiss domes in the Shuswap complex are ca. 20 km/Myr, which is significantly faster than tectonic exhumation associated with extension (Whitney et al., 2004c; Whitney et al., 2013). Rapid decompression should produce a narrow range of ages, which is at odds with the wide range of ages (≥ 10 Myr) and the remobilization of melts prior to emplacement observed in some CAB localities. Furthermore, (re) melting events related to repeated or prolonged decompression are difficult to reconcile with dehydration melting as the protolith becomes increasingly refractory and requires increasingly high temperatures to make new melts. Regardless, once upward movement and decompression is initiated, there is a positive feedback between melting, viscosity reduction, and exhumation resulting in relatively large volumes (≥ 20%) of dehydration-related leucocratic melt (Whitney et al., 2004b; Rey et al., 2009), consistent with some locations in the northern CAB (e.g., Priest River complex, Stevens et al., 2015, 2016). The positive P-T slope of dehydration melting solidi suggests that melting can occur throughout the decompression process and that emplacement in the middle-to-upper crust is efficient.

Decompression melting is considered less likely in the central and southern CAB, in part because the timing of extension and exhumation is younger than crustal melting (Fig. 9). However, P-T paths from metamorphic rocks in many Cordilleran core complexes suggest that decompression is a near-isothermal process that would not be expected to be recorded by thermochronometers. For example, by some estimates, the Ruby-East Humboldt complex experienced ~4 kbar (~15 km) decompression at ca. 750–650 °C from ca. 85–55 Ma (McGrew et al., 2000; Henry et al., 2011) (Fig. 10), which largely overlaps with the crystallization ages of CAB rocks in the complex (Howard et al., 2011). How this period of decompression occurred is unclear because the complex exposes a series of stacked and folded nappes, rather than discrete gneiss domes or evidence for diapirism (Howard, 1980). Deep structural levels within the Ruby-East Humboldt complex show some evidence for lateral crustal flow (MacCready et al., 1997) and numerical models suggest that relatively slow extension rates may have kept the

complex from developing more defined migmatitic gneiss domes (Rey et al., 2009). Another possibility is that the recumbently folded nappes in the Ruby Mountains record flattening strain during Late Cretaceous to Eocene decompression and that they sit above an even deeper structural level (not exposed) that records vertical, diapir-like exhumation. Regardless, diapiric exhumation of the lower crust has not been seriously proposed to have generated anatectic melting in North America outside of the northern CAB.

There is also evidence for syn-convergent, Late Cretaceous extension (prior to core complex extensional faulting) in the central and southern CAB (Carl et al., 1991; Wells and Hoisch, 2008; Druschke et al., 2009; Wells et al., 2012; Long et al., 2015). In some cases, this extension has been proposed to have caused decompression melting. Examples include the Iron Mountains and Old Woman Mountains in southeast California (Wells and Hoisch, 2008) and the Death Valley region (Hodges and Walker, 1990; Applegate et al., 1992; Applegate and Hodges, 1995). However, the amount of Late Cretaceous extension documented in the U.S Cordillera is limited (Miller et al., 2012; Lund Snee et al., 2016) and it is uncertain whether there was enough extension to cause widespread decompression melting.

Relating anatectic melting to near-isothermal decompression in the central and northern CAB is possible because migmatite and metamorphic rocks are exposed, enabling P-T-t paths to be reconstructed and deep crustal strain to be evaluated. These types of rocks are generally not exposed in the southern CAB, specifically in Arizona and Sonora, and as a result, decompression melting has not been seriously proposed or evaluated in that region. However, one end-member interpretation is that intrusive rocks in the southern CAB signify a period of decompression in the deep crust that is otherwise inscrutable. As such, the northern core complexes and CAB may provide a template for understanding deep crustal process in the southern U.S. and northern Mexican Cordillera.

7.2. Radiogenic heat and thermal relaxation

Radiogenic heating and relaxation of isotherms following crustal thickening has also been proposed to account for CAB rocks (Haxel et al., 1984; Miller and Gans, 1989; Patiño-Douce et al., 1990; Wright and Wooden, 1991). The Laramide orogeny (ca. 80–40 Ma) overlaps in age with the CAB, however, Laramide deformation is chiefly characterized by slip on high-angle reverse faults that produced limited horizontal shortening and hence limited crustal thickening (Yonkee and Weil, 2015). In addition, thermal models suggest that maximum temperatures in the middle to lower crust are attained 40–60 Myr after (instantaneous) crustal thickening (England and Thompson, 1984, 1986; Clark et al., 2011), ruling out Laramide-age crustal thickening as a cause of crustal anatexis in the CAB. In contrast, the Sevier orogeny caused significant crustal thickening and the time elapsed between the end of shortening (ca. 100–80 Ma) and the onset of crustal melting in the CAB is ca. 10–50 Myr, consistent with the thermal models. These models implicitly assume that the crust, perhaps in the form of an orogenic plateau, remained thick after the end of crustal thickening. Anatexis resulting from crustal thickening was modelled explicitly for the North American Cordillera by Patiño-Douce et al. (1990) who suggested that a 10–15 km thick migmatite layer at 30–40 km depth would develop by the end of the Sevier orogeny if the crust was thickened to 50–55 km, consistent with estimates of crustal thickness for the Nevadaplano (Coney and Harms, 1984; Chapman et al., 2015). Modeling by both Patiño-Douce et al. (1990) and England and Thompson (1984, 1986) assumed that free water was not present in the melt source region and that relatively high temperatures ($>$ 850 °C) were required to produce biotite dehydration melting in order to generate the melt volumes (20–40%) observed. To generate these high temperatures, the models required mid-crustal layers with moderately high radiogenic heat production ($>$2 μW/m^3). The high temperatures required for biotite-dehydration melting are one of the main arguments against crustal thickening as a primary mechanism to generate the CAB rocks (e.g., Wells and Hoisch, 2008, 2012; Wells et al., 2012). If water-excess or water-deficient melting are important processes in the origin of the CAB, then melting at lower temperatures and the production of large melt volumes is less problematic for hypotheses relating anatexis to crustal thickening (Fig. 13).

Much of the southern CAB is located southeast of the deformational limit of the Sevier thrust belt (Fig. 1) and southeast of the Maria contractional belt in western Arizona and southeast California (Spencer and Reynolds, 1990; Boettcher et al., 2002). This region (southern Arizona and Sonora) experienced limited shortening during the Laramide orogeny, but the amount of documented shortening (ca. 30 km; Davis, 1979; Haxel et al., 1984) is not enough to significantly thicken the crust. Nonetheless, geochemical data suggest that the crust in southern Arizona and northern Sonora was relatively thick (55–60 km) during Late Cretaceous to early Paleogene time (Chapman et al., 2020), which may be related to magmatic thickening (Erdman et al., 2016). If the southern CAB is related to crustal thickening and radiogenic heating, then the age of the intrusive rocks could be interpreted as the age of peak metamorphism in the deep crust, which is otherwise unconstrained.

Total horizontal shortening in the Sevier thrust belt is greatest (~350 km) in the central U.S. Cordillera (DeCelles and Coogan, 2006) and decreases to the north (e.g., Fuentes et al., 2012) and to the south (e.g., Giallorenzo et al., 2018). This fact may help explain why the central CAB is older than the northern and southern CAB – because the crust was thickened more and/or faster and reached peak metamorphic conditions earlier. The wide range of ages and evidence for melt remobilization in the CAB (e.g., Catalina-Rincon complex, Davis et al., 2019; Ducea et al., 2020) is consistent with melts formed during prograde metamorphism that remained at high temperature and pressure, existing at near-solidus or partially-molten conditions until melt extraction or exhumation.

7.3. Water present melting

Melting involving free water in the parent rock has not received much attention as a significant cause for anatexis in the CAB. As mentioned in Section 6, Hoisch (1987) suggested that fluids exsolved from crystallizing magmas at depth resulted in water-flux melting in the Big Maria Mountains, California and hypothesized that crustal melting in the nearby Old Woman Mountains, California may be analogous. Wells and Hoisch (2008) proposed that delamination and mantle upwelling was a primary cause of crustal melting throughout the CAB (see next section), but they also suggested that dehydration of the Farallon slab could have played a role. The timing of low-angle subduction of the Farallon slab beneath the CAB matches closely with the age of CAB intrusive rocks. Many studies have suggested that the mantle lithosphere was hydrated during the Laramide orogeny (Dumitru et al., 1991; Humphreys et al., 2003; Farmer et al., 2008) and several studies in the last decade have suggested that the lower crust was hydrated as well (Jones et al., 2015; Butcher et al., 2017; Porter et al., 2017; Levandowski et al., 2018). Other potential sources of free water include metamorphic reactions within the crust (e.g., underthrusting of crustal lithologies) and small amounts of relict water in pore spaces.

The geochemistry of the CAB rocks does not support water-excess melting (Fig. 12), but it is consistent with water-deficient melting, which is difficult to distinguish from water-absent melting by geochemistry alone. The relatively low calculated zircon saturation temperatures for the CAB may even require some degree of water-added melting because some temperature estimates are below the solidus for muscovite dehydration melting (Fig. 11). Melts produced by water-absent and water-deficient melting are both water-undersaturated and are more likely to ascend through the crust to form intrusive bodies. Periodic fluid influx could also explain the wide range of crystallization ages at individual CAB locations.

7.4. Mantle heat flux

The two main hypotheses proposed for CAB rocks that involve increased mantle heat flow are 1) asthenospheric upwelling following delamination and 2) mantle upwelling above a subducting slab. The delamination hypothesis suggests that upwelling following delamination of the mantle lithosphere resulted in decompression melting of the asthenosphere and basaltic underplating/intrusion that provided additional heat to melt the overlying crust (Wells and Hoisch, 2008, 2012; Wells et al., 2012). Delamination is common in areas of thickened crust (e.g., England and Houseman, 1989), consistent with the position of the CAB and reconstructions of the orogenic interior and the Nevadaplano (Coney and Harms, 1984; DeCelles, 2004). The delamination model has been applied specifically in the Great Basin and Mojave regions where melting is generally Late Cretaceous in age (Wells and Hoisch, 2008). The model could be extended to the northern and southern CAB, where melting is generally early to middle Paleogene in age, if delamination migrated spatially through time or if there were separate delamination events. However, geophysical studies suggest that many parts of the northern and southern CAB have intact, ancient, cratonic (or peri-cratonic) mantle lithosphere preserved, which suggests delamination has not occurred (e.g., Li et al., 2007).

The subduction hypothesis suggests that the upwelling arm of corner flow (also called counterflow or induced mantle flow) in the mantle wedge above a subducting slab may steadily heat up the base of the lithosphere and could eventually cause crustal melting (Armstrong, 1982; Farmer and DePaolo, 1983; Barton, 1990). A variation of this model was proposed for the Death Valley region and suggests that asthenospheric upwelling above steepened portions of the Farallon slab may have caused crustal melting (Lima et al., 2018). Some studies have suggested that thermal convection or other processes in (non-extending) back-arc regions may produce temperatures high-enough to cause crustal melting (Currie and Hyndman, 2006; Wolfram et al., 2019). But most studies indicate that corner-flow and normal subduction processes (including changes in slab dip) do not provide enough heat to cause (water-absent) crustal melting in the upper plate, particularly during periods of low-angle to flat-slab subduction when the upper mantle and lithosphere are cooled by the slab (English et al., 2003; Liu and Currie, 2016). The timing and progression direction of Farallon slab roll-back in the U.S. Cordillera is also at odds with the timing and progression direction of the CAB. Flare-up magmatism related to slab roll-back is oldest in the northern and southern U.S. Cordillera and youngest in the central U.S. Cordillera (Humphreys, 1995), whereas the CAB is oldest in the central U.S. Cordillera and becomes younger to the north and south (Fig. 9). Nonetheless, individual parts of the CAB coincide with the timing of Farallon slab roll-back and have been interpreted to be related to mantle upwelling or mantle-derived magmatic intrusion (e.g., Konstantinou and Miller, 2015).

Both the delamination and subduction hypotheses suggest that mantle processes are required to produce temperatures high enough (> 800 °C) to cause biotite dehydration melting to explain the large volumes of CAB rocks (Wells and Hoisch, 2012; Barton, 1990). This is not supported by the zircon saturation temperatures (Fig. 8), assuming that those temperatures are representative of partial melting temperatures (see Section 5.2). The rarity of mantle-derived magmatic products in CAB locations is another argument against a significant role for the mantle in the formation of the CAB (e.g., Wright and Wooden, 1991).

8. Conclusions

The North American Cordilleran Anatectic Belt (CAB) is a chain of Late Cretaceous to Eocene intrusive rocks and anatectic rocks produced by crustal melting that is exposed from southern British Columbia, Canada to northern Sonora, Mexico in the interior, or hinterland, of the North American Cordilleran orogenic system. The duration of melting at any given location was often protracted, lasting ~10 Myr, and characterized by repeated melt remobilization and reworking. The CAB rocks are generally leucocratic (SiO_2 > 70 wt. %), peraluminous (ASI > 1.0), contain igneous muscovite ± garnet, have evolved radiogenic isotopic compositions ($^{87}Sr/^{86}Sr_i$ > 0.706), and have elevated (crustal-like) $\delta^{18}O$. The CAB was chiefly produced by partial melting of metasedimentary rocks (e.g., schist, greywacke) and has no little or no mantle-derived component, including partial melting of basalt/amphibolite. Geochemically, the CAB rocks are consistent with muscovite dehydration melting and/or water-deficient melting, but not water-excess melting. Zircon saturation temperatures for the CAB cluster between 600–800 °C with an average of 724 ± 48 °C, which is too low for biotite or amphibole dehydration melting. CAB rocks were primarily emplaced as sills, dikes, laccoliths, or large sheeted complexes and lack extrusive equivalents. Late aplite and pegmatite dikes are common and suggest relatively hydrous melts, which is also consistent with muscovite dehydration melting or water-added melting. A small amount of free water during melting may be required by the relatively large melt volumes within the CAB, supporting water-deficient conditions. The source of this free water is unknown, but may have been in relict pore fluids, exsolved from magmas, produced by metamorphic reactions, or liberated by dehydration of the Farallon slab. Crystallization ages of rocks in the CAB overlap with the timing of the Laramide orogeny and many of these rocks were emplaced during a period of low-angle to flat-slab subduction when the Farallon slab was located beneath the CAB.

There is a close spatial correlation between the CAB and the belt of Cordilleran metamorphic core complexes, and a large majority of the rocks in the CAB are found in the footwalls of core complexes. Only in a few locations, however, have CAB intrusive rocks been demonstrated to have originated from melting of the rocks (i.e., migmatite) exposed at the surface in the core complexes. An unanswered question in the CAB is whether the prevalence of crustal melting in core complexes is related to the core complexes themselves or is an artifact of core complexes exposing middle to lower crust, where the CAB magmas appear to have been commonly emplaced. In the northern CAB, the timing for core complex extension/exhumation and anatexis overlap, supporting a shared origin between the two and emphasizing the role of decompression melting. This overlap in ages is not observed in the central and southern CAB where core complex extension/exhumation is up to 50 Myr younger than crustal melting, suggesting that mechanisms other than decompression melting are required there.

The CAB formed in a region of previously thickened crust, interpreted as an orogenic plateau. Radiogenic heating and relaxation of isotherms following crustal thickening during the Sevier orogeny may explain crustal melting, particularly in the central CAB where horizontal shortening in the retroarc thrust belt is the greatest. Horizontal shortening during the Laramide orogeny was not large enough to significantly thicken the crust structurally. In addition, the oldest rocks in the CAB occur in the central CAB and are younger to the north and to the south. Melting associated with crustal thickening may not be applicable to the southern CAB because the Sevier thrust belt did not extend that far south and crustal shortening was limited.

A prominent role of delamination, mantle upwelling, or other mechanisms that increase mantle heat flux in producing the CAB is difficult to assess but appears unlikely. Most locations in the CAB do not contain mantle-derived, co-genetic igneous rocks and those that do have been interpreted to reflect processes other than crustal anatexis. Arguments that a component of elevated mantle heat flow is required to produce temperatures high enough to initiate biotite dehydration melting to account for large melt volumes are not supported by thermometry or geochemistry, and estimated melt volumes can best be reconciled with water-deficient melting.

Declaration of Competing Interest

The authors declare that they have no known competing financial interests or personal relationships that could have appeared to influence

the work reported in this paper.

Acknowledgements

Chapman acknowledges support from U.S. National Science Foundation grant EAR-1928312. Comments from three anonymous reviewers helped improved the manuscript.

Appendix A. Supplementary data

Supplementary data to this article can be found online at https://doi.org/10.1016/j.earscirev.2021.103576.

References

Anderson, J.L., Cullers, R.L., 1990. Middle to upper crustal plutonic construction of a magmatic arc; An example from the Whipple Mountains metamorphic core complex. In: Anderson, J.L. (Ed.), The Nature and Origin of Cordilleran Magmatism: Geological Society of America Memoir, 174, pp. 47–69.
Anderson, J.L., Barth, A.P., Young, E.D., 1988. Mid-crustal Cretaceous roots of Cordilleran metamorphic core complexes. Geology 16, 366–369.
Anderson, T.H., Silver, L.T., Salas, G.A., 1980. Distribution and U-Pb isotope ages of some lineated plutons, northwestern Mexico. In: Crittenden, M.D., Coney, P.J., Davis, G.H. (Eds.), Cordilleran Metamorphic Core Complexes, Geological Society of America Memoir, 153, pp. 269–283.
Annen, C., Blundy, J.D., Sparks, R.S.J., 2006. The genesis of intermediate and silicic magmas in deep crustal hot zones. J. Petrol. 47, 505–539.
Applegate, J.D.R., Hodges, K.V., 1995. Mesozoic and Cenozoic extension recorded by metamorphic rocks in the Funeral Mountains, California. Geol. Soc. Am. Bull. 107, 1063–1076.
Applegate, J.D.R., Walker, J.D., Hodges, K.V., 1992. Late Cretaceous extensional unroofing in the Funeral Mountains metamorphic core complex, California. Geology 20, 519–522.
Armstrong, R.L., 1982. Cordilleran metamorphic core complexes-From Arizona to southern Canada. Annu. Rev. Earth Planet. Sci. 10, 129–154.
Armstrong, R.L., 1988. Mesozoic and early Cenozoic magmatic evolution of the Canadian Cordillera. In: Clark, S.P., Burchfiel, B.C., Suppe, J. (Eds.), Processes in continental lithospheric deformation: Geological Society of America Special Paper, 218, pp. 55–91.
Armstrong, R.L., Ward, P., 1991. Evolving geographic patterns of Cenozoic magmatism in the North American Cordillera: The temporal and spatial association of magmatism and metamorphic core complexes. J. Geophys. Res. Solid Earth 96, 13201–13224.
Arnold, A.H., 1986. Geologic Implications of a Geochemical Study of Three Two-Mica Granites in Southern Arizona. University of Arizona. MS thesis.
Asmerom, Y., Ikramuddin, M., Kinart, K., 1988. Geochemistry of Late Cretaceous granitoids from northeastern, Washington: Implication for genesis of two-mica, Cordilleran granites. Geology 16, 431–435.
Banks, N.G., 1980. Geology of a zone of metamorphic core complexes in southeastern Arizona. In: Crittenden Jr., M.D., Coney, P.J., Davis, G.H. (Eds.), Cordilleran metamorphic core complexes: Geological Society of America Memoir, 153, pp. 177–215.
Barbarin, B., 1996. Genesis of the two main types of peraluminous granitoids. Geology 24, 295–298.
Barker, D.S., 1987. Tertiary alkaline magmatism in Trans-Pecos Texas. Geol. Soc. Lond., Spec. Publ. 30, 415–431.
Barnes, C.G., Burton, B.R., Burling, T.C., Wright, J.E., Karlsson, H.R., 2001. Petrology and geochemistry of the late Eocene Harrison Pass pluton, Ruby Mountains core complex, northeastern Nevada. J. Petrol. 42, 901–929.
Barth, A.P., Wooden, J.L., 2006. Timing of magmatism following initial convergence at a passive margin, southwestern US Cordillera, and ages of lower crustal magma sources. J. Geol. 114, 231–245.
Barton, M.D., 1987. Lithophile-element mineralization associated with Late Cretaceous two-mica granites in the Great Basin. Geology 15, 337–340.
Barton, M.D., 1990. Cretaceous magmatism, metamorphism, and metallogeny in the east-central Great Basin. The nature and origin of Cordilleran magmatism. Geol. Soc. Am. Mem. 174, 283–302.
Barton, M.D., 1996. Granitic magmatism and metallogeny of southwestern North America: Transactions of the Royal Society of Edinburgh. Earth Sci. 87, 261–280.
Barton, M.D., 2000. Overview of the lithophile element-bearing magmatic-hydrothermal system at Birch Creek, White Mountains, California. In: Dilles, J.H., Barton, M.D., Johnson, D.A., Proffett, J.M., Einaudi, M.T., Crafford, E.J. (Eds.), Contrasting Styles of Intrusion Associated Hydrothermal Systems: Society of Economic Geologists Guide Book, 32, pp. 9–26.
Barton, M.D., Trim, H.E., 1991. Late Cretaceous two-mica granites and lithophile-element mineralization in the Great Basin. In: Raines, G.L., Lisle, R.E., Schafer, R.W., Wilkinson, W.H. (Eds.), Geology and ore deposits of the Great Basin, pp. 529–538.
Barton, M.D., Girardi, J.D., Kreiner, D.C., Seedorff, E., Zurcher, L., Dilles, J.H., Haxel, G. B., Johnson, D.A., Steininger, R.C., Pennell, W.M., 2011. Jurassic igneous-related metallogeny of southwestern North America: Great Basin Evolution and Metallogeny. In: Proceedings of the Geological Society of Nevada Symposium, pp. 373–396.
Bea, F., Montero, P., 1999. Behavior of accessory phases and redistribution of Zr, REE, Y, Th, and U during metamorphism and partial melting of metapelites in the lower crust: an example from the Kinzigite Formation of Ivrea-Verbano, NW Italy. Geochim. Cosmochim. Acta 63, 1133–1153.
Beard, J.S., Lofgren, G.E., 1991. Dehydration melting and water-saturated melting of basaltic and andesitic greenstones and amphibolites at 1, 3, and 6. 9 kb. J. Petrol. 32, 365–401.
Bendick, R., Baldwin, J., 2009. Dynamic models for metamorphic core complex formation and scaling: The role of unchannelized collapse of thickened continental crust. Tectonophysics 477, 93–101.
Best, M.G., Brimhall, W.H., 1974. Late Cenozoic alkalic basaltic magmas in the western Colorado Plateaus and the Basin and Range transition zone, USA, and their bearing on mantle dynamics. Geol. Soc. Am. Bull. 85, 1677–1690.
Best, M.G., Christiansen, E.H., 1991. Limited extension during peak Tertiary volcanism, Great Basin of Nevada and Utah. J. Geophys. Res. Solid Earth 96, 13509–13528.
Best, M.G., Barr, D.L., Christiansen, E.H., Gromme, S., Deino, A.L., Tingey, D.G., 2009. The Great Basin Altiplano during the middle Cenozoic ignimbrite flareup: Insights from volcanic rocks. Int. Geol. Rev. 51, 589–633.
Bickford, M.E., Mueller, P.A., Condie, K.C., Hanan, B.B., Kamenov, G.D., 2019. Ages and Hf isotopic compositions of detrital zircons in the Pinal schist, southern Arizona, USA: Provenance, tectonic setting, and evidence for pre-1.7 Ga crust in SW Laurentia. Precambrian Research 331, 105374.
Boehnke, P., Watson, E.B., Trail, D., Harrison, T.M., Schmitt, A.K., 2013. Zircon saturation re-revisited. Chem. Geol. 351, 324–334.
Boettcher, S.S., Mosher, S., Tosdal, R.M., 2002. Structural and tectonic evolution of Mesozoic basement-involved fold nappes and thrust faults in the Dome Rock Mountains, Arizona. In: Barth, A. (Ed.), Contributions to Crustal Evolution of the Southwestern United States: Boulder, Colorado, Geological Society of America Special Paper, 365, pp. 73–97.
Borisov, A., Aranovich, L., 2019. Zircon solubility in silicate melts: New experiments and probability of zircon crystallization in deeply evolved basic melts. Chem. Geol. 510, 103–112.
Brandon, A.D., Lambert, R.S., 1993. Geochemical characterization of mid-Cretaceous granitoids of the Kootenay Arc in the southern Canadian Cordillera. Can. J. Earth Sci. 30, 1076–1090.
Brandon, A.D., Lambert, R.S., 1994. Crustal melting in the Cordilleran Interior: the mid-Cretaceous White Creek batholith in the southern Canadian Cordillera. J. Petrol. 35, 239–269.
Brandon, A.D., Smith, A.D., 1994. Mesozoic granitoid magmatism in southeast British Columbia: implications for the origin of granitoid belts in the North American Cordillera. J. Geophys. Res. Solid Earth 99, 11879–11896.
Breitsprecher, K., Thorkelson, D.J., Groome, W.G., Dostal, J., 2003. Geochemical confirmation of the Kula-Farallon slab window beneath the Pacific Northwest in Eocene time. Geology 31, 351–354.
Brown, K.L., Hart, W.K., Stuck, R.J., 2018. Temporal and geochemical signatures in granitoids of northwestern Nevada: Evidence for the continuity of the Mesozoic magmatic arc through the western Great Basin. Lithosphere 10, 327–350.
Bryant, B., Wooden, J.L., 2008. Geology of the Northern Part of the Harcuvar Complex, West-Central, Arizona. U.S. Geol. Surv. Profess. Paper 1752, 52.
Burchfiel, B.C., Davis, G.A., 1975. Nature and controls of Cordilleran orogenesis, western United States: Extensions of an earlier synthesis. Am. J. Sci. 275, 363–396.
Burri, T., Berger, A., Engi, M., 2005. Tertiary migmatites in the Central Alps: regional distribution, field relations, conditions of formation, and tectonic implications. Schweiz. Mineral. Petrogr. Mitt. 85, 215–232.
Butcher, L.A., Mahan, K.H., Allaz, J.M., 2017. Late Cretaceous crustal hydration in the Colorado Plateau, USA, from xenolith petrology and monazite geochronology. Lithosphere 9, 561–578.
Camilleri, P.A., Chamberlain, K.R., 1997. Mesozoic tectonics and metamorphism in the Pequop Mountains and Wood Hills region, northeast Nevada: Implications for the architecture and evolution of the Sevier orogen. Geol. Soc. Am. Bull. 109, 74–94.
Carl, B.S., Miller, C.F., Foster, D.A., 1991. Western old Woman Mountains shear zone: Evidence for late ductile extension in the Cordilleran orogenic belt. Geology 19, 893–896.
Carlson, D.H., Fleck, R., Moye, F.J., Fox, K.F., 1991. Geology, geochemistry, and isotopic character of the Colville Igneous Complex, northeastern Washington. J. Geophys. Res. Solid Earth 96, 13313–13333.
Carr, S.D., 1992. Tectonic setting and U-Pb geochronology of the early Tertiary Ladybird leucogranite suite, Thor-Odin-Pinnacles area, southern Omineca belt, British Columbia. Tectonics 11, 258–278.
Cassel, E.J., Smith, M.E., Jicha, B.R., 2018. The impact of slab rollback on earth's surface: uplift and extension in the hinterland of the North American Cordillera. Geophys. Res. Lett. 45.
Castro, A., 2013. Tonalite–granodiorite suites as cotectic systems: a review of experimental studies with applications to granitoid petrogenesis. Earth Sci. Rev. 124, 68–95.
Castro, A., Douce, A.E.P., Corretgé, L.G., Jesús, D., El-Biad, M., El-Hmidi, H., 1999. Origin of peraluminous granites and granodiorites, Iberian massif, Spain: an experimental test of granite petrogenesis. Contrib. Mineral. Petrol. 135, 255–276.
Cawthorn, R.G., Brown, P.A., 1976. A model for the formation and crystallization of corundum-normative calc-alkaline magmas through amphibole fractionation. J. Geol. 84, 467–476.
Cecil, M.R., Rotberg, G.L., Ducea, M.N., Saleeby, J.B., Gehrels, G.E., 2012. Magmatic growth and batholithic root development in the northern Sierra Nevada, California. Geosphere 8, 592–606.

Chapman, J.B., Ducea, M.N., DeCelles, P.G., Profeta, L., 2015. Tracking changes in crustal thickness during orogenic evolution with Sr/Y: An example from the North American Cordillera. Geology 43, 919–922.
Chapman, J.B., Dafov, M.N., Gehrels, G., Ducea, M.N., Valley, J.W., Ishida, A., 2018. Lithospheric architecture and tectonic evolution of the southwestern US Cordillera: Constraints from zircon Hf and O isotopic data. Geol. Soc. Am. Bull. 130, 2031–2046.
Chapman, J.B., Greig, R., Haxel, G.B., 2020. Geochemical evidence for an orogenic plateau in the southern US and northern Mexican Cordillera during the Laramide orogeny. Geology 48, 164–168.
Chappell, B.W., White, A.J., 2001. Two contrasting granite types: 25 years later. Aust. J. Earth Sci. 48, 489–499.
Chappell, B.W., White, A.J.R., Wyborn, D., 1987. The importance of residual source material (restite) in granite petrogenesis. J. Petrol. 28, 11–38.
Chappell, B.W., Bryant, C.J., Wyborn, D., 2012. Peraluminous I-type granites. Lithos 153, 142–153.
Chen, J.H., Moore, J.G., 1982. Uranium-lead isotopic ages from the Sierra Nevada batholith, California. J. Geophys. Res. Solid Earth 87, 4761–4784.
Clark, C., Fitzsimons, I.C., Healy, D., Harley, S.L., 2011. How does the continental crust get really hot? Elements 7, 235–240.
Clarke, D.B., 2019. The origins of strongly peraluminous granitoid rocks. Can. Mineral. 57, 529–550.
Clarke, G.L., Daczko, N.R., Klepeis, K.A., Rushmer, T., 2005. Roles for fluid and/or melt advection in forming high-P mafic migmatites, Fiordland, New Zealand. J. Metamorph. Geol. 23, 557–567.
Clemens, J.D., Droop, G.T.R., 1998. Fluids, P–T paths and the fates of anatectic melts in the Earth's crust. Lithos 44, 21–36.
Clemens, J.D., Stevens, G., 2012. What controls chemical variation in granitic magmas? Lithos 134–135, 317–329.
Clemens, J.D., Stevens, G., Bryan, S.E., 2020. Conditions during the formation of granitic magmas by crustal melting–hot or cold; drenched, damp or dry? Earth-Science Reviews 200, 102982.
Clemens, J.D., Vielzeuf, D., 1987. Constraints on melting and magma production in the crust. Earth Planet. Sci. Lett. 86, 287–306.
Collins, W.J., 1996. Lachlan Fold Belt granitoids: products of three-component mixing. Trans. R. Soc. Edinb. Earth Sci. 87, 171–181.
Collins, W.J., Huang, H.Q., Jiang, X., 2016. Water-fluxed crustal melting produces Cordilleran batholiths. Geology 44, 143–146.
Coney, P.J., Harms, T.A., 1984. Cordilleran metamorphic core complexes: Cenozoic extensional relics of Mesozoic compression. Geology 12, 550–554.
Coney, P.J., Reynolds, S.J., 1977. Cordilleran Benioff zones. Nature 270, 403–406.
Connolly, J.A.D., 1990. Multivariable phase diagrams; an algorithm based on generalized thermodynamics. Am. J. Sci. 290, 666–718.
Connolly, J.A.D., 2005. Computation of phase equilibria by linear programming: A tool for geodynamic modeling and its application to subduction zone decarbonation. Earth Planet. Sci. Lett. 236, 524–541.
Connolly, J.A.D., Petrini, K., 2002. An automated strategy for calculation of phase diagram sections and retrieval of rock properties as a function of physical conditions. J. Metamorph. Geol. 20, 697–708.
Conrad, W.K., Nicholls, I.A., Wall, V.J., 1988. Water-saturated and-undersaturated melting of metaluminous and peraluminous crustal compositions at 10 kb: evidence for the origin of silicic magmas in the Taupo Volcanic Zone, New Zealand, and other occurrences. J. Petrol. 29, 765–803.
Constenius, K.N., 1996. Late Paleogene extensional collapse of the Cordilleran foreland fold and thrust belt. Geol. Soc. Am. Bull. 108, 20–39.
Constenius, K.N., Esser, R.P., Layer, P.W., 2003. In: Raynolds, R.G., Flores, R.M. (Eds.), Extensional collapse of the Charleston-Nebo salient and its relationship to space-time variations in Cordilleran orogenic belt tectonism and continental stratigraphy. Cenozoic Systems of the Rocky Mountain Region: SEPM Rocky Mountain Section, pp. 303–353.
Cooper, F.J., Platt, J.P., Anczkiewicz, R., Whitehouse, M.J., 2010. Footwall dip of a core complex detachment fault: Thermobarometric constraints from the northern Snake Range (Basin and Range, USA). J. Metamorph. Geol. 28, 997–1020.
Cooper, J.R., Silver, L.T., 1964. Geology and ore deposits of the Dragoon quadrangle, Cochise County, 416. U.S. Geological Survey Professional Paper, Arizona, pp. 165–168.
Copeland, P., Condie, K.C., 1986. Geochemistry and tectonic setting of lower Proterozoic supracrustal rocks of the Pinal Schist, Southeastern Arizona. Geol. Soc. Am. Bull. 97, 1512–1520.
Copeland, P., Currie, C.A., Lawton, T.F., Murphy, M.A., 2017. Location, location, location: The variable lifespan of the Laramide orogeny. Geology 45, 223–226.
Creasey, S.C., Banks, N.G., Ashley, R.P., Theodore, T.G., 1977. Middle Tertiary plutonism in the Santa Catalina and Tortolita Mountains, Arizona: U.S. Geological Survey. Journal of Researc 5, 705–717.
Crowley, J.L., Brown, R.L., Parrish, R.R., 2001. Diachronous deformation and a strain gradient beneath the Selkirk allochthon, northern Monashee complex, southeastern Canadian Cordillera. J. Struct. Geol. 23, 1103–1121.
Crowley, J.L., Brown, R.L., Gervais, F., Gibson, H.D., 2008. Assessing inheritance of zircon and monazite in granitic rocks from the Monashee Complex, Canadian Cordillera. J. Petrol. 49, 1915–1929.
Cubley, J.F., Pattison, D.R., Tinkham, D.K., Fanning, C.M., 2013. U–Pb geochronological constraints on the timing of episodic regional metamorphism and rapid high-T exhumation of the Grand Forks complex, British Columbia. Lithos 156, 241–267.
Currie, C.A., Hyndman, R.D., 2006. The thermal structure of subduction zone back arcs: Journal of Geophysical Research. Solid Earth 111.
Davis, G.H., 1979. Laramide folding and faulting in southeastern Arizona. Am. J. Sci. 279, 543–569.
Davis, G.H., Spencer, J.E., Gehrels, G.E., 2019. Field-trip guide to the Catalina-Rincon metamorphic core complex, Tucson, Arizona. In: Geologic Excursions in Southwestern North America, Geological Society of America Field Trip Guide, 55.
DeCelles, P.G., 2004. Late Jurassic to Eocene evolution of the Cordilleran thrust belt and foreland basin system, western USA. Am. J. Sci. 304, 105–168.
DeCelles, P.G., Coogan, J.C., 2006. Regional structure and kinematic history of the Sevier fold-and-thrust belt, central Utah. Geol. Soc. Am. Bull. 118, 841–864.
DePaolo, D.J., 1981. Trace element and isotopic effects of combined wallrock assimilation and fractional crystallization. Earth Planet. Sci. Lett. 53, 189–202.
Dewitt, E.D., Reynolds, S.J., 1990. Late Cretaceous plutonism and cooling in the Maria fold and thrust belt, west-central Arizona. Geol. Soc. Am. Abstr. Programs 22 (3), 18.
Dickinson, W.R., 2004. Evolution of the North American Cordillera. Annu. Rev. Earth Planet. Sci. 32, 13–45.
Dickinson, W.R., 2006. Geotectonic evolution of the Great Basin. Geosphere 2, 353–368.
Dickinson, W.R., Snyder, W.S., 1978. Plate tectonics of the Laramide orogeny. In: Matthews, V. (Ed.), Laramide Folding Associated with Basement Block Faulting in the Western United States: Geological Society of America Memoir, 151, pp. 355–366.
Dickinson, W.R., Kay, S.M., Ramos, V.A., 2009. Anatomy and global context of the North American Cordillera. Backbone of the Americas: Shallow subduction, plateau uplift, and ridge and terrane collision. Geol. Soc. Am. Mem. 204, 1–29.
Doughty, P.T., Chamberlain, K.R., 2007. Age of Paleoproterozoic basement and related rocks in the Clearwater complex, northern Idaho, U.S.A. In: Link, P.K., Lewis, R.L. (Eds.), Proterozoic geology of western North America and Siberia: Society of Economic Paleontologists and Mineralogists Special Publication, 86, pp. 9–35.
Doughty, P.T., Price, R.A., 1999. Tectonic evolution of the Priest River complex, northern Idaho and Washington: A reappraisal of the Newport fault with new insights on metamorphic core complex formation. Tectonics 18, 375–393.
Droop, G.T.R., Brodie, K.H., 2012. Anatectic melt volumes in the thermal aureole of the Etive Complex, Scotland: The roles of fluid-present and fluid-absent melting. J. Metamorph. Geol. 30, 843–864.
Druschke, P., Hanson, A.D., Wells, M.L., Rasbury, T., Stockli, D.F., Gehrels, G., 2009. Synconvergent surface-breaking normal faults of Late Cretaceous age within the Sevier hinterland, east-central Nevada. Geology 37, 447–450.
Ducea, M.N., Triantafyllou, A., and Krcmaric, J., 2020, New timing and depth constraints for the Catalina Metamorphic Core complex, Southeast Arizona: Tectonics, v. 39, e2020TC006383.
Dumitru, T.A., Gans, P.B., Foster, D.A., Miller, E.L., 1991. Refrigeration of the western Cordilleran lithosphere during Laramide shallow-angle subduction. Geology 19, 1145–1148.
Duncan, I.J., 1984. Structural evolution of the Thor-Odin gneiss dome. Tectonophysics 101, 87–130.
Economos, R.C., Barth, A.P., Wooden, J.L., Howard, K.A., Wiegand, B.A., 2010. Comparing batholith-source connections for the Cadiz Valley Batholith and a deeper sheeted intrusive complex in the Mojave Desert, CA through whole rock and pre-magmatic zircon geochemistry: Abstract V51E-02, 2010 AGU Annual Fall Meeting, San Francisco, California.
Egger, A.E., Dumitru, T.A., Miller, E.L., Savage, C.F., Wooden, J.L., 2003. Timing and nature of Tertiary plutonism and extension in the Grouse Creek Mountains, Utah. Int. Geol. Rev. 45, 497–532.
Elison, M.W., 1995. Causes and consequences of Jurassic magmatism in the northern Great Basin: Implications for tectonic development. In: Miller, D.M., Busby, C. (Eds.), Jurassic Magmatism and Tectonics of the North American Cordillera, Geological Society of America Special Paper, 299, pp. 249–265.
England, P., Houseman, G., 1989. Extension during continental convergence, with application to the Tibetan Plateau. J. Geophys. Res. Solid Earth 94, 17561–17579.
England, P.C., Thompson, A., 1984. Pressure-temperature-time paths of regional metamorphism I. Heat transfer during the evolution of regions of thickened continental crust. J. Petrol. 25, 894–928.
England, P.C., Thompson, A., 1986. Some thermal and tectonic models for crustal melting in continental collision zones. Geol. Soc. Lond., Spec. Publ. 19, 83–94.
English, J.M., Johnston, S.T., Wang, K., 2003. Thermal modelling of the Laramide orogeny: testing the flat-slab subduction hypothesis. Earth Planet. Sci. Lett. 214, 619–632.
Erdman, M.E., Lee, C.T.A., Levander, A., Jiang, H., 2016. Role of arc magmatism and lower crustal foundering in controlling elevation history of the Nevadaplano and Colorado Plateau: A case study of pyroxenitic lower crust from central Arizona, USA. Earth Planet. Sci. Lett. 439, 48–57.
Evans, S.L., Styron, R.H., van Soest, M.C., Hodges, K.V., Hanson, A.D., 2015. Zircon and apatite (U-Th)/He evidence for Paleogene and Neogene extension in the Southern Snake Range, Nevada, USA. Tectonics 34, 2142–2164.
Farmer, G.L., DePaolo, D.J., 1983. Origin of Mesozoic and Tertiary granite in the western United States and implications for Pre-Mesozoic crustal structure: 1. Nd and Sr isotopic studies in the geocline of the Northern Great Basin. J. Geophys. Res. Solid Earth 88, 3379–3401.
Farmer, G.L., DePaolo, D.J., 1984. Origin of Mesozoic and Tertiary granite in the western United States and implications for Pre-Mesozoic crustal structure: 2. Nd and Sr isotopic studies of unmineralized and Cu-and Mo-mineralized granite in the Precambrian Craton. J. Geophys. Res. Solid Earth 89, 10141–10160.
Farmer, G.L., Bailey, T., Elkins-Tanton, L.T., 2008. Mantle source volumes and the origin of the mid-Tertiary ignimbrite flare-up in the southern Rocky Mountains, Western US. Lithos 102, 279–294.
Fayon, A.K., Peacock, S.M., Stump, E., Reynolds, S.J., 2000. Fission track analysis of the footwall of the Catalina detachment fault, Arizona: Tectonic denudation, magmatism, and erosion. J. Geophys. Res. Solid Earth 105, 11047–11062.
Ferguson, C.A., Johnson, B.J., Skotnicki, J.S., Maher, J.D., Spencer, J.E., Gilbert, W.G., Richard, S.M., Youberg, A., Demsey, K.A., House, P.K., 2003. Geologic Map of the

Tortolita Mountains, Pinal and Pima Counties. Arizona Geological Survey Digital Geologic Map DGM-26, Arizona.
Ferrari, L., López-Martínez, M., Rosas-Elguera, J., 2002. Ignimbrite flare-up and deformation in the southern Sierra Madre Occidental, western Mexico: Implications for the late subduction history of the Farallon plate. Tectonics 21.
Fitz-Díaz, E., Lawton, T.F., Juárez-Arriaga, E., Chávez-Cabello, G., 2018. The Cretaceous-Paleogene Mexican orogen: Structure, basin development, magmatism and tectonics. Earth Sci. Rev. 183, 56–84.
Force, E.R., 1997. Geology and mineral resources of the Santa Catalina Mountains, Southeastern Arizona: a cross-sectional approach: Mineral Resource Science Monograph, v. 1., Center for Mineral Resources. University of Arizona, p. 135.
Fornash, K.F., Patchett, P.J., Gehrels, G.E., Spencer, J.E., 2013. Evolution of granitoids in the Catalina metamorphic core complex, southeastern Arizona: U-Pb, Nd, and Hf isotopic constraints. Contrib. Mineral. Petrol. 165, 1295–1310.
Foster, D.A., John, B.E., 1999. Quantifying tectonic exhumation in an extensional orogen with thermochronology: examples from the southern Basin and Range Province. Geol. Soc. Lond., Spec. Publ. 154, 343–364.
Foster, D.A., Raza, A., 2002. Low-temperature thermochronological record of exhumation of the Bitterroot metamorphic core complex. northern Cordilleran Orogen: Tectonophysics 349, 23–36.
Foster, D.A., Harrison, T.M., Miller, C.F., 1989. Age, inheritance, and uplift history of the Old Woman-Piute batholith, California and implications for K-feldspar age spectra. J. Geol. 97, 232–243.
Foster, D.A., Schafer, C., Fanning, C.M., Hyndman, D.W., 2001. Relationships between crustal partial melting, plutonism, orogeny, and exhumation: Idaho–Bitterroot batholith. Tectonophysics 342, 313–350.
Foster, D.A., Doughty, P.T., Kalakay, T.J., Fanning, C.M., Coyner, S., Grice, W.C., Vogl, J., Till, A.B., Roeske, S.M., Sample, J.C., 2007. Kinematics and timing of exhumation of metamorphic core complexes along the Lewis and Clark fault zone, northern Rocky Mountains, USA. In: Till, A.B. (Ed.), Exhumation associated with continental strike-slip fault systems: Geological Society of America Special Paper, 434, pp. 207–232.
Foster, D.A., Grice, W.C., Kalakay, T.J., 2010. Extension of the Anaconda metamorphic core complex: 40Ar/39Ar thermochronology and implications for Eocene tectonics of the northern Rocky Mountains and the Boulder batholith. Lithosphere 2, 232–246.
Frost, B.R., Barnes, C.G., Collins, W.J., Arculus, R.J., Ellis, D.J., Frost, C.D., 2001. A geochemical classification for granitic rocks. J. Petrol. 42, 2033–2048.
Fryxell, J.E., 1988. Geologic map and description of stratigraphy and structure of the west-central Grant Range, Nye County, Nevada. Geol. Soc. Am. Map Chart Ser. 16. MCH064.
Fuentes, F., DeCelles, P.G., Constenius, K.N., 2012. Regional structure and kinematic history of the Cordilleran fold-thrust belt in northwestern Montana, USA. Geosphere 8, 1104–1128.
Gans, P.B., 1989. Synextensional magmatism in the Basin and Range province: A case study from the eastern Great Basin. Geol. Soc. Am. Spec. Paper 233, 53.
Gao, P., Zheng, Y.F., Zhao, Z.F., 2016. Experimental melts from crustal rocks: a lithochemical constraint on granite petrogenesis. Lithos 266, 133–157.
Gaschnig, R.M., Vervoort, J.D., Lewis, R.S., McClelland, W.C., 2010. Migrating magmatism in the northern US Cordillera: in situ U–Pb geochronology of the Idaho batholith. Contrib. Mineral. Petrol. 159, 863–883.
Gaschnig, R.M., Vervoort, J.D., Lewis, R.S., Tikoff, B., 2011. Isotopic evolution of the Idaho batholith and Challis intrusive province, northern US Cordillera. J. Petrol. 52, 2397–2429.
Gaschnig, R.M., Vervoort, J.D., Lewis, R.S., Tikoff, B., 2013. Probing for Proterozoic and Archean crust in the northern US Cordillera with inherited zircon from the Idaho batholith. Geol. Soc. Am. Bull. 125, 73–88.
Gehrels, G., Rusmore, M., Woodsworth, G., Crawford, M., Andronicos, C., Hollister, L., Patchett, J., Ducea, M., Butler, R., Klepeis, K., Davidson, C., 2009. U-Th-Pb geochronology of the Coast Mountains batholith in north-coastal British Columbia: Constraints on age and tectonic evolution. Geol. Soc. Am. Bull. 121, 1341–1361.
Genier, F., Bussy, F., Epard, J.L., Baumgartner, L., 2008. Water-assisted migmatization of metagraywackes in a Variscan shear zone, Aiguilles–Rouges massif, western Alps. Lithos 102, 575–597.
Gervais, F., Brown, R.L., 2011. Testing modes of exhumation in collisional orogens: Synconvergent channel flow in the southeastern Canadian Cordillera. Lithosphere 3, 55–75.
Gervasoni, F., Klemme, S., Rocha-Júnior, E.R., Berndt, J., 2016. Zircon saturation in silicate melts: a new and improved model for aluminous and alkaline melts. Contrib. Mineral. Petrol. 171 (21).
Ghosh, D.K., 1995. U–Pb geochronology of Jurassic to early Tertiary granitic intrusives from the Nelson-Castlegar area, southeastern British Columbia, Canada. Can. J. Earth Sci. 32, 1668–1680.
Giallorenzo, M.A., Wells, M.L., Yonkee, W.A., Stockli, D.F., Wernicke, B.P., 2018. Timing of exhumation, Wheeler Pass thrust sheet, southern Nevada and California: Late Jurassic to middle Cretaceous evolution of the southern Sevier fold-and-thrust belt. Geol. Soc. Am. Bull. 130, 558–579.
González-Becuar, E., Pérez-Segura, E., Vega-Granillo, R., Solari, L., González-León, C.M., Solé, J., Martínez, M.L., 2017. Laramide to Miocene syn-extensional plutonism in the Puerta del Sol area, central Sonora, Mexico. Rev. Mexic. Cienc. Geol. 34, 45–61.
González-León, C.M., Solari, L., Solé, J., Ducea, M.N., Lawton, T.F., Bernal, J.P., Becuar, E.G., Gray, F., Martínez, M.L., Santacruz, R.L., 2011. Stratigraphy, geochronology, and geochemistry of the Laramide magmatic arc in north-central Sonora, Mexico. Geosphere 7, 1392–1418.
Goodwin, L.B., Haxel, G.B., 1990. Structural evolution of the Southern Baboquivari Mountains, south-central Arizona and north-central Sonora. Tectonics 9, 1077–1095.
Gordon, S.M., Whitney, D.L., Teyssier, C., Grove, M., Dunlap, W.J., 2008. Timescales of migmatization, melt crystallization, and cooling in a Cordilleran gneiss dome: Valhalla complex, southeastern British Columbia. Tectonics 27.
Gottardi, R., McAleer, R., Casale, G., Borel, M., Iriondo, A., Jepson, G., 2020. Exhumation of the Coyote Mountains metamorphic core complex (Arizona): implications for orogenic collapse of the southern North American Cordillera. Tectonics 39 e2019TC006050.
Gottlieb, E.S., 2017. Geologic Insights from Zircon Inheritance. Ph.D. dissertation. Stanford University, p. 354.
Grice, W.C., 2006. Exhumation and Cooling History of the Middle Eocene Anaconda Metamorphic Core Complex. University of Florida, Western Montana. PhD Dissertation.
Grijalva-Noriega, F.J., Roldan-Quintana, J., 1998. An overview of the Cenozoic tectonic and magmatic evolution of Sonora, northwestern Mexico. Rev. Mexic. Cienc. Geol. 15, 145–156.
Grove, M., Jacobson, C.E., Barth, A.P., Vucic, A., 2003. Temporal and spatial trends of Late Cretaceous-early Tertiary underplating of Pelona and related schist beneath southern California and southwestern Arizona, in, Johnson, S.E., Paterson, S.R., Fletcher, J.M., Girty, G.H., Kimbrough, D.L., and Martín-Barajas, A., eds., Tectonic evolution of northwestern Mexico and the southwestern USA: Geological Society of America Special Paper, v. 374 p. In: 381-406.
Guevara, V., 2012. Structural, thermochronological, and stratigraphic constraints on the evolution of the Clearwater metamorphic core complex. University of Montana, Idaho. MS Thesis.
Hallett, B.W., Spear, F.S., 2014. The P–T history of anatectic pelites of the Northern East Humboldt Range, Nevada: Evidence for tectonic loading, decompression, and anatexis. J. Petrol. 55, 3–36.
Hallett, B.W., Spear, F.S., 2015. Monazite, zircon, and garnet growth in migmatitic pelites as a record of metamorphism and partial melting in the East Humboldt Range, Nevada. Am. Mineral. 100, 951–972.
Hamilton, W., 1987. Mesozoic geology and tectonics of the Big Maria Mountains region, southeastern California. Mesozoic rocks of southern Arizona and adjacent areas. Arizona Geol. Soc. Digest 18, 33–47.
Haney, E.M., 2008. Pressure-temperature evolution of metapelites within the Anaconda metamorphic core complex, Southwestern Montana. University of Montana. M.S. thesis.
Hansen, V.L., Goodge, J.W., 1988. Metamorphism, structural petrology, and regional evolution of the Okanogan Complex, northeastern Washington. Rubey colloquium on metamorphism and crustal evolution of the Western United States 7, 233–270.
Harris, N., Massey, J., 1994. Decompression and anatexis of Himalayan metapelites. Tectonics 13, 1537–1546.
Harris, N., Massey, J., Inger, S., 1993. The role of fluids in the formation of High Himalayan leucogranites. Geol. Soc. Lond., Spec. Publ. 74, 391–400.
Harris, N.B.W., Inger, S., 1992. Trace element modelling of pelite-derived granites. Contrib. Mineral. Petrol. 110, 46–56.
Hawkesworth, C., Turner, S., Gallagher, K., Hunter, A., Bradshaw, T., Rogers, N., 1995. Calc-alkaline magmatism, lithospheric thinning and extension in the Basin and Range. J. Geophys. Res. Solid Earth 100, 10271–10286.
Haxel, G.B., Tosdal, R.M., May, D.J., Wright, J.E., 1984. Latest Cretaceous and early Tertiary orogenesis in south-central Arizona: Thrust faulting, regional metamorphism, and granitic plutonism. Geol. Soc. Am. Bull. 95, 631–653.
Hayama, Y., Shibata, K., Takeda, H., 1984. K-Ar ages of the low-grade metamorphic rocks in the Altar massif, northwest Sonora, Mexico. J. Geol. Soc. Jpn. 90, 589–596.
Henry, C.D., John, D.A., 2013. Magmatism, ash-flow tuffs, and calderas of the ignimbrite flareup in the western Nevada volcanic field, Great Basin, USA. Geosphere 9, 951–1008.
Henry, C.D., McGrew, A.J., Colgan, J.P., Snoke, A.W., Brueseke, M.E., Lee, J., Evans, J.P., 2011. Timing, distribution, amount, and style of Cenozoic extension in the northern Great Basin. Geologic Field Trips to the Basin and Range, Rocky Mountains, Snake River Plain, and Terranes of the US Cordillera. Geol. Soc. Am. Field Guide 21, 27–66.
Hinchey, A.M., Carr, S.D., 2006. The S-type Ladybird leucogranite suite of southeastern British Columbia: Geochemical and isotopic evidence for a genetic link with migmatite formation in the North American basement gneisses of the Monashee complex. Lithos 90, 223–248.
Hinchey, A.M., Carr, S.D., McNeill, P.D., Rayner, N., 2006. Paleocene–Eocene high-grade metamorphism, anatexis, and deformation in the Thor–Odin dome, Monashee complex, southeastern British Columbia. Can. J. Earth Sci. 43, 1341–1365.
Hodges, K.V., Walker, J.D., 1990. Petrologic constraints on the unroofing history of the Funeral Mountain metamorphic core complex, California. J. Geophys. Res. Solid Earth 95, 8437–8445.
Hodges, K.V., Walker, J.D., 1992. Extension in the Cretaceous Sevier orogen, North American Cordillera. Geol. Soc. Am. Bull. 104, 560–569.
Hodges, K.V., Snoke, A.W., Hurlow, H.A., 1992. Thermal evolution of a portion of the Sevier hinterland: the northern Ruby Mountains-East Humboldt Range and Wood Hills, northeastern Nevada. Tectonics 11, 154–164.
Hoisch, T.D., 1987. Heat transport by fluids during Late Cretaceous regional metamorphism in the Big Maria Mountains, southeastern California. Geol. Soc. Am. Bull. 98, 549–553.
Hoisch, T.D., Simpson, C., 1993. Rise and tilt of metamorphic rocks in the lower plate of a detachment fault in the Funeral Mountains, Death Valley, California. J. Geophys. Res. Solid Earth 98, 6805–6827.
Hoisch, T.D., Wells, M.L., Beyene, M.A., Styger, S., Vervoort, J.D., 2014. Jurassic Barrovian metamorphism in a western US Cordilleran metamorphic core complex, Funeral Mountains, California. Geology 42, 399–402.

Holk, G.J., Taylor Jr., H.P., 1997. $^{18}O/^{16}O$ homogenization of the middle crust during anatexis: The Thor-Odin metamorphic core complex, British Columbia. Geology 25, 31–34.
Holk, G.J., Taylor Jr., H.P., 2000. Water as a petrologic catalyst driving $^{18}O/^{16}O$ homogenization and anatexis of the middle crust in the metamorphic core complexes of British Columbia. Int. Geol. Rev. 42, 97–130.
Holland, T.J.B., Powell, R., 2011. An improved and extended internally consistent thermodynamic dataset for phases of petrological interest, involving a new equation of state for solids. J. Metamorph. Geol. 29, 333–383.
Holm, D.K., Dokka, R.K., 1991. Major late Miocene cooling of the middle crust associated with extensional orogenesis in the Funeral Mountains. California: Geophys. Res. Lett. 18, 1775–1778.
Holtz, F., Johannes, W., 1991. Genesis of peraluminous granites I. Experimental investigation of melt compositions at 3 and 5 kb and various H2O activities. J. Petrol. 32, 935–958.
Howard, K.A., 1980. Metamorphic infrastructure in the northern Ruby Mountains, Nevada. In: Crittenden, M.D., Coney, P.J., Davis, G.H. (Eds.), Cordilleran metamorphic core complexes: Geological Society of America Memoir, 153, pp. 335–347.
Howard, K.A., 2002. Geologic Map of the Sheep Hole Mountains 30'x 60'quadrangle, San Bernardino and Riverside Counties. U.S. Geological Survey Geologic Investigations Series I-2344, California.
Howard, K.A., John, B.E., 1987. Crustal extension along a rooted system of imbricate low-angle faults: Colorado River extensional corridor, California and Arizona. Geol. Soc. Lond., Spec. Publ. 28, 299–311.
Howard, K.A., Wooden, J.L., Barnes, C.G., Premo, W.R., Snoke, A.W., Lee, S.Y., 2011. Episodic growth of a Late Cretaceous and Paleogene intrusive complex of pegmatitic leucogranite, Ruby Mountains core complex, Nevada, USA. Geosphere 7, 1220–1248.
Humphreys, E., Hessler, E., Dueker, K., Farmer, G.L., Erslev, E., Atwater, T., 2003. How Laramide-age hydration of North American lithosphere by the Farallon slab controlled subsequent activity in the western United States. Int. Geol. Rev. 45, 575–595.
Humphreys, E.D., 1995. Post-Laramide removal of the Farallon slab, western United States. Geology 23, 987–990.
Hyndman, D.W., 1983. The Idaho Batholith and associated plutons, Idaho and western Montana. In: Roddick, J.A. (Ed.), Circum-Pacific Plutonic Terranes: Geological Society of America, Memoir, 159, pp. 213–240.
Hyndman, D.W., Foster, D.A., 1988. The role of tonalites and mafic dikes in the generation of the Idaho batholith. J. Geol. 96, 31–46.
Inger, S., Harris, N., 1993. Geochemical constraints on leucogranite magmatism in the Langtang Valley, Nepal Himalaya. J. Petrol. 34, 345–368.
Isachsen, C., Gehrels, G., Freguson, C., Skotnicki, S., Richard, S.M., Spencer, J.E., 1998. U-Pb zircon dates from nine granitic rocks in central and western Arizona. Arizona Geol. Surv. Open File Rep. 98, 35.
Johannes, W., Holtz, F., 1996. Petrogenesis and Experimental Petrology of Granitic Rocks. Springer, p. 335.
Johannes, W., Ehlers, C., Kriegsman, L.M., Mengel, K., 2003. The link between migmatites and S-type granites in the Turku area, southern Finland. Lithos 68, 69–90.
John, B.E., 1988. Structural reconstruction and zonation of a tilted mid-crustal magma chamber: The felsic Chemehuevi Mountains plutonic suite. Geology 16, 613–617.
John, B.E., Mukasa, S.B., 1990. Footwall rocks to the Mid-Tertiary Chemehuevi Detachment Fault: A window into the middle crust in the Southern Cordillera. J. Geophys. Res. Solid Earth 95, 463–485.
John, B.E., Wooden, J., 1990. Petrology and geochemistry of the metaluminous to peraluminous Chemehuevi Mountains Plutonic Suite, southeastern California: The Nature and Origin of Cordilleran Magmatism. Geol. Soc. Am. Mem. 174, 71–98.
Johnson, K.M., Lewis, R.S., Bennett, E.H., Kiilsgaard, T.H., 1988. Cretaceous and Tertiary intrusive rocks of south-central Idaho. Guidebook to the geology of central and southern Idaho. Idaho Geol. Surv. Bull. 27, 55–86.
Johnson, M.G., 1977. Geology and mineral deposits of Pershing County. Nevada Bureau of Mines and Geology Bulletin, Nevada, p. 89.
Jones, C.H., Mahan, K.H., Butcher, L.A., Levandowski, W.B., Farmer, G.L., 2015. Continental uplift through crustal hydration. Geology 43, 355–358.
Jones, J.V., 1999. Deformational, magmatic, and metamorphic history of the central Ruby Mountains, Elko County, Nevada. M.S. thesis. University of Wyoming.
Kapp, J.D.A., Miller, C.F., Miller, J.S., 2002. Ireteba pluton, Eldorado Mountains, Nevada: Late, deep-source, peraluminous magmatism in the Cordilleran Interior. J. Geol. 110, 649–669.
Keith, S.B., Reynolds, S.J., Damon, P.E., Shafiqullah, M., Livingston, D.E., Pushkar, P.D., 1980. Evidence for multiple intrusion and deformation within the Santa Catalina Rincon-Tortolita crystalline complex, southeastern Arizona. In: Crittenden, M.D., Coney, P.J., Davis, G.H. (Eds.), Cordilleran Metamorphic Core Complexes: Geological Society of America Memoir, 153, pp. 217–267.
Kemp, A.I., Hawkesworth, C.J., Foster, G.L., Paterson, B.A., Woodhead, J.D., Hergt, J.M., Gray, C.M., Whitehouse, M.J., 2007. Magmatic and crustal differentiation history of granitic rocks from Hf–O isotopes in zircon. Science 315, 980–983.
Ketcham, R.A., 1996. Thermal models of core-complex evolution in Arizona and New Guinea: Implications for ancient cooling paths and present-day heat flow. Tectonics 15, 933–951.
King, E.M., Valley, J.W., 2001. The source, magmatic contamination, and alteration of the Idaho batholith. Contrib. Mineral. Petrol. 142, 72–88.
King, E.M., Valley, J.W., Stockli, D.F., Wright, J.E., 2004. Oxygen isotope trends of granitic magmatism in the Great Basin: Location of the Precambrian craton boundary as reflected in zircons. Geol. Soc. Am. Bull. 116, 451–462.
Kistler, R.W., Anderson, J.L., 1990. Two different lithosphere types in the Sierra Nevada, California. The nature and origin of Cordilleran magmatism. Geol. Soc. Am. Mem. 174, 271–281.
Kistler, R.W., Peterman, Z.E., 1973. Variations in Sr, Rb, K, Na, and initial Sr87/Sr86 in Mesozoic granitic rocks and intruded wall rocks in central California. Geol. Soc. Am. Bull. 84, 3489–3512.
Kistler, R.W., Ghent, E.D., O'Neil, J.R., 1981. Petrogenesis of garnet two-mica granites in the Ruby Mountains, Nevada. J. Geophys. Res. Solid Earth 86, 10591–10606.
Knapp, J.H., Heizler, M.T., 1990. Thermal history of crystalline nappes of the Maria fold and thrust belt, west central Arizona. J. Geophys. Res. Solid Earth 95, 20049–20073.
Kohn, M.J., 2014. Himalayan metamorphism and its tectonic implications. Annu. Rev. Earth Planet. Sci. 42, 381–419.
Konstantinou, A., Miller, E., 2015. Evidence for a long-lived accommodation/transfer zone beneath the Snake River Plain: A possible influence on Neogene magmatism? Tectonics 34, 2387–2398.
Konstantinou, A., Strickland, A., Miller, E.L., Wooden, J.P., 2012. Multistage Cenozoic extension of the Albion–Raft River–Grouse Creek metamorphic core complex: Geochronologic and stratigraphic constraints. Geosphere 8, 1429–1466.
Konstantinou, A., Strickland, A., Miller, E., Vervoort, J., Fisher, C.M., Wooden, J., Valley, J., 2013. Synextensional magmatism leading to crustal flow in the Albion–Raft River–Grouse Creek metamorphic core complex, northeastern Basin and Range. Tectonics 32, 1384–1403.
Kruckenberg, S.C., Whitney, D.L., Teyssier, C., Fanning, C.M., Dunlap, W.J., 2008. Paleocene-Eocene migmatite crystallization, extension, and exhumation in the hinterland of the northern Cordillera: Okanogan dome, Washington, USA. Geol. Soc. Am. Bull. 120, 912–929.
Laberge, J.D., Pattison, D.R.M., 2007. Geology of the western margin of the Grand Forks complex, southern British Columbia: high-grade Cretaceous metamorphism followed by early Tertiary extension on the Granby fault. Can. J. Earth Sci. 44, 199–228.
Lang, J.R., Titley, S.R., 1998. Isotopic and geochemical characteristics of Laramide magmatic systems in Arizona and implications for the genesis of porphyry copper deposits. Econ. Geol. 93, 138–170.
Le Breton, N., Thompson, A.B., 1988. Fluid-absent (dehydration) melting of biotite in metapelites in the early stages of crustal anatexis. Contrib. Mineral. Petrol. 99, 226–237.
Le Fort, P., Cuney, M., Deniel, C., France-Lanord, C., Sheppard, S.M.F., Upreti, B.N., Vidal, P., 1987. Crustal generation of the Himalayan leucogranites. Tectonophysics 134, 39–57.
Leclair, A.D., Parrish, R.R., Archibald, D.A., 1993. Evidence for Cretaceous deformation in the Kootenay Arc on U-Pb and 40Ar/39Ar dating, southeastern British Columbia. In: Current Research, Part A: Geological Survey of Canada, Paper 93-1A, pp. 207–220.
Lederer, G.W., Cottle, J.M., Jessup, M.J., Langille, J.M., Ahmad, T., 2013. Timescales of partial melting in the Himalayan middle crust: insight from the Leo Pargil dome, northwest India. Contrib. Mineral. Petrol. 166, 1415–1441.
Lee, D.E., Christiansen, E.H., 1983. The granite problem as exposed in the southern Snake Range, Nevada. Contrib. Mineral. Petrol. 83, 99–116.
Lee, D.E., Marvin, R.F., 1981. Markedly discordant K-Ar ages for coexisting biotite and muscovite from a two-mica granite in the Toano Range, Elko County, Nevada: Isochron/West, 32, p. 19.
Lee, D.E., Kistler, R.W., Friedman, I., Van Loenen, R.E., 1981. Two-mica granites of northeastern Nevada. J. Geophys. Res. Solid Earth 86, 10607–10616.
Lee, D.E., Stacey, J.S.D., Fisher, L., 1986. Muscovite phenocrystic two-mica granites of NE Nevada are Late Cretaceous in age, in Shorter contributions to isotope research: U.S. Geol. Den. Surv. Bull. 1622, 31–39.
Lee, J., Blackburn, T., Johnston, S., 2017. Timing of mid-crustal ductile extension in the northern Snake Range metamorphic core complex, Nevada: Evidence from U/Pb zircon ages. Geosphere 13, 439–459.
Lee, S.Y., Barnes, C.G., Snoke, A.W., Howard, K.A., Frost, C.D., 2003. Petrogenesis of Mesozoic, peraluminous granites in the Lamoille Canyon area, Ruby Mountains, Nevada, USA. J. Petrol. 44, 713–732.
Levandowski, W., Jones, C.H., Butcher, L.A., Mahan, K.H., 2018. Lithospheric density models reveal evidence for Cenozoic uplift of the Colorado Plateau and Great Plains by lower-crustal hydration. Geosphere 14, 1150–1164.
Leveille, R.A., Stegen, R.J., 2012. The southwestern North America porphyry copper province. In: Hedenquist, J.W., Harris, M.O., Camus, F. (Eds.), Geology and Genesis of Major Copper Deposits and Districts of the World: A Tribute to Richard H. Sillitoe: Society of Economic Geologists Special Publication, 16, pp. 361–401.
Li, X., Yuan, X., Kind, R., 2007. The lithosphere-asthenosphere boundary beneath the western United States. Geophys. J. Int. 170, 700–710.
Lima, R.D., Prior, M.G., Stockli, D.F., Hayman, N.W., 2018. Protracted heating of the orogenic crust in Death Valley, California, USA. Geology 46, 315–318.
Liu, S., Currie, C.A., 2016. Farallon plate dynamics prior to the Laramide orogeny: Numerical models of flat subduction. Tectonophysics 666, 33–47.
Long, S.P., Kohn, M.J., 2020. Distributed ductile thinning during thrust emplacement: A commonly overlooked exhumation mechanism. Geology 48, 368–373.
Long, S.P., Soignard, E., 2016. Shallow-crustal metamorphism during Late Cretaceous anatexis in the Sevier hinterland plateau: Peak temperature conditions from the Grant Range, eastern Nevada, USA. Lithosphere 8, 150–164.
Long, K.B., Gehrels, G.E., Baldwin, S.L., 1995. Tectonothermal evolution of the Pinaleno-Jackson Mountain core complex, southeast Arizona. Geological Society of America Bulletin 107, 1231–1240.
Long, S.P., Thomson, S.N., Reiners, P.W., Di Fiori, R.V., 2015. Synorogenic extension localized by upper-crustal thickening: An example from the Late Cretaceous Nevadaplano. Geology 43, 351–354.

Lund, K., Beard, S.L., Colgan, J.P., 2014. Shrimp U-Pb dating of zircon reveals Oligocene, Late Cretaceous, and Late Jurassic ages in Troy granite, east-central Nevada. Geol. Soc. Am. Abstr. Programs 46 (5), 30.
Lund Snee, J.E., Miller, E.L., Grove, M., Hourigan, J.K., Konstantinou, A., 2016. Cenozoic paleogeographic evolution of the Elko Basin and surrounding region, northeast Nevada. Geosphere 12, 464–500.
Luth, W.C., Jahns, R.H., Tuttle, O.F., 1964. The granite system at pressures 4–10 kilobars. J. Geophys. Res. 69, 759–773.
MacCready, T., Snoke, A.W., Wright, J.E., Howard, K.A., 1997. Mid-crustal flow during Tertiary extension in the Ruby Mountains core complex, Nevada. Geol. Soc. Am. Bull. 109, 1576–1594.
Mahood, G.A., Nibler, G.E., Halliday, A.N., 1996. Zoning patterns and petrologic processes in peraluminous magma chambers: Hall Canyon pluton, Panamint Mountains, California. Geol. Soc. Am. Bull. 108, 437–453.
Mallery, C., Barth, A., Roldan-Quintana, J., Haxel, G., Wooden, J., Jacobson, C., 2018. A geochemical model of the origin of the Pan Tak Granite, the granite of Presumido Peak, and the granite of Sierra San Juan during the Laramide orogeny, southern Arizona and northern Sonora. Geol. Soc. Am. Ann. Meet. abstract no. 315.
Marvin, R.F., Zartman, R.E., Obradovich, J.D., Harrison, J.E., 1984. Geochronometric and lead isotope data on samples from the Wallace 1 degrees by 2 degrees Quadrangle, Montana and Idaho: United States Geological Survey Miscellaneous Field Studies Map, MF-1354-G.
Mattinson, C.G., Colgan, J.P., Metcalf, J.R., Miller, E.L., Wooden, J.L., 2007. Late Cretaceous to Paleocene metamorphism and magmatism in the Funeral Mountains metamorphic core complex, Death Valley, California. In: Cloos, M., Carlson, W.D., Gilbert, M.C., Liou, J.G., Sorenson, S.S. (Eds.), Convergent margin terranes and associated regions: a tribute to W.G. Ernst: Geological Society of America Special Paper, 419, pp. 205–223.
May, D.J., Haxel, G., 1980. Reconnaissance bedrock geologic map of the Sells quadrangle. Pima County, Arizona: US Geological Survey Miscellaneous Field Studies Map MF-1166, scale, 1:62,500.
McFarlane, D.N., 1981. Oreana tungsten-bearing pegmatite and related Rocky Canyon stock. University of Nevada, Reno, MS thesis, Pershing County, Nevada.
McGrew, A.J., Snee, L.W., 1994. 40Ar/39Ar thermochronologic constraints on the tectonothermal evolution of the northern East Humboldt Range metamorphic core complex, Nevada. Tectonophysics 238, 425–450.
McGrew, A.J., Peters, M.T., Wright, J.E., 2000. Thermobarometric constraints on the tectonothermal evolution of the East Humboldt Range metamorphic core complex, Nevada. Geol. Soc. Am. Bull. 112, 45–60.
Meijer, A., 2014. The Pinal Schist of southern Arizona: A Paleoproterozoic forearc complex with evidence of spreading ridge–trench interaction at ca. 1.65 Ga and a Proterozoic arc obduction event. Geol. Soc. Am. Bull. 126, 1145–1163.
Miller, C.F., 1985. Are strongly peraluminous magmas derived from pelitic sedimentary sources? J. Geol. 93, 673–689.
Miller, C.F., Barton, M.D., 1990. Phanerozoic plutonism in the Cordilleran interior, USA. In: Kay, S.M., Rapela, C.W. (Eds.), Plutonism from Antarctica to Alaska: Geological Society of America Special Paper, 241, pp. 213–231.
Miller, C.F., Bradfish, L.J., 1980. An inner Cordilleran belt of muscovite-bearing plutons. Geology 8, 412–416.
Miller, C.F., Wooden, J.L., 1994. Anatexis, hybridization and the modification of ancient crust: Mesozoic plutonism in the Old Woman Mountains area, California. Lithos 32, 111–133.
Miller, C.F., Stoddard, E.F., Bradfish, L.J., Dollase, W.A., 1981. Composition of plutonic muscovite: Genetic implications. Can. Mineral. 19, 25–34.
Miller, C.F., Wooden, J.L., Bennett, V.C,. Wright, J.E., Solomon, G.C., and Hurst, R.W., 1990b, Petrogenesis of the composite peraluminous-metaluminous Old Woman-Piute range batholith, southeastern California: isotopic constraints, in, Anderson, J. L., ed., The Nature and Origin of Cordilleran Magmatism: Geological Society of America Memoir, v. 174, p. 99-109.
Miller, C.F., McDowell, S.M., Mapes, R.W., 2003. Hot and cold granites? Implications of zircon saturation temperatures and preservation of inheritance. Geology 31, 529–532.
Miller, D.M., Nakata, J.K., Glick, L.L., 1990. K-Ar ages of Jurassic to Tertiary plutonic and metamorphic rocks, northwestern Utah and northeastern Nevada: U.S. Geol. Den. Surv. Bull. 1096, 17p.
Miller, D.M., Hoisch, T.D., Busby, C., 1995. Jurassic tectonics of northeastern Nevada and northwestern Utah from the perspective of barometric studies. In: Miller, D.M., Busby, C. (Eds.), Jurassic Magmatism and Tectonics of the North American Cordillera, Geological Society of America Special Paper, 299, pp. 267–294.
Miller, E.L., Gans, P.B., 1989. Cretaceous crustal structure and metamorphism in the hinterland of the Sevier thrust belt, western US Cordillera. Geology 17, 59–62.
Miller, E.L., Dumitru, T.A., Brown, R.W., Gans, P.B., 1999. Rapid Miocene slip on the Snake Range–Deep Creek range fault system, east-central Nevada. Geol. Soc. Am. Bull. 111, 886–905.
Miller, E.L., Konstantinou, A., Strickland, A., 2012. Comment on Geodynamics of synconvergent extension and tectonic mode switching: Constraints from the Sevier-Laramide orogen by Michael L. Wells et al. Tectonics 31, 3.
Miller, F.K., Clark, L.D., Engels, J.C., 1975. Geology of the Chewelah-Loon Lake area, Stevens and Spokane Counties, Washington: U.S. Geological Survey Professional Paper, 806, p. 50.
Miller, J.S., Glazner, A.F., Crowe, D.E., 1996. Muscovite-garnet granites in the Mojave Desert: Relation to crustal structure of the Cretaceous arc. Geology 24, 335–338.
Miller, J.S., Glazner, A.F., Farmer, G.L., Suayah, I.B., Keith, L.A., 2000. A Sr, Nd, and Pb isotopic study of mantle domains and crustal structure from Miocene volcanic rocks in the Mojave Desert, California. Geol. Soc. Am. Bull. 112, 1264–1279.
Miller, M.G., Friedman, R.M., 1999. Early Tertiary magmatism and probable Mesozoic fabrics in the Black Mountains, Death Valley, California. Geology 27, 19–22.
Milliard, A.K., Ressel, M.W., Henry, C.D., Ricks, C., Loptien, G., 2015. Spatial and temporal constraints on Carlin-type gold mineralization at the Pequop Mountains footwall to the Ruby Mountain-East Humboldt metamorphic core complex. In: Pennell, W.M., Garside, L.J. (Eds.), New Concepts and Discoveries: Geological Society of Nevada Symposium, 1, pp. 895–923.
Misch, P., Hazzard, J.C., 1962. Stratigraphy and metamorphism of Late Precambrian rocks in central northeastern Nevada and adjacent Utah. AAPG Bull. 46, 289–343.
Monger, J.W.H., Price, R.A., Tempelman-Kluit, D.J., 1982. Tectonic accretion and the origin of the two major metamorphic and plutonic welts in the Canadian Cordillera. Geology 10, 70–75.
Moye, F.J., Hackett, W.R., Blakley, J.D., Snider, L.G., 1988. Regional geologic setting and volcanic stratigraphy of the Challis volcanic field, central Idaho. Guidebook to the geology of central and southern Idaho. Idaho Geol. Surv. Bull. 27, 87–97.
Moynihan, D.P., Pattison, D.R.M., 2013. Barrovian metamorphism in the central Kootenay Arc, British Columbia: petrology and isograd geometry. Can. J. Earth Sci. 50, 769–794.
Nabelek, P.I., 2019. Petrogenesis of leucogranites in collisional orogens. Geol. Soc. Lond., Spec. Publ. 491, 179–207.
Naney, M.T., 1983. Phase equilibria of rock-forming ferromagnesian silicates in granitic systems. Am. J. Sci. 283, 993–1033.
Nelson, J.L., Colpron, M., Israel, S., 2013. The cordillera of British Columbia, Yukon, and Alaska: tectonics and metallogeny. In: Colpron, M., Bissig, T., Rusk, B.G., Thompson, J.F.H. (Eds.), Tectonics, Metallogeny, and Discovery: The North American Cordillera and Similar Accretionary Settings: Society of Economic Geologists Special Publication, 17, pp. 53–109.
Norlander, B.H., Whitney, D.L., Teyssier, C., Vanderhaeghe, O., 2002. Partial melting and decompression of the Thor-Odin Dome, Shuswap metamorphic core complex, Canadian Cordillera. Lithos 61, 103–125.
Nourse, J.A., Anderson, T.H., Silver, L.T., 1994. Tertiary metamorphic core complexes in Sonora, northwestern Mexico. Tectonics 13, 1161–1182.
Nourse, J.A., Jacques-Ayala, C., González-León, C.M., Roldan-Quintana, J., 1995. Jurassic-Cretaceous paleogeography of the Magdalena region, northern Sonora, and its influence on the positioning of Tertiary metamorphic core complexes. In: Jacques-Ayala, C., Gonzalez-Leon, C.M., Roldan-Quintana, J. (Eds.), Studies on the Mesozoic of Sonora and adjacent areas: Geological Society of America Special Paper, 301, pp. 59–78.
Parker, D.F., Ren, M., Adams, D.T., Tsai, H., Long, L.E., 2012. Mid-Tertiary magmatism in western Big Bend National Park, Texas, USA: Evolution of basaltic source regions and generation of peralkaline rhyolite. Lithos 144, 161–176.
Parrish, R.R., Carr, S.D., Parkinson, D.L., 1988. Eocene extensional tectonics and geochronology of the southern Omineca Belt, British Columbia and Washington. Tectonics 7, 181–212.
Patiño Douce, A.E., 2005. Vapor-absent melting of tonalite at 15–32 kbar. J. Petrol. 46, 275–290.
Patiño-Douce, A.E., 1996. Effects of pressure and H2O content on the compositions of primary crustal melts. Earth Environ. Sci. Trans. R. Soc. Edinb. 87, 11–21.
Patiño-Douce, A.E., 1999. What do experiments tell us about the relative contributions of crust and mantle to the origin of granitic magmas? Geol. Soc. Lond. Spec. Publ. 168, 55–75.
Patiño-Douce, A.E., Beard, J.S., 1995. Dehydration-melting of biotite gneiss and quartz amphibolite from 3 to 15 kbar. J. Petrol. 36, 707–738.
Patiño-Douce, A.E., Beard, J.S., 1996. Effects of P, f(O2) and Mg/Fe ratio on dehydration melting of model metagreywackes. J. Petrol. 37, 999–1024.
Patiño-Douce, A.E., Harris, N., 1998. Experimental constraints on Himalayan anatexis. J. Petrol. 39, 689–710.
Patiño-Douce, A.E., Humphreys, E.D., Johnston, A.D., 1990. Anatexis and metamorphism in tectonically thickened continental crust exemplified by the Sevier hinterland, western North America. Earth Planet. Sci. Lett. 97, 290–315.
Peterman, E.M., Hourigan, J.K., Grove, M., 2014. Experimental and geologic evaluation of monazite (U–Th)/He thermochronometry: Catnip Sill, Catalina Core Complex, Tucson, AZ. Earth Planet. Sci. Lett. 403, 48–55.
Peto, P., 1976. An experimental investigation of melting reactions involving muscovite and paragonite in the silica-undersaturated portion of the system K2O–Na2O–Al2O3–SiO2–H2O. Prog. Exp. Petrol. 3, 41–45.
Porter, R., Hoisch, T., Holt, W.E., 2017. The role of lower-crustal hydration in the tectonic evolution of the Colorado Plateau. Tectonophysics 712, 221–231.
Premo, W.R., Castiñeiras, P., Wooden, J.L., 2008. SHRIMP-RG U-Pb isotopic systematics of zircon from the Angel Lake orthogneiss, East Humboldt Range, Nevada: Is this really Archean crust? Geosphere 4, 963–975.
Prince, C., Harris, N., Vance, D., 2001. Fluid-enhanced melting during prograde metamorphism. J. Geol. Soc. 158, 233–241.
Prior, M.G., Stockli, D.F., Singleton, J.S., 2016. Miocene slip history of the Eagle Eye detachment fault, Harquahala Mountains metamorphic core complex, west-central Arizona. Tectonics 35, 1913–1934.
Rapp, R.P., Watson, E.B., 1995. Dehydration melting of metabasalt at 8–32 kbar: implications for continental growth and crust-mantle recycling. J. Petrol. 36, 891–931.
Rapp, R.P., Watson, E.B., Miller, C.F., 1991. Partial melting of amphibolite/eclogite and the origin of Archean trondhjemites and tonalites. Precambrian Res. 51, 1–25.
Rehrig, W.A., Reynolds, S., 1980. Geologic and geochronologic reconnaissance of a northwest-trending zone of metamorphic core complexes in southern and western Arizona. Geol. Soc. Am. Mem. 153, 131–157.
Rey, P.F., Teyssier, C., Whitney, D.L., 2009. Extension rates, crustal melting, and core complex dynamics. Geology 37, 391–394.

Reynolds, S.J., Wood, Steven E., Pearthree, Philip A., Field, John J., 2002. Geologic Map of the White Tank Mountains, Central Arizona: Arizona Geological Survey Digital Geologic Map DGM-14, map scale 1:24,000.
Richard, S.M., Fryxell, J.E., Sutter, J.F., 1990. Tertiary structure and thermal history of the Harquahala and Buckskin Mountains, west central Arizona: Implications for denudation by a major detachment fault system. J. Geophys. Res. Solid Earth 95, 19973–19987.
Rivers, T., Ketchum, J., Indares, A., Hynes, A., 2002. The high pressure belt in the Grenville Province: architecture, timing and exhumation. Can. J. Earth Sci. 39, 867–893.
Roldán-Quintana, J., 1991. Geology and chemical composition of the Jaralito and Aconchi batholiths in east-central Sonora, México. In: Perez-Segura, E., Jacques-Ayala, C. (Eds.), Studies of Sonoran Geology: Geological Society of America Special Paper, 254, pp. 69–80.
Rosenberg, C.L., Handy, M.R., 2005. Experimental deformation of partially melted granite revisited: implications for the continental crust. J. Metamorph. Geol. 23, 19–28.
Rudnick, R.L., 1992. Restites, Eu anomalies and the lower continental crust. Geochim. Cosmochim. Acta 56, 963–970.
Runyon, S.E., Seedorff, E., Barton, M.D., Steele-MacInnis, M., Lecumberri-Sanchez, P., Mazdab, F.K., 2019. Coarse muscovite veins and alteration in porphyry systems. Ore Geol. Rev. 113.
Saleeby, J., 2003. Segmentation of the Laramide slab–Evidence from the southern Sierra Nevada region. Geol. Soc. Am. Bull. 115, 655–668.
Sawyer, E.W., 1987. The role of partial melting and fractional crystallization in determining discordant migmatite leucosome compositions. J. Petrol. 28, 445–473.
Scaillet, B., Pichavant, M., Roux, J., 1995. Experimental crystallization of leucogranite magmas. J. Petrol. 36, 663–705.
Schwindinger, M., Weinberg, R.F., 2017. A felsic MASH zone of crustal magmas—feedback between granite magma intrusion and in situ crustal anatexis. Lithos 284, 109–121.
Schwindinger, M., Weinberg, R.F., Clos, F., 2019. Wet or dry? The difficulty of identifying the presence of water during crustal melting. J. Metamorph. Geol. 37, 339–358.
Seedorff, E., Dilles, J.H., Proffett, J.M., Einaudi, M.T., Zurcher, L., Stavast, W.J.A., Johnson, D.A., Barton, M.D., 2005. Porphyry deposits: Characteristics and origin of hypogene features. In: Hedenquist, J.W., Thompson, J.F.H., Goldfarb, R.J., Richards, J.P. (Eds.), Economic Geology 100th Anniversary Volume, pp. 251–298.
Seedorff, E., Barton, M.D., Stavast, W.J., Maher, D.J., 2008. Root zones of porphyry systems: Extending the porphyry model to depth. Econ. Geol. 103, 939–956.
Seedorff, E., Barton, M.D., Gehrels, G.E., Valencia, V.A., Johnson, D.A., Maher, D.J., Stavast, W.J., Marsh, T.M., 2019. Temporal evolution of the Laramide arc: U-Pb geochronology of plutons associated with porphyry copper mineralization in east-central Arizona. Geol. Soc. Am. Field Guide 55, 369–400.
Sevigny, J.H., Parrish, R.R., 1993. Age and origin of late Jurassic and Paleocene granitoids, Nelson Batholith, southern British Columbia. Can. J. Earth Sci. 30, 2305–2314.
Shafiqullah, M., Damon, P.E., Lynch, D.J., Reynolds, S.J., Rehrig, W.A., Raymond, R.H., 1980. K-Ar geochronology and geologic history of southwestern Arizona and adjacent areas. Studies in western Arizona. Arizona Geol. Soc. Digest 12, 201–260.
Shaw, A.L., Guilbert, J.M., 1990. Geochemistry and metallogeny of Arizona peraluminous granitoids with reference to Appalachian and European occurrences. In: Stein, H.J., Hannah, J.L. (Eds.), Ore-bearing granite systems; petrogenesis and mineralizing processes: Geological Society of America Special Paper, 246, pp. 317–356.
Shawe, D.R., Marvin, R.F., Andriessen, P.A.M., Mehnert, H.H., Merritt, V.M., 1986. Ages of igneous and hydrothermal events in the Round Mountain and Manhattan gold districts, Nye County, Nevada. Econ. Geol. 81, 388–407.
Siégel, C., Bryan, S.E., Allen, C.M., Gust, D.A., 2018. Use and abuse of zircon-based thermometers: a critical review and a recommended approach to identify antecrystic zircons. Earth Sci. Rev. 176, 87–116.
Silver, L.T., Chappell, B.W., 1988. The Peninsular Ranges Batholith: an insight into the evolution of the Cordilleran batholiths of southwestern North America. Earth Environ. Sci. Trans. R. Soc. Edinb. 79, 105–121.
Silverberg, D.S., 1990. The Tectonic Evolution of the Pioneer Metamorphic Core Complex, South-Central Idaho. Massachusetts Institute of Technology. Ph.D. dissertation.
Singleton, J.S., 2015. The transition from large-magnitude extension to distributed dextral faulting in the Buckskin-Rawhide metamorphic core complex, west-central Arizona. Tectonics 34, 1685–1708.
Singleton, J.S., Stockli, D.F., Gans, P.B., Prior, M.G., 2014. Timing, rate, and magnitude of slip on the Buckskin-Rawhide detachment fault, west central Arizona. Tectonics 33, 1596–1615.
Sizemore, T., Wielicki, M.M., Çemen, I., Stockli, D., Heizler, M., Robinson, D., 2019. Structural evolution of central Death Valley, California, using new thermochronometry of the Badwater turtleback. Lithosphere 11, 436–447.
Sola, A.M., Hasalová, P., Weinberg, R.F., Suzaño, N.O., Becchio, R.A., Hongn, F.D., Botelho, N., 2017. Low-P melting of metapelitic rocks and the role of H2O: Insights from phase equilibria modelling. J. Metamorph. Geol. 35, 1131–1159.
Solar, G.S., Brown, M., 2001. Petrogenesis of migmatites in Maine, USA: possible source of peraluminous leucogranite in plutons? J. Petrol. 42, 789–823.
Solomon, G.C., Taylor Jr., H.P., 1989. Isotopic evidence for the origin of Mesozoic and Cenozoic granitic plutons in the northern Great Basin. Geology 17, 591–594.
Spear, F.S., 2004. Fast cooling and exhumation of the Valhalla metamorphic core complex. southeastern British Columbia: International Geology Review 46, 193–209.
Spear, F.S., Parrish, R.R., 1996. Petrology and cooling rates of the Valhalla complex, British Columbia. Canada: Journal of Petrology 37, 733–765.
Spencer, J.E., Reynolds, S.J., 1990. Relationship between Mesozoic and Cenozoic tectonic features in west central Arizona and adjacent southeastern California. J. Geophys. Res. Solid Earth 95, 539–555.
Spencer, J.E., Isachsen, C.E., Ferguson, C.A., Richard, S.M., Skotnicki, S.J., Wooden, J., Riggs, N.R., 2003. U-Pb isotope geochronologic data from 23 igneous rock units in cenrtal and southeastern Arizona. Arizona Geol. Surv. Open File Rep. 40. OFR-03-08.
Stevens, G., Clemens, J.D., 1993. Fluid-absent melting and the roles of fluids in the lithosphere: a slanted summary? Chem. Geol. 108, 1–17.
Stevens, G., Clemens, J.D., Droop, G.T., 1997. Melt production during granulite-facies anatexis: experimental data from “primitive” metasedimentary protoliths. Contrib. Mineral. Petrol. 128, 352–370.
Stevens, G., Villaros, A., Moyen, J.F., 2007. Selective peritectic garnet entrainment as the origin of geochemical diversity in S-type granites. Geology 35, 9–12.
Stevens, L.M., Baldwin, J.A., Cottle, J.M., Kylander-Clark, A.R.C., 2015. Phase equilibria modelling and LASS monazite petrochronology: P–T–t constraints on the evolution of the Priest River core complex, northern Idaho. J. Metamorph. Geol. 33, 385–411.
Stevens, L.M., Baldwin, J.A., Crowley, J.L., Fisher, C.M., Vervoort, J.D., 2016. Magmatism as a response to exhumation of the Priest River complex, northern Idaho: Constraints from zircon U–Pb geochronology and Hf isotopes. Lithos 262, 285–297.
Stewart, J. H., 1980, Geology of Nevada: Nevada Bureau of Mines and Geology Special Publication, v. 4, 136 p.
Stewart, J.H., McKee, E.H., Stager, H.K., 1977. Geology and mineral deposits of Lander County, Nevada. Nevada Bureau Mines Geol. Bull. 88, 106.
Stewart, J.H., McManamin, M.A., Morales-Ramirez, J.M., 1984. Upper Proterozoic and Cambrian rocks in the Caborca region, Sonora, Mexico - Physical stratigraphy, biostratigraphy, paleocurrent studies, and regional relations. U.S. Geol. Surv. Profess. Paper 1309, 36.
Strickland, A., Miller, E.L., Wooden, J.L., Kozdon, R., Valley, J.W., 2011. Syn-extensional plutonism and peak metamorphism in the Albion–Raft River–Grouse Creek metamorphic core complex. Am. J. Sci. 311, 261–314.
Sylvester, A.G., Ortel, G., Nelson, C.A., Christie, J.M., 1978. Papoose Flat pluton: A granitic blister in the Inyo Mountains, California. Geol. Soc. Am. Bull. 89, 1205–1219.
Terrien, J., 2012. The Role of Magmatism in the Catalina Metamorphic Core Complex, Arizona: Insights from Integrated Thermochronology, Gravity and Aeromagnetic Data. Syracuse University. Ph.D. Dissertation.
Teyssier, C., Whitney, D.L., 2002. Gneiss domes and orogeny. Geology 30, 1139–1142.
Thompson, A.B., 1983. Fluid-absent metamorphism. J. Geol. Soc. 140, 533–547.
Thompson, A.B., Connolly, J.A., 1995. Melting of the continental crust: some thermal and petrological constraints on anatexis in continental collision zones and other tectonic settings. J. Geophys. Res. Solid Earth 100, 15565–15579.
Valencia-Moreno, M., Ruiz, J., Barton, M.D., Patchett, P.J., Zürcher, L., Hodkinson, D.G., Roldán-Quintana, J., 2001. A chemical and isotopic study of the Laramide granitic belt of northwestern Mexico: Identification of the southern edge of the North American Precambrian basement. Geol. Soc. Am. Bull. 113, 1409–1422.
van der Molen, I., Paterson, M.S., 1979. Experimental deformation of partially-melted granite. Contrib. Mineral. Petrol. 70, 299–318.
Vanderhaeghe, O., 2009. Migmatites, granites and orogeny: Flow modes of partially-molten rocks and magmas associated with melt/solid segregation in orogenic belts. Tectonophysics 477, 119–134.
Vanderhaeghe, O., Teyssier, C., 2001. Partial melting and flow of orogens. Tectonophysics 342, 451–472.
Vanderhaeghe, O., Teyssier, C., Wysoczanski, R., 1999. Structural and geochronological constraints on the role of partial melting during the formation of the Shuswap metamorphic core complex at the latitude of the Thor-Odin dome, British Columbia. Can. J. Earth Sci. 36, 917–943.
Vanderhaeghe, O., Teyssier, C., McDougall, I., Dunlap, W.J., 2003. Cooling and exhumation of the Shuswap Metamorphic Core Complex constrained by 40Ar/39Ar thermochronology. Geol. Soc. Am. Bull. 115, 200–216.
Vielzeuf, D., Montel, J.M., 1994. Partial melting of metagreywackes. Part I. Fluid-absent experiments and phase relationships. Contrib. Mineral. Petrol. 117, 375–393.
Vielzeuf, D., Schmidt, M.W., 2001. Melting relations in hydrous systems revisited: application to metapelites, metagreywackes and metabasalts. Contrib. Mineral. Petrol. 141, 251–267.
Villaros, A., Laurent, O., Couzinié, S., Moyen, J.F., Mintrone, M., 2018. Plutons and domes: the consequences of anatectic magma extraction—example from the southeastern French Massif Central. Int. J. Earth Sci. 107, 2819–2842.
Vogl, J.J., Foster, D.A., Fanning, C.M., Kent, K.A., Rodgers, D.W., Diedesch, T., 2012. Timing of extension in the Pioneer metamorphic core complex with implications for the spatial-temporal pattern of Cenozoic extension and exhumation in the northern US Cordillera. Tectonics 31.
Wallace, C.A., Lidke, D.J., Elliott, J.E., Desmarais, N.R., Obradovich, J.D., Lopez, D.A., Zarske, S.E., Heise, B.A., Blaskowski, M.J., Lean, J.S., 1992. Geologic map of the Anaconda-Pintlar Wilderness and contiguous roadless area, Granite, Deer Lodge, Beaverhead, and Ravalli counties, western Montana. U.S. Geol. Surv. Miscell. Field Stud. Map 1633-C.
Watson, E.B., Harrison, T.M., 1983. Zircon saturation revisited: temperature and composition effects in a variety of crustal magma types. Earth Planet. Sci. Lett. 64, 295–304.
Watts, K.E., John, D.A., Colgan, J.P., Henry, C.D., Bindeman, I.N., Schmitt, A.K., 2016. Probing the volcanic–plutonic connection and the genesis of crystal-rich rhyolite in a deeply dissected supervolcano in the Nevada Great Basin: source of the Late Eocene Caetano Tuff. J. Petrol. 57, 1599–1644.

Webster, E.R., Pattison, D., DuFrane, S.A., 2017. Geochronological constraints on magmatism and polyphase deformation and metamorphism in the southern Omineca Belt, British Columbia. Can. J. Earth Sci. 54, 529–549.
Weinberg, R.F., 2016. Himalayan leucogranites and migmatites: nature, timing and duration of anatexis. J. Metamorph. Geol. 34, 821–843.
Weinberg, R.F., Hasalová, P., 2015. Water-fluxed melting of the continental crust: A review. Lithos 212, 158–188.
Wells, M.L., Hoisch, T.D., 2008. The role of mantle delamination in widespread Late Cretaceous extension and magmatism in the Cordilleran orogen, western United States. Geol. Soc. Am. Bull. 120, 515–530.
Wells, M.L., Hoisch, T.D., 2012. Reply to comment by E.L. Miller et al. on Geodynamics of synconvergent extension and tectonic mode switching: Constraints from the Sevier-Laramide orogen. Tectonics 31.
Wells, M.L., Spell, T.L., Grove, M., 2002. Late Cretaceous intrusion and extensional exhumation of the Cadiz Valley batholith, Iron Mountains, southeastern California: Geological Society of America Annual Meeting. Abstracts with Programs.
Wells, M.L., Hoisch, T.D., Cruz-Uribe, A.M., Vervoort, J.D., 2012. Geodynamics of synconvergent extension and tectonic mode switching: Constraints from the Sevier-Laramide orogen. Tectonics 31.
White, A.J.R., Clemens, J.D., Holloway, J.R., Silver, L.T., Chappell, B.W., Wall, V.J., 1986. S-type granites and their probable absence in southwestern North America: Geology 14, 115–118.
Whitehouse, M.J., Stacey, J.S., Miller, F.K., 1992. Age and nature of the basement in northeastern Washington and northern Idaho: isotopic evidence from Mesozoic and Cenozoic granitoids. J. Geol. 100, 691–701.
Whitmeyer, S.J., Karlstrom, K.E., 2007. Tectonic model for the Proterozoic growth of North America. Geosphere 3, 220–259.
Whitney, D.L., Paterson, S.R., Schmidt, K.L., Glazner, A.F., Kopf, C.F., 2004a. Growth and demise of continental arcs and orogenic plateaux in the North American Cordillera: From Baja to British Columbia. In: Grocott, J., McCaffrey, K.J.W., Taylor, G., Tikoff, B. (Eds.), Vertical Coupling and Decoupling in the Lithosphere: Geological Society, London, Special Publication, 227, pp. 167–175.
Whitney, D.L., Teyssier, C., Vanderhaeghe, O., 2004b. Gneiss domes and crustal flow. In: Whitney, D.L., Teyssier, C., Siddoway, C.S. (Eds.), Gneiss domes in orogeny: Geological Society of America Special Paper, 380, pp. 15–34.
Whitney, D.L., Teyssier, C., Fayon, A.K., 2004c. Isothermal decompression, partial melting and exhumation of deep continental crust. Geol. Soc. Lond., Spec. Publ. 227, 313–326.
Whitney, D.L., Teyssier, C., Rey, P., Buck, W.R., 2013. Continental and oceanic core complexes. Geol. Soc. Am. Bull. 125, 273–298.
Wolfram, L.C., Weinberg, R.F., Nebel, O., Hamza, K., Hasalová, P., Míková, J., Becchio, R., 2019. A 60-Myr record of continental back-arc differentiation through cyclic melting. Nat. Geosci. 12, 215–219.
Wong, M.S., Gans, P.B., 2008. Geologic, structural, and thermochronologic constraints on the tectonic evolution of the Sierra Mazatán core complex, Sonora, Mexico: New insights into metamorphic core complex formation. Tectonics 27.
Wong, M.S., Gans, P.B., Scheier, J., 2010. The 40Ar/39Ar thermochronology of core complexes and other basement rocks in Sonora, Mexico: Implications for Cenozoic tectonic evolution of northwestern Mexico. J. Geophys. Res. Solid Earth 115.
Wong, M.S., O'Brien, H.P., Bunting, K.C., Gans, P.B., 2011. 40Ar/39Ar K-feldspar thermochronology of the Harcuvar core complex, western Arizona: New insight into the timing of extension and degree of footwall tilt. Geol. Soc. Am. Ann. Meet. Abstr. Progr. 43, 53.
Wooden, J.L., Kistler, R.W., Tosdal, R.M., 1999. Strontium, lead, and oxygen isotopic data for granitoid and volcanic rocks from the northern Great Basin and Sierra Nevada, California, Nevada and Utah. U.S. Geol. Surv. Open File Rep. 99-569, 20.
Wright, J.E., Haxel, G., 1982. A garnet-two-mica granite, Coyote Mountains, southern Arizona: Geologic setting, uranium-lead isotopic systematics of zircon, and nature of the granite source region. Geol. Soc. Am. Bull. 93, 1176–1188.
Wright, J.E., Snoke, A.W., 1993. Tertiary magmatism and mylonitization in the Ruby-East Humboldt metamorphic core complex, northeastern Nevada: U-Pb geochronology and Sr, Nd, and Pb isotope geochemistry. Geol. Soc. Am. Bull. 105, 935–952.
Wright, J.E., Wooden, J.L., 1991. New Sr, Nd, and Pb isotopic data from plutons in the northern Great Basin: Implications for crustal structure and granite petrogenesis in the hinterland of the Sevier thrust belt. Geology 19, 457–460.
Wust, S.L., 1986. Regional correlation of extension directions in Cordilleran metamorphic core complexes. Geology 14, 828–830.
Wyld, S.J., 2002. Structural evolution of a Mesozoic backarc fold-and-thrust belt in the US Cordillera: New evidence from northern Nevada. Geol. Soc. Am. Bull. 114, 1452–1468.
Wyllie, P.J., 1977. Crustal anatexis: an experimental review. Tectonophysics 43, 41–71.
Wyllie, P.J., Wolf, M.B., 1993. Amphibolite dehydration-melting: sorting out the solidus: Geological Society. London, Special Publications 76, 405–416.
Yardley, B.W., Barber, J.P., 1991. Melting reactions in the Connemara Schists: the role of water infiltration in the formation of amphibolite facies migmatites. Am. Mineral. 76, 848–856.
Yonkee, W.A., Weil, A.B., 2015. Tectonic evolution of the Sevier and Laramide belts within the North American Cordillera orogenic system. Earth Sci. Rev. 150, 531–593.
Zen, E.A., 1986. Aluminum enrichment in silicate melts by fractional crystallization: some mineralogic and petrographic constraints. J. Petrol. 27, 1095–1117.
Zen, E.A., 1988. Phase relations of peraluminous granitic rocks and their petrogenetic implications. Annu. Rev. Earth Planet. Sci. 16, 21–51.